ACTIVITY REPORT 2026

CNRNANO

ISTITUTO NANOSCIENZE CONSIGLIO NAZIONALE DELLE RICERCHE

Table of contents

Institute director
Gaetano Scamarcio
(Till 08/31/2024, Lucia Sorba)

Coordinators of units
Modena: Arrigo Calzolari
(Till 10/15/2025, Massimo Rontani)

Administrative director
Giovanna Diprima

Executive board
Cnr researchers
Stefania Benedetti, Deborah Prezzi, Elia Strambini, Valentina Tozzini, Filippo Troiani, Miriam Serena Vitiello
Cnr technical/administrative staff
Maria Grazia Angelini
Affiliated researchers
Stefano Frabboni, Stefano Roddaro

Former board
(Till 04/22/2024)
Cnr researchers
Stefania Benedetti, Giorgia Brancolini, Marco Cecchini, Stefan Heun, Valentina Tozzini, Filippo Troiani
Cnr technical/administrative staff
Maria Grazia Angelini
Affiliated researchers
Elisa Molinari, Alessandro Tredicucci

Contacts
Piazza San Silvestro, 12
I-56127 Pisa, Italy
ph. +39 050 509418
e-mail: segreteria.nest@nano.cnr.it

Via Campi, 213A
I-41125 Modena, Italy
ph. +39 059 2055629
e-mail: segreteria.s3@nano.cnr.it

website: www.nano.cnr.it

Foreword

This Activity Report presents the scientific highlights of the research carried out during the years 2024–2025 within the core areas of the Institute: fundamental and translational nanobiophysics; physics and technology of light at the nanoscale; solid-state quantum technology; surfaces and interfaces, including nanofabrication, imaging, and spectroscopy; and nanoscale theory, modelling, and computation.

To provide a comprehensive overview of the Institute's activities and achievements, the report also includes a complete list of ongoing projects, publication output, and scientific events organized during this period, together with a detailed description of the rich variety and high quality of the available research facilities. The high number of publications in leading international journals, including those of the Nature portfolio, testifies to the scientific excellence and global relevance of Cnr Nano research.

A distinctive element of this period has been the strong engagement of the Institute in large-scale national and European initiatives, including projects funded within the Next Generation EU framework and other competitive programs. This broad participation has strengthened interdisciplinary collaborations, expanded scientific capabilities, and contributed to the consolidation of Cnr Nano as a key player in the national and international research landscape.

Equally important has been the effort to reinforce the sense of community and shared vision within the Institute. Over 170 researchers, technologists, and staff gathered in Modena on 5–6 June 2025 for the 4th Cnr Nano Scientific Meeting, under the theme "Reconnecting, inspiring interactions". Beyond its scientific value, the meeting fostered dialogue across labs and career stages, while a public evening concert highlighted the connection between science, creativity, and society.

Over these two years, the Institute has continued to grow. The current staff comprises 74 researchers and technologists, 27 postdoctoral fellows, 41 research associates, and 14 administrative and technical personnel, reflecting a sustained commitment to strengthening both scientific and support activities.

I would like to express my sincere gratitude to all those who contributed to the preparation of this report. In particular, I acknowledge the editorial coordination of Maddalena Scandola; the editorial board, including Luisa Neri, Maria Bartolacelli, and Susanna Cavicchioli; and the scientific committee composed of Stefania Benedetti, Guido Paolicelli, Stefano Pittalis, Antonella Sgarbossa, Fabio Taddei, Stefano Veronesi, and Simone Zanotto.

I would like to thank all members of the Institute for their dedication, creativity, and commitment. Our work continues to drive the scientific excellence and collaborative spirit that define Cnr Nano. I am confident that the Institute will further strengthen its role in addressing fundamental scientific challenges while contributing to technological innovation and societal impact.

Gaetano Scamarcio
Director of Cnr Nano

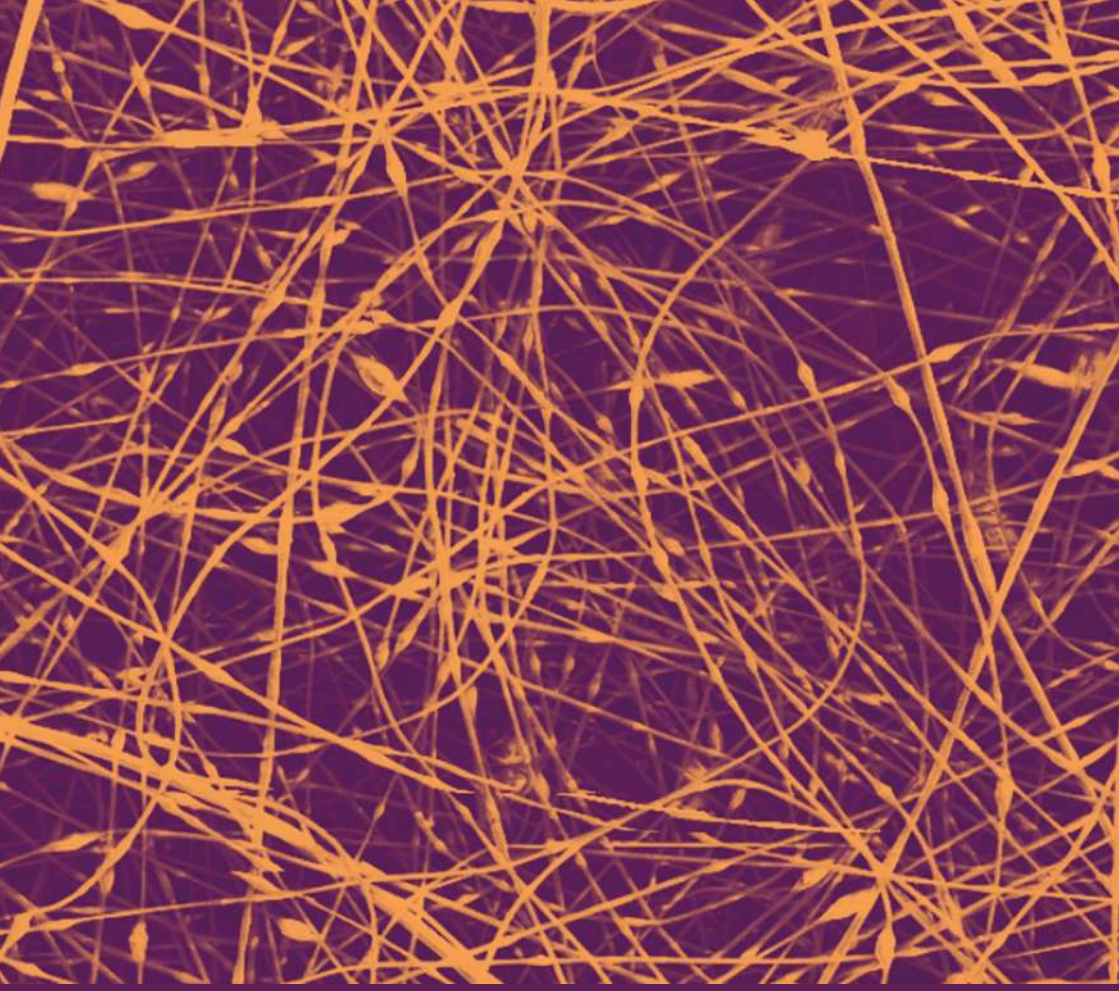

Highlights - Fundamental and translational nanobiophysics

Nanobiophysics is an interdisciplinary field that combines biology, physics, chemistry, biotechnology, and nanotechnology to study biological systems at the nanoscale. The research highlights we present address key challenges in disease understanding, diagnostics, and therapeutic intervention in the regenerative medicine, oncology, and infectious diseases through an integrated strategy that combines advanced biocompatible materials, multiscale computational modeling, nanoscale sensing technologies, and clinically relevant biological models.

Advanced materials for biomedical applications. Advanced polymeric biomaterials combined with additive manufacturing (AM) techniques enable the fabrication of complex, biologically relevant scaffolds. Computer-aided wet-spinning (CAWS) was employed to produce 3D chitosan/alginate hydrogel scaffolds for cancer modeling and biodegradable PLGA scaffolds reinforced with hydroxyapatite for bone regeneration. Together, these systems demonstrate the versatility of AM-enabled biomaterials for disease modeling and regenerative medicine.

Among 2D nanomaterials, stable and photoactive black phosphorus nanoflakes have been produced via liquid-phase exfoliation. Their ability to generate singlet oxygen when irradiated with visible light, combined with their intrinsic biocompatibility, supports applications in antimicrobial phototherapy, bioimaging, and inhibition of pathological amyloid aggregation. These materials represent a promising class of multifunctional platforms for future theragnostic strategies.

Computational biophysics and molecular design. Computational modeling plays a central role in understanding and predicting protein aggregation, a pervasive phenomenon relevant to both disease and biotechnology.
AlphaFold (AF) software and molecular dynamics (MD) performances have been compared on the behaviour of variants of the Intrinsically Fluorescent Proteins (FP) with different aggregation propensity. Despite differences in sampling, both approaches converged on similar preferential interaction interfaces, highlighting their complementarity. This integration establishes a general framework for combining AI-driven structure prediction with physics-based simulations to study complex biomolecular assemblies.
Multiscale modeling and atomistic simulations guided the development of a patented GFP-based FRET biosensor for detecting SARS-CoV-2 spike,

optimizing domain organization and linker sequences for efficient signal transduction. This integrated strategy that combines experimental validation, supercomputer simulations, and in silico design yields reliable, scalable, and modular diagnostic tools that can be quickly implemented in response to new emerging infective threats.

Nanoscale and label-free sensing technologies. Acoustic biosensing using Quartz Crystal Microbalance with Dissipation Monitoring (QCM-D) was developed for direct polyphenol analysis in wine. Peptide-functionalized sensors provided robust, quantitative responses without pre-treatment, enabling cost-effective, real-time monitoring for food quality control and precision oenology.

A novel quantum relaxometry approach based on nitrogen-vacancy centres in diamond was developed for label-free detection of negatively charged biomolecules like miRNA-21, frequently overexpressed in a wide variety of human cancers. By exploiting biomolecule-induced localization of paramagnetic ions, the method achieves nanomolar sensitivity while overcoming charge-screening limitations. Molecular dynamics simulations quantitatively linked nanoscale ion distributions to quantum signal readout, strengthening the mechanistic foundation of this emerging diagnostic technology.

Biomedical applications and translational impact. Biomimetic scaffolds were developed to address unmet needs in tissue repair. Directional glycerol–chitosan membranes and nanofibers, engineered to match nerve tissue mechanics and anisotropy, guided Schwann cell migration, neurite outgrowth, and axonal alignment. Validation across in vitro, ex vivo, and in vivo models demonstrated enhanced nerve regeneration in clinically relevant injury scenarios.

The nanoscale organization of the immune checkpoint protein PD-L1 was resolved in cancer cells. PD-L1 was shown to form raft-confined nanoclusters arranged in a mesoscopic lattice, providing new insight into immune escape mechanisms and inspiring future therapeutic strategies in immuno-oncology.

[OA] *in the References indicates an Open Access publication.*

Additive manufacturing of functional biopolymeric scaffolds for cancer modeling and bone regeneration

The strategic combination of additive manufacturing (AM) and biomaterial design is leading to tailored scaffolds in two distinct areas of tissue engineering: cancer modeling and bone regeneration. Cancer modeling is the creation of artificial systems that mimic human cancer. These models aim to give an insight into cancer initiation, progression, and response to treatment, to predict disease outcomes and optimize therapeutic strategies. Bone tissue engineering is a promising approach in regenerative medicine aimed at repairing or replacing damaged bone tissue. In both these fields, the advent of AM has provided a boost to the production of novel biocompatible functional devices.

Advances in polymeric biomaterials formulation and AM techniques are constantly improving the design and fabrication of novel biomedical devices for the investigation and treatment of several pathological conditions. For instance, according to the cancer modeling strategy, realistic tumor models are grown in vitro to get information about their onset, evolution, stability, and response to drugs.

In this context, computer-aided wet-spinning (CAWS) was used to fabricate chitosan/alginate polyelectrolyte complex hydrogels for an *in vitro* 3D ovarian cancer model (Cs/Alg, Fig. 1). The resulting scaffolds were stable for long-term culture (up to 63 days) and successfully supported colonization by cancer cells that retained aggressive tumor characteristics. Critically, the developed 3D model demonstrated significantly lower sensitivity to chemotherapeutic agents (cisplatin and eugenol) compared to standard 2D cell cultures, validating the scaffold utility for more accurate pre-clinical drug testing.

The combination of advanced materials and novel AM techniques finds its proper employment also in the fabrication of biocompatible and biodegradable scaffolds for tissue regeneration. Thanks to CAWS, poly(D,L-lactide-co-glycolide) (PLGA) scaffolds reinforced with PLGA-grafted hydroxyapatite (PgHA) were prepared (PLGA/PgHA, Fig. 1). The functionalization of hydroxyapatite with PLGA substantially enhanced its compatibility with the polymeric matrix. This resulted in composite scaffolds with enhanced mechanical properties and prolonged *in vitro* structural stability. The scaffolds supported preosteoblast viability and differentiation toward the osteoblastic phenotype, highlighting their potential for personalized bone tissue engineering.

These two studies together show the versatility and efficacy of combining biocompatible polymers design with precision AM to engineer functionally optimized scaffolds for advanced biomedical applications.

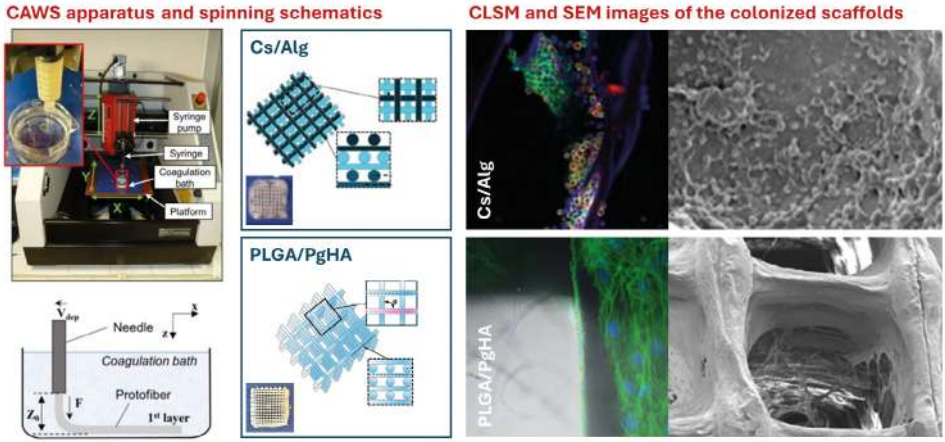

Fig. 1
Left: CAWS apparatus, deposition scheme and prototype for the two different scaffolds. Right: CLSM and SEM images of the colonized scaffolds. For Cs/Alg A2780cis cells were stained with Phalloidin Alexa Fluor 488, DAPI and β1 integrin CD29 monoclonal antibody and imaged at day 28. For PLGA/PgHA MC3T3 cells were stained with Phalloidin Alexa Fluor 488 and DAPI and imaged at day 28.

Contact persons
Antonella Battisti (antonella.battisti@nano.cnr.it)

References
[1] Functionalized Hydroxyapatite Loading Enhances the Mechanical and Biodegradation Properties of Wet-Spun Poly(Lactide-co-Glycolide) Scaffolds by Additive Manufacturing. G. Pecorini, E. Martinelli, A. Corti, A. Battisti, and D. Puppi. Macromolecular Bioscience 25, 2400486 (2025). [OA]
[2] Chitosan/alginate polyelectrolyte complex hydrogels by additive manufacturing for *in vitro* 3D ovarian cancer modeling. S. Braccini, G. Pecorini, S. Biagini, C. Tacchini, A. Battisti, and D. Puppi. International Journal of Biological Macromolecules 296, 13979 (2025).

Projects
Ateneo Research Projects (PRA) 2020-University of Pisa, project nr. PRA_2020_37.

Atomistic design of an intramolecular fret biosensor for emerging viruses

RosettaFold design principles, pioneered by Nobel laureate David Baker, inspired the development of an integrated computational–experimental strategy leading to a patented GFP-based FRET biosensor for SARS-CoV-2 Spike detection. Multiscale modelling allowed engineering of a single protein combining the Spike RBM and the de novo–designed LCB1 fragment mimicking ACE2 helices. Optimized linkers ensure structural stability and efficient energy transfer. The sensor is genetically encoded and functionalized via click chemistry, it offers dual fluorescence readouts. This study shows how atomistic insight can drive next-generation protein nanosensors.

An integrated computational–experimental strategy for the rational design of fluorescent protein-based nanosensors has been developed, leading to the creation of a patented GFP-based FRET biosensor for the detection of the SARS-CoV-2 Spike antigen (patent no. 102022000025416). The design combined multiscale molecular modeling and dynamics simulations to guide the engineering of a single protein sequence composed of three modules: a Spike-derived recognition domain namely RBM, a central region inspired by the human ACE2 receptor for viral binding namely LCB1, and Green Fluorescent Protein (GFP), which produces a detectable fluorescent signal upon target recognition. The sensor incorporates the LCB1 sequence, designed via de novo design by Rosetta fold, mimicking the two α-helices of ACE2 responsible for RBM interaction.

The main innovation lies in the atomistic-level guidance applied to optimize FRET detection mechanisms, bridging molecular insight and experimental implementation. Optimized linker sequences (AAASSGGGASGAGG and LEAPAPA) ensure structural stability and efficient energy transfer. Fully genetically encoded and expressed in E. coli, the biosensor supports dual fluorescence readouts. The biosensor was realized using click chemistry techniques in collaboration with Prof. E. Da Pozzo at the University of Pisa.

This integrated approach, combining in silico design, supercomputer simulations, and experimental validation, provides the creation of stable, modular, and flexible protein nanosensors capable of detecting emerging viral threats and contributing to future pandemic preparedness. The modular architecture allows each component to be tuned, ensuring that recognition elements can be redesigned to detect new viruses, offering a robust platform for next-generation biosensing technologies.

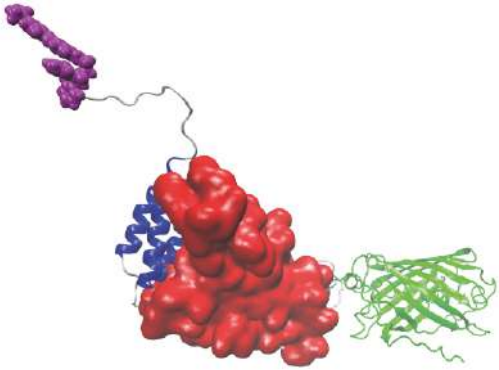

Fig. 1
Schematic picture of the FRET sensor prototype. Reporter 1 (violet) corresponds to a Gly(His)$_6$ peptide sequence, composed of six histidine residues preceded by glycine, essential for biosensor purification and enabling covalent conjugation to an organic quencher. Interaction element 1 (red) is the receptor-binding motif (RBM) of the SARS-CoV-2 Spike protein, which mediates binding to the human ACE2 receptor. Interaction element 2 (blue) corresponds to the LCB1 sequence, designed to mimic the two α-helices of the N-terminal region of ACE2 responsible for RBM interaction. Reporter 2 (green) is the Enhanced Green Fluorescent Protein (EGFP), a bright GFP variant that generates the fluorescent signal upon target recognition.

Contact persons
Giorgia Brancolini (giorgia.brancolini@nano.cnr.it)
Valentina Tozzini (valentina.tozzini@nano.cnr.it)

References
[1] An intramolecular FRET biosensor for the detection of SARS-CoV-2 in biological fluids. D. Montepietra, L. Germelli, L. Marchetti, V. Tozzini, E. Angeloni, C. Giacomelli, B. Storti, R. Bizzarri, E. Barresi, S. Taliani, G. Brancolini, and E. Da Pozzo. Nanoscale 17, 8803-8815 (2025). [OA]

Projects
MIUR PRIN 2021, PACECOR, project nr. 2020LW7XWH.

Combining AI with Coarse Grained Molecular dynamics to explore protein aggregation

The Nobel prize 2024 to Baker, Hassabis, and Jumper for studies on protein structure prediction made clear that AI has wildly stepped into bio-modelling. Indeed, proteins fold prediction relies on the exploration and classification of huge conformational and sequential spaces, a task where artificial neural networks (NN) excel, allowing the AlphaFold (AF) software to fold proteins with 97% accuracy. Conversely, it still shows flaws on disordered proteins, and on multimeric ones or aggregates. We explore this issue by comparing the performances of AF and molecular dynamics (MD) on the behaviour of variants of the Intrinsically Fluorescent Proteins (FP) with different aggregation propensity.

Aggregation is a pervasive phenomenon, affecting both disordered and well-folded proteins. Therefore, probing a tool such as AF, destined to become routine [1], on this aspect is crucial. The choice of FPs as study case has the added value that the knowledge of their intrinsic aggregation helps designing molecular sensors using them as chromophores. The knowledge of FPs' intrinsic aggregation may help the design of molecular sensors that use the same FPs as chromophores.

FPs are also an ideal system for the test: the variants have same fold and different sequence and aggregation tendency, allowing to compare the capability of different popular inter-residue level potentials (Calvados, COCOMO, Trovato) and of AF to reproduce the inter-molecular interactions. We performed extensive MD simulations [2] exploring the phase diagram of aggregation (Fig. 1, panel a). Our results reproduce the diffusivity and aggregation order of the variants for all FFs, and indicate that COCOMO better matches the experimental viscosities. Furthermore, the simulations return the aggregate structures and contact interfaces of different variants, determined by their sequences, and allow to calculate the contact probability matrix. The latter is the primary output of AF (Fig. 1 panel b). In this case, the *multimer* contact probability matrix is returned, and, based on this, the multimer structures are generated and compared with the cluster structures of similar size from MD. Despite MD trajectories explore multiple relative conformations, while AF returns only a limited number of structures, we observe that MD and AF return similar preferential interfaces in the different variants. This is confirmed by the similarity of the monomer-monomer contact probability matrix, obtained by averaging the AF multimeric one with that obtained with MD, especially for one of the FFs (Trovato), which also returns interfaces and aggregate structures more consistent with those of AF.

Our results are useful to guide the choice or design of inter-residue potentials, to highlight the contacts between two complementary approaches, and to outline a possible scheme to integrate AlphaFold outcomes and molecular dynamics simulations.

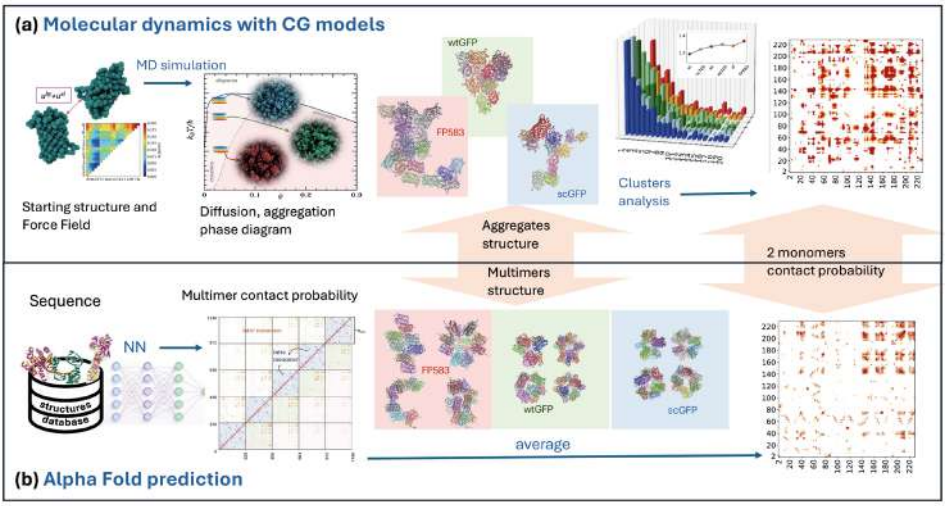

Fig. 1
Comparative workflows of Molecular Dynamics (MD) and AlphaFold (AF). (a) A residue-level representation of the proteins is built, and the phase diagram of aggregation studied with MD simulations. The clusters' structure and size distribution are also returned, allowing evaluation of the monomer contact probability matrix. (b) The AF evaluates the contact probability matrix for multimers directly from the sequence and returns multimer structures. The monomer probability matrix is obtained averaging the out-of-diagonal blocks of the multimer ones.

Contact persons
Valentina Tozzini (valentina.tozzini@nano.cnr.it)

References
[1] Editorial: Revolutionizing Life Sciences: The Nobel Leap in Artificial Intelligence-Driven Biomodeling. V. Tozzini and C. Giulivi. Frontiers in Molecular Biosciences 11, 1540823 (2025). [OA]
[2] Aggregation of Intrinsically Fluorescent Proteins: Combining Coarse-Grained Molecular Dynamics with AlphaFold Predictions. M. Bini, G. Brancolini, and V. Tozzini. ACS Omega 10, 54341-54356 (2025). [OA]

Projects
Next Generation-EU PNRR, Tuscany Health Ecosystem, project nr. ECS_00000017.
INFN CSN5, FRIDA project.
INFN CSN5, MIRO project.
CINECA award, IsB27_SETE, project nr. HP10BSTFDD.
CINECA award, IsCb7_AG-ABETA project nr. HP10C8JNX2.

Exploring Gelatin-A and Mouse Proline-Rich Protein 5 as probes for wine polyphenol analysis by quartz crystal microbalance with dissipation monitoring

Polyphenols play a crucial role in shaping wine quality, influencing color, astringency, bitterness, and overall stability. Since conventional analytical techniques are often expensive and slow, faster and more accessible approaches are desirable. Quartz Crystal Microbalance with Dissipation Monitoring (QCM-D) offers rapid, reliable, label-free detection. Using Gelatin A and Mouse Proline-Rich Protein 5 (MP5) as probes, QCM-D enables effective evaluation of wine polyphenols. With MP5, dissipation responds linearly to total polyphenols and hydroxybenzoic acids, highlighting its potential for real-time monitoring during the winemaking process.

This work explores the use of Quartz Crystal Microbalance with Dissipation Monitoring (QCM-D) for direct polyphenol analysis in wine, offering a faster and simpler alternative to traditional methods. Two probes were tested: Gelatin Type A (Gel-A) and a peptide fragment of Mouse Proline-Rich Protein 5 (MP5), both immobilized on QCM sensors using optimized protocols (Fig. 1).

Functionalization was confirmed by frequency shifts and AFM imaging, revealing network-like structures and increased surface wettability. MP5 achieved a molecular density of 2.1×10^{14} molecules cm^{-2}, significantly higher than Gel-A (5.1×10^{12} molecules cm^{-2}), due to its smaller size. In wine detection tests, MP5 consistently produced negative frequency shifts (mass loading) and positive dissipation shifts, indicating increased viscoelasticity upon polyphenol binding. Importantly, MP5 showed a linear correlation between dissipation and total polyphenol concentration, as well as hydroxybenzoic acids, enabling quantitative analysis (Fig. 2). Gel-A exhibited more complex behaviour: both positive and negative frequency shifts were observed, likely due to dehydration effects from cross-linked structures formed with procyanidins. Dissipation values for Gel-A were negative, confirming network formation. These differences suggest MP5 provides more predictable and robust sensing performance, while Gel-A interactions depend on wine composition, particularly tannin content.

The system offers key advantages: direct analysis without pre-treatment, cost-effective probes compared to enzyme-based sensors, and adaptability for on-site use. Future work will address sensor stability and storage to enable pre-functionalized sensors for wineries, supporting real-time monitoring during fermentation, aging, and blending. This approach could extend beyond wine to other agri-food sectors such as olive oil, where polyphenols affect flavor and nutritional quality, ultimately evolving into a versatile platform for precision oenology and food quality control.

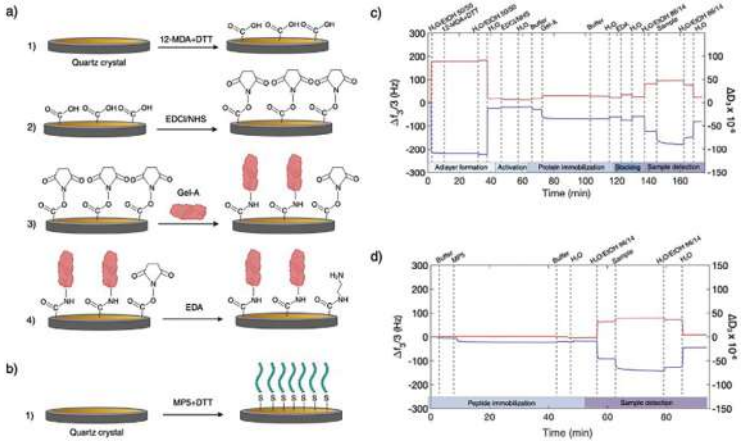

Fig. 1
Schematic of the quartz crystal functionalization (not in scale) a) in 1. the formation of the 12-MDA adlayer; in 2. the activation via EDCI/NHS chemistry; in 3. Gel-A protein immobilization; in 4. deactivation. b) MP5 peptide immobilization. c) Typical $\Delta f_3/3$ (blue line) and ΔD_3 (red line) vs time for Gel-A functionalization. d) Typical $\Delta f_3/3$ (blue line) and ΔD_3 (red line) vs time for MP5-based functionalization (events: Peptide immobilization, Sample detection). Created in BioRender. Tori, G. (2025) https://BioRender.com/o95t497.

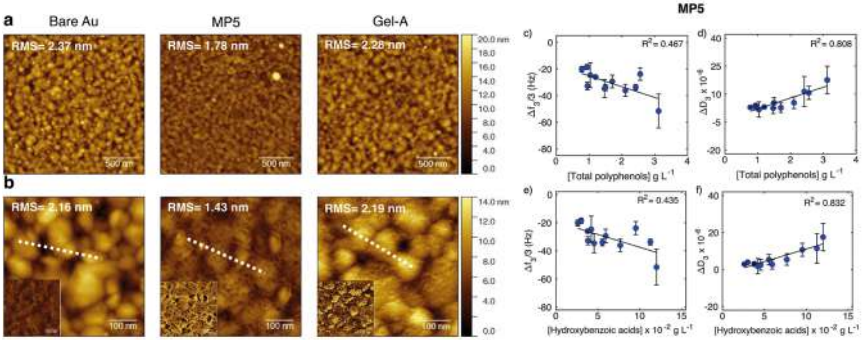

Fig. 2
(a, b) AFM topography images of quartz crystals before (Bare Au) and after functionalization with MP5 and Gel-A. (c-f) Calibration of $\Delta f_3/3$ and ΔD_3 for the total polyphenols or hydroxybenzoic acids concentration obtained with wine samples.

Contact persons
Marco Cecchini (marco-cecchini@cnr.it)
Mariacristina Gagliardi (mariacristina.gagliardi@cnr.it)

References

[1] Exploring Gelatin-A and Mouse Proline-Rich Protein 5 as Probes for Wine Polyphenol Analysis by Quartz Crystal Microbalance with Dissipation Monitoring. G. Tori et al. Advanced Sensor Research 4, e00140 (2025). [OA]
[2] The effect of probe density coverage on the detection of oenological tannins in quartz crystal microbalance with dissipation monitoring (QCM-D) experiments. M. Gagliardi et al. Journal of the Science of Food and Agriculture 105, 1476 (2024).

Projects

MIUR FISR 2019, VioLOC, project nr. FISR2019-03020.

Quantum sensing of microRNAs with nitrogen-vacancy centers in diamond

We introduce a quantum biosensing platform based on Nitrogen-Vacancy (NV) centres in diamond, for label-free detection of nucleic acids such as microRNAs. The technique employs paramagnetic Mn^{2+} ions as magnetic reporters, which accumulate locally, due to the negative charge of the microRNA. All-atom Molecular Dynamics (MD) simulations provided critical validation, confirming the formation of an Mn^{2+} ion cloud at the diamond/miRNA interface. The MD approach allowed us to quantify the magnetic noise generated by these accumulated ions, providing a theoretical prediction for the enhanced NV spin relaxation (T_1), which is at the basis of the operational optical readout of miRNA concentration.

Detection of biomolecules for diagnostics purposes is typically accomplished using fluorescence labels and labour-intensive amplification methods. Achieving label-free detection with high sensitivity would be of great importance for accessible and early diagnosis of diseases such as cancer. Our work addresses this fundamental challenge in biomolecular sensing, by developing a novel quantum relaxometry technique utilizing Nitrogen-Vacancy centres (NV) in diamond.

NV spin relaxation is sensitive to magnetic field fluctuations (magnetic noise), and can be manipulated and read optically, because the different spin states have different fluorescence intensity. The proposed technique exploits the strong negative charge of nucleic acids (miRNA-21 in our study) to attract paramagnetic ions, such as Mn^{2+}, and localize them close to the surface (Fig. 1). The increased magnetic noise due to the Mn^{2+} enhances the spin-lattice relaxation rate ($1/T_1$) of the NV centres.

This mechanism was validated by all-atom Molecular Dynamics (MD) simulations. The MD models confirmed that the negative charges on the miRNA and its propensity to interact with the functionalized diamond surface result in a dense accumulation of Mn^{2+} ions at the interface (Fig. 2), much higher than background concentration. Crucially, the simulations allowed for the precise quantification of the magnetic noise intensity - $\langle B_\perp^2 \rangle$ - generated by the ion distribution across various scenarios, directly linking the microscopic structures to the observed quantum relaxation signals. The experimental results, in line with the MD predictions, demonstrated sensitive, label-free detection of miRNA-21 down to the 10 nM range.

This quantum-sensing approach provides robust nanoscale detection of negatively charged molecules, paving the way for high-sensitive diagnostics that are label free and overcome the inherent limitations of charge screening in biological environments.

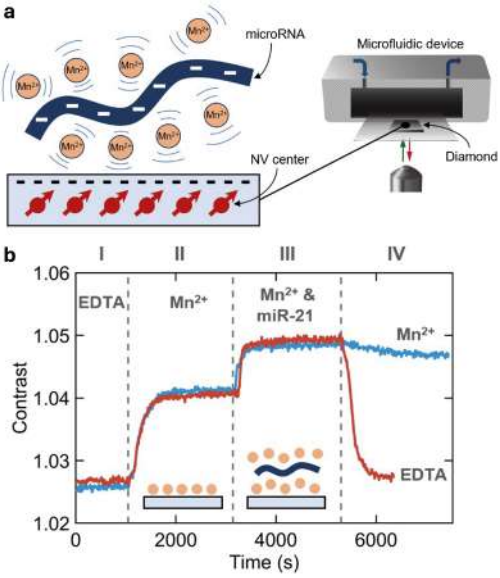

Fig. 1
Experimental setup and detection protocol. a) Mn^{2+} ions counteract the intrinsic charge of microRNA-21 (miR-21) and mediate the interaction with the diamond surface. The NV centres (red circles) are distributed 7±3 nm below the surface. The diamond sample is attached to a coverslip placed inside the microfluidic device, which is used for sequential liquid injection. b) Spin relaxation contrast (the ratio of two NV fluorescence readouts, one at 10 μs and one at 400 μs, after preparation with a suitable laser pulse sequence) during sequential injection of: EDTA (a chelating agent), Mn^{2+} solution, miR-21 in Mn^{2+} solution, finally and EDTA (red line) or Mn^{2+} solution (blue line).

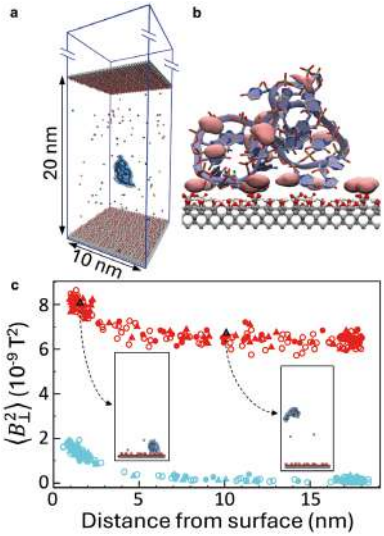

Fig. 2
a) The MD simulation setup consists of a capped box, two slabs of diamond along the z-axis and one single miR-21. The volume between the diamond slabs is filled with ions and aqueous solution (not shown) and each diamond surface is terminated with hydroxyl/epoxy, carbonyl, ether, and carboxyl functional groups. b) Isosurfaces (pink) of Mn^{2+} density calculated for one representative MD trajectory. Each surface corresponds to an ion interacting either with the diamond surface, with miR-21 or with both. c) $\langle B_\perp^2 \rangle$ – average fluctuation intensity of the magnetic field due to the Mn^{2+} – experienced by a NV at 7-nm depth as a function of the distance of the miR-21 to the diamond surface for negatively charged (red) and neutral (cyan) diamond surface states.

Contact persons
Riccardo Nifosì (riccardo.nifosi@cnr.it)
Luca Bellucci (luca.bellucci@cnr.it)

References
[1] Quantum sensing of microRNAs with nitrogen-vacancy centers in diamond. J. Zalieckas, M. M. Greve, L. Bellucci, G. Sacco, V. Håkonsen, V. Tozzini, and R. Nifosì. Communications Chemistry 7, 101 (2024). [OA]

Phosphorene as an innovative photodynamic therapeutic platform for biomedical applications: antibacterial and antiamyloidogenic strategies

Phosphorene, a two-dimensional nanomaterial derived from black phosphorus through exfoliation, exhibits unique physicochemical properties-tunable bandgap, high surface area, efficient photothermal conversion and ability to generate singlet oxygen under visible/NIR irradiation-that make it suitable for photothermal and photodynamic therapy. Phosphorene-based nanomaterials can be engineered as innovative platform in antimicrobial phototherapy to successfully eradicate persistent infections. Its biocompatibility and ability to cross the blood–brain barrier enable applications also in antiamyloidogenic interventions, including inhibition of formation and disassembly of amyloid fibrils.

Among 2D materials, black Phosphorus (bP) monolayers, known as Phosphorene, have attracted recent scientific attention for biomedical applications due to their unique characteristics. Few-layered bP nanosheets have been shown to be effective photosensitizers exhibiting a broad-spectrum light absorption ranging from the UV light to the near-infrared region, producing singlet oxygen ($^1O_2$) with a high quantum yield. In addition to these favorable properties, bP-nanosheets are biocompatible and nontoxic materials, which is the essential criteria for *in vivo* applications.

Phosphorene has been studied and proposed for many biomedical applications, such as bioimaging, biosensing, and theranostics. Recently, studies on its potential antimicrobial applications, especially against antibiotic-resistant pathogens, have been gaining growing attention [Pharmaceutics 15, 2748 (2023)]. In addition, direct effects of inhibition and disintegration of amyloid fibrils associated with the development of various neurodegenerative diseases (e.g., Alzheimer's disease) and metabolic disorders (e.g., diabetes) have been reported.

Preparation of phosphorene suspensions for biomedical applications using black phosphorus liquid phase exfoliation have been performed. To achieve this goal, two liquid exfoliating media were employed: deionized water (biocompatible and safe) and Cyrene, a new-generation bio-based and potentially biocompatible solvent that has not been used previously for liquid phase exfoliation of bP. The obtained bP nanoflakes suspensions have been characterized and their stability over time as well as their photoactivity have been investigated. Preliminary data on the potential biomedical application of bP-nanosheets to inhibit the insulin self-assembly into amyloid aggregates as well as to cause fibrils disassembling through simple incubation or photoactivity, are presented [1].

The use of bP-nanoflakes, both alone and combined with natural photosensitizers, in antimicrobial phototherapy is under investigation in order to eradicate antibiotic resistant bacteria commonly found in chronic wound infections [2].

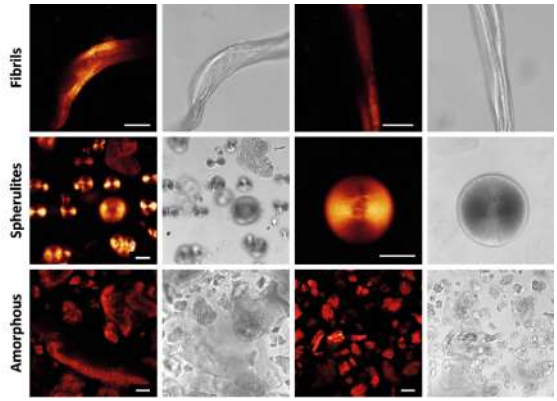

Fig. 1
Confocal fluorescence (columns 1 and 3) and transmission (columns 2 and 4) images of insulin aggregates with different morphologies after ThT staining. Insulin aggregates sometimes appear as long fibril bundles (10–50 μm), but aggregates with different morphologies are often present in the same sample. The shape of these aggregates (that often converge in large superstructures) can be fibrillar, amorphous, or even spherical (spherulites). Scale bars: 25 μm.

Fig. 2
Confocal fluorescence (columns 2 and 4) and transmission (columns 1 and 3) images of insulin aggregates with and without incubation with 2D-bP at different times after ThT staining. 2D-bP significantly inhibited the formation of amyloid structures in the first 7 h. After 24 h, many intensively emitting aggregates stained by ThT were revealed in both the treated and control samples, indicating that the insulin self-assembly could no longer be blocked by 2D-bP probably due to nanoflakes degradation. Scale bars: 50 μm.

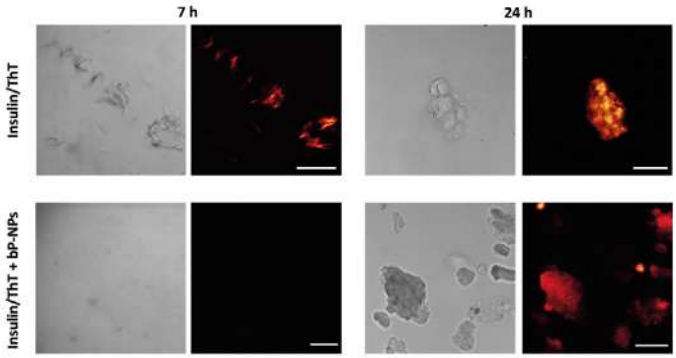

Contact persons
Antonella Sgarbossa (antonella.sgarbossa@nano.cnr.it)

References
[1] Cyrene-and water-based exfoliation of black phosphorus for potential nanolayer-mediated disaggregation of insulin fibrils. C. Caponio, A. Costanzo, S. Coiai, F. Cicogna, E. Pitzalis, S. Borsacchi, G. Lorenzetti, E. Bramanti, A. Papalini, A. Battisti, A. Sgarbossa, and E. Passaglia. FlatChem 45, 100665 (2024). [OA]
[2] Natural Biomolecules and Light: Antimicrobial Photodynamic Strategies in the Fight Against Antibiotic Resistance. G. Amendola, M. Di Luca, and A. Sgarbossa. Int. J. Mol. Sci. 26, 7993 (2025). [OA]

Projects
Next Generation EU PNRR, PE13 INF-ACT, project nr. PE00000007.

Nanoscale engagement of programmed death ligand 1 (PD-L1) in membrane lipid raft domains of cancer cells

Several tumors have evolved the ability to evade the immune system by expressing programmed death ligand 1 (PD-L1) on the membrane of neoplastic cells. The molecular organization of PD-L1 on the membrane is still rather obscure. Here, we investigated the plasma membrane organization of PD-L1 by a multiscale fluorescence imaging toolbox reaching the nanoscale by super-resolution microscopy. The significant colocalization of PD-L1 with lipid raft markers supports a raft-driven organization of PD-L1, which may follow its extended palmitoylation upon expression. This pattern was also demonstrated in living cells. These results may afford novel targets for improved immuno-oncology strategies.

In recent years, PD-L1 has become a major therapeutic target in oncology due to its role as a cellular checkpoint enabling immune escape in multiple cancers. Despite this relevance, its membrane organization remains unclear.

Exploiting the high basal expression of PD-L1 in the HCC827 NSCLC cell line, we investigated its membrane arrangement [1] using a multiscale fluorescence microscopy toolbox previously applied in other contexts [Comput Struct Biotechnol J 19, 6140–6156 (2021)]. Following the hierarchical framework proposed by Kusumi, we examined the mesoscale (100–300 nm) and nanoscale (<100 nm) organization of PD-L1 using SMLM (TIRF-dSTORM) and SPLIT-STED [1]. SPLIT-STED revealed a clear clustered distribution of membrane PD-L1 (Fig. 1a, b). After single-cluster identification (Fig. 1e, f), we quantified cluster density (ρc) and nearest-neighbour distance (NNd).dSTORM, which exploits stochastic fluorophore activation to achieve nanometric spatial resolution (Fig. 1c), produced DDC-corrected maps (Fig. 1d) with a density of 101 ± 8 localizations/μm^2. We observed that PD-L1 forms clusters confined within ~25 nm corrals, assembling into an irregular mesoscopic lattice with an average interdomain spacing of ~180 nm. This architecture likely reflects synergistic effects of raft confinement driven by post-translational palmitoylation and homotypic PD-L1 interactions. Although fixed cells allow higher-resolution imaging, we extended the analysis to living cells using line-scan FCS with PD-L1-EGFP.

For colocalization, GPI and Cav-1 were transiently expressed as EGFP fusion proteins. The strong colocalization of PD-L1 with lipid raft markers, together with similar raft-confined diffusion behaviour, supports a raft-driven organizational model potentially linked to extensive palmitoylation. Pearson's coefficient R quantitatively confirmed these associations. These findings were integrated into the molecular model of membrane PD-L1 organization shown in Fig. 2 and may help guide future immuno-oncology strategies.

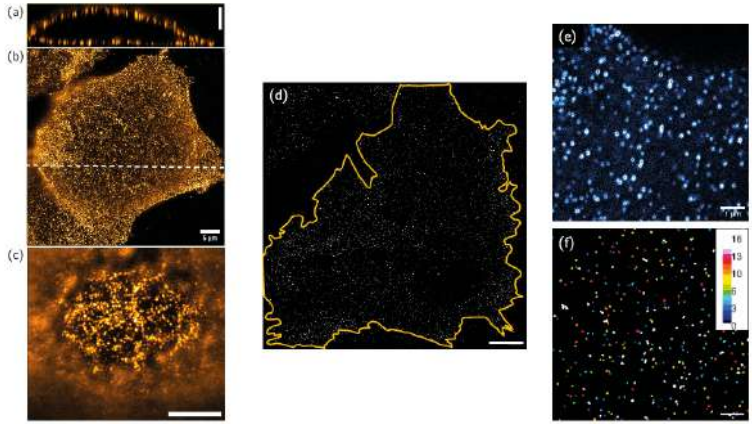

Fig. 1
Super-resolution imaging of plasma membrane PD-L1. (a – c) SPLIT-STED microscopy image of a representative cell indirectly immunostained by the antibody couple αPD-L1/αr647; (a) orthogonal (xz) view; (b) basal (xy) view: the dashed line represents the position of the xz sectioning plane visualized in (a). (c) apical (xy) view. (d) Gaussian rendering of TIRF-d-STORM map of a representative basal membrane immunostained by the Alexa647-conjugated αPD-L1-647 primary antibody. (e) SPLIT-STED zoom highlighting single PD-L1 clusters, marked with a small red cross, in a 10 µm ×10 µm representative basal membrane region. (f) Quantitative clustering map of a 10 µm ×10 µm representative basal membrane region according to Getis and Franklin's local point pattern analysis of a dSTORM map; the pseudo-colour scale refers to the number of emitters enclosed in each cluster. Scale bar (a–c): 5 µm, (d): 2 µm, (e, f): 1 µm.

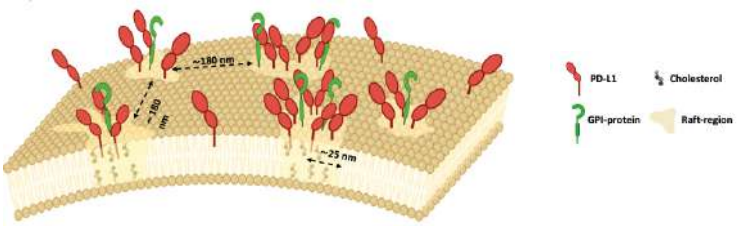

Fig. 2
Model of PD-L1 organization in the plasma membrane of the cell. PD-L1 is engaged in raft regions of 25 nm radius, marked by GPI proteins, and organized in a mesoscale “lattice” with 180 nm intercluster distance. Raft-engaged PD-L1 undergoes restricted diffusion, whereas non-raft PD-L1 is almost free to diffuse in the 2D membrane bilayer

Contact persons
Barbara Storti (barbara.storti@nano.cnr.it)
Ranieri Bizzarri (ranieri.bizzarri@unipi.it)

References
[1] Nanoscale engagement of programmed death ligand 1 (PD-L1) in membrane lipid raft domains of cancer cells. S. Civita et al. The FEBS Journal 292, 5979-5997 (2025).

Soft biocompatible nano/micro-structured scaffolds for nerve regeneration applications

Peripheral nerve injuries are a significant clinical issue, often resulting in incomplete functional recovery due to the limitations of current treatments. Biomaterial-based scaffolds that mimic the mechanical and topographical features of native nerve tissues represent a promising strategy to support nerve regeneration. We developed glycerol-blended chitosan scaffolds, nano/micro-structured with directional cues and with a nerve-mechanically compliant stiffness, with the aim to improve glial and neuronal cell growth for peripheral nerve repair applications.

We developed membranes made of biocompatible chitosan and glycerol, by solvent casting, and micro-patterned them with directional geometries having different levels of axial symmetry (Fig. 1a). These glycerol (10%)-blended chitosan membranes (Gly-Chi M) were optimized in terms of topography (groove width ≈ 4 μm) and mechanical properties, thus presenting a nerve physiological-grade Young's modulus (≈ 0.7 MPa) [1]. In parallel, we developed aligned glycerol plasticized chitosan nanofibers (Gly–Chi NFs) by electrospinning, thus obtaining continuous Gly (2%)-Chi NFs with a diameter of 184 ± 6 nm and a high level of anisotropy [2]. These Gly-Chi scaffolds were tested in vitro as first with Schwann cells (SCs), the glial cells with a primary role in the nerve regeneration process. Gly-Chi scaffolds were biocompatible, and effective in directing SC polarization; Gly-Chi M resulted highly performant in boosting collective cell migration [1, 2].

We investigated the regenerative potential of Gly-Chi microstructured membranes with in vitro models with increasing biological complexity [3]. These soft directional membranes promoted invasion, polarization, and alignment of primary SCs (Fig. 1b), and further promoted neurite outgrowth and directional guidance of human iPSC-derived sensory neurons when co-cultured on SCs (Fig. 1c). Moreover, tests with rat dorsal root ganglia *ex vivo* explants confirmed the ability of these scaffolds to orient axonal extension (Fig. 1d). We finally tested our Gly-Chi M *in vivo*, in a rat iatrogenic nerve damage model of the periprostatic neurovascular bundles [4]. Gly-Chi M promoted nerve fiber regeneration *in vivo* (Fig. 1e) in a nerve lesion model that resembles the damage occurring in men after radical prostatectomy, a clinical issue involved in prostate cancer. Overall, our findings demonstrate that glycerol-blended chitosan scaffolds with a nerve-mechanically compliant stiffness, and micro-structured with directional cues effectively support both glial and neuronal organization and represent a robust biomimetic platform for peripheral nerve repair.

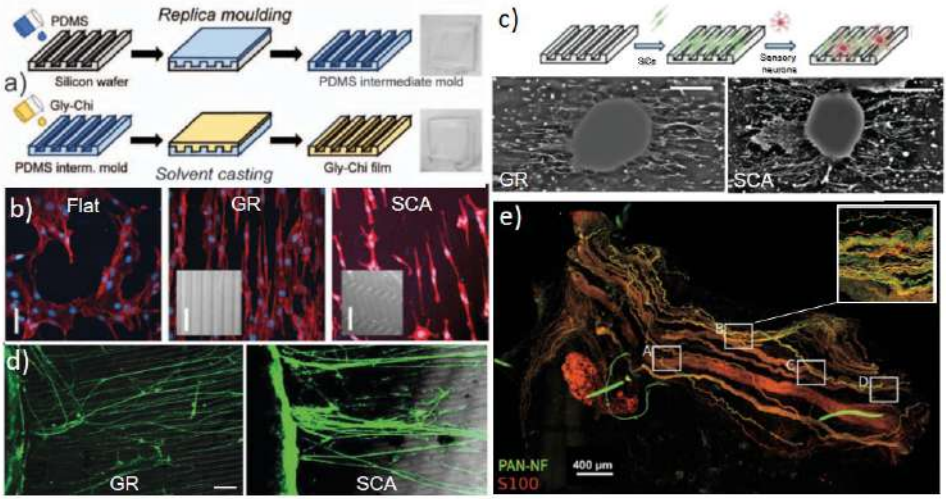

Fig. 1
a) Gly-Chi microstructured membranes fabrication process with two molds, by solvent casting. b) Confocal images of RT4-SCs cultured on FLAT, gratings- (GR) and scalene triangles- (SCA) micropatterned Gly-Chi membranes: nuclei (*blue*), actin fibres (*red*), patterns' bright field inserts; scale bars= 20 µm. c) Nerve-in-vitro model: confocal images of sensory neurons (*immunostained for* β*III-tubulin*) cultured with primary SC on Gly-Chi membranes, after 7 days of culture; scale bar = 500 µm. d) Representative images of ex vivo rat DRG explant cultures (*immunostained for* β*III-tubulin*) on GR and SCA M; scale bar = 100 µm. e) Gly-Chi membrane fully colonized by regenerated nerve fibres in vivo: immunolabeling of regenerating fibres using PAN neurofilament marker for axonal staining (*green*) and S100β marker for glial cells (*red*).

Contact persons
Ilaria Tonazzini (ilaria.tonazzini@cnr.it)
Marco Cecchini (marco-cecchini@cnr.it)

References
[1] Glycerol-blended chitosan membranes with directional micro-grooves and reduced stiffness improve Schwann cell wound healing. L. Scaccini et al. Biomed. Mater. 19, 065005 (2024). [OA]
[2] Chitosan-glycerol blended nanofibers for peripheral nerve regeneration applications. L. Scaccini et al. Nanoscale Advances 7, 6132 (2025). [OA]
[3] Soft Scaffolds for Nerve Repair: Investigating Glycerol-Plasticized Chitosan Microstructures with In Vitro Complex Models. L. Scaccini et al. J Biomed Mat Res - Part B Applied Biomaterials 113, e35660 (2025). [OA]
[4] Exploring the potential of chitosan-blended membranes for nerve regeneration post-radical prostatectomy: a novel rat model for studying bilateral cavernous nerve damage in vivo. F. Fregnan et al. Minerva Urology and Nephrology 77, 91 (2025). [OA]

Projects
MUR PRIN 2022, ENGInerve, project nr. 2022ZH5M72.

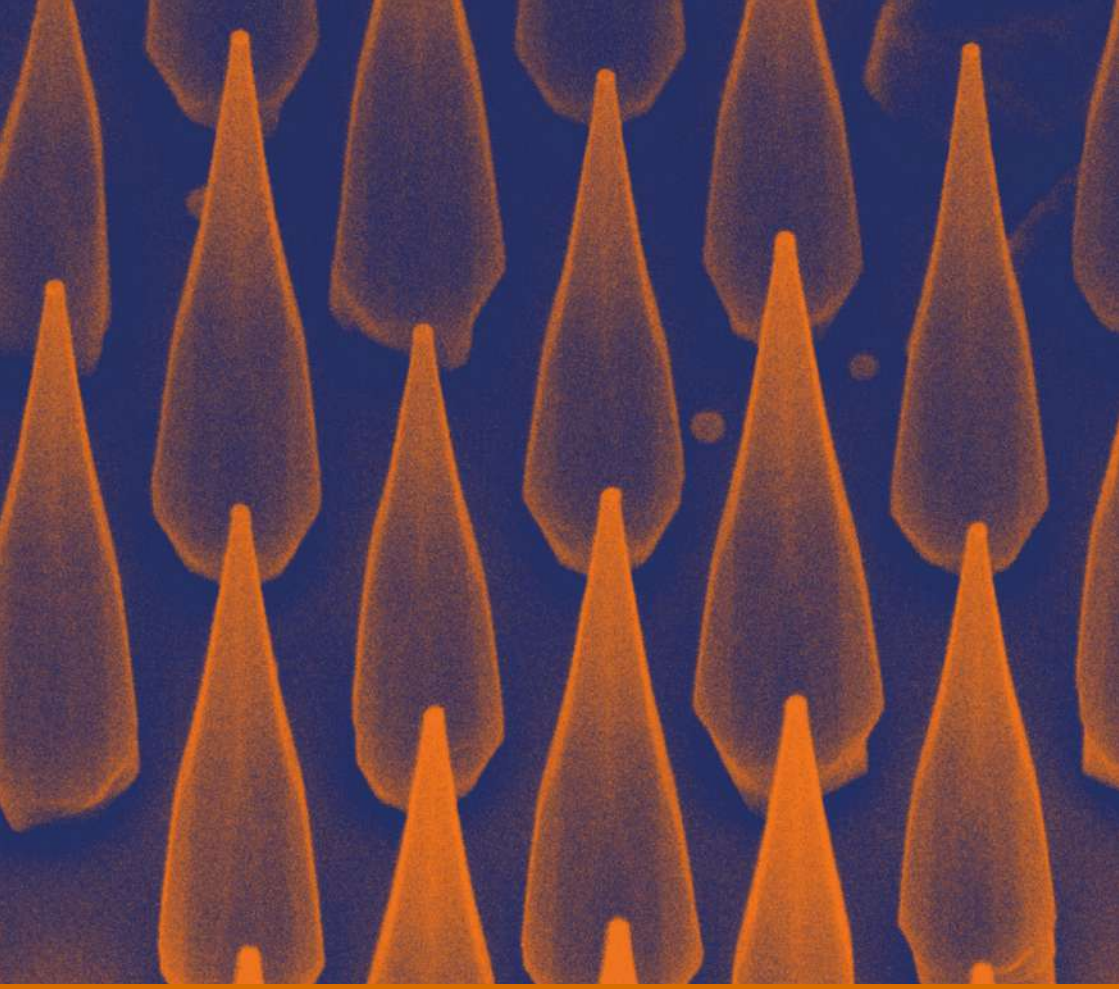

Highlights
-
Physics and technology of light at the nanoscale

Light plays a central role in modern technology. Beyond vision, it enables global communication through lasers and optical fibers, high-resolution imaging in microscopes, and the exploitation of photons' quantum properties. In all these applications, precise control of light-matter interactions at the nanoscale is crucial. When materials are structured as atom-thick layers, nanowires, or 3D composites, light behaves in unusual ways that can be harnessed for advanced technological applications. Cnr Nano is actively engaged in a wide range of research exploring and developing innovative applications of light at the nanoscale.

A wide gamut of materials. Researchers at Cnr Nano explored a broad variety of base substances upon which novel nanosystems have been created. They involve both organic and inorganic chemistry, as well as specialized physical techniques for their ad-hoc nanostructuration. Investigations involved 3d-printed polymers embedding molecules with reconfigurable chemical structures, 2d materials such as bismuth selenide and graphene, hybrid thin films including transparent oxides and ferroelectrics, phase change alloys, and epitaxially grown, zero-dimensional quantum dots.

From structure to functionality. Our studies, while retaining a fundamental character, are always oriented towards innovations with a technological role. For instance, we devised light emitters operating at various wavelengths, from the near-infrared (telecom window) to the far-infrared (Terahertz), covering needs such as quantum telecommunication and vibrational spectroscopy. In parallel, we studied systems capable of optical computation, or of scanning a beam such as in a LIDAR. Moreover, we analyzed epsilon-near-zero low-voltage optical switches, and Terahertz detectors with record performance.

Knowledge from collaboration. Multidisciplinarity underpins most of the work performed at Cnr Nano. As first, we practice an intense internal knowledge sharing aimed at overcoming the traditional barriers between individual disciplines such as physics, chemistry, optical and telecommunication engineering. We rely on an advanced set of laboratories including visible, near-infrared and far-infrared spectroscopy; polymer synthesis, printing and molding; semiconductor, metal and oxide growth; and cleanroom-based nanostructuration. All this is sided by advanced electromagentic and structural simulation tools. Additionally, we are always open to external, often international collaborations, to pursue cutting-edge results as witnessed by the high-level of publication venues.

Addressing today's global challenges. While pursuing scientific and technological innovation, we always look for how these will impact our future world at a large scale. For instance, Terahertz-enabled vibrational spectroscopy could enable more precise hydrocarbon detection, and ultimately to monitor the presence of pollutants before the onset of dangerous physiological effects. Another example involves optical computers, where the information is processed at the speed of light without the need for energy-consumptive conversions between the electronic and optical domain, ultimately decreasing the carbon footprint of technologies like neural networks.

[OA] *in the References indicates an Open Access publication.*

Active modulation of the optical response of transparent conducting oxide films in the near infrared range

We have exploited well-controlled Al:ZnO films to actively tune the optical response of the film in the near-infrared range by means of an applied external voltage. A hybrid transparent conductive oxide/electro-optic stack has been realized in form of a microcapacitor by means of electron beam lithography to observe a field effect at room temperature and low voltage. We have thus investigated the optical response by means of spectroscopic ellipsometry. In parallel, the quality of the film has been investigated by means of positron annihilation spectroscopy to clarify the presence of defects complexes that can play a role in the film properties and optical/electrical response.

Transparent conductive oxides (TCOs) can adjust the free carrier concentration through the doping level and allow epsilon-near-zero condition to be tuned in the near-infrared telecommunication window. A great challenge is the control by external stimuli of TCO optoelectronic properties, which would pave the way for intriguing applications in photonic devices.

We have demonstrated room-temperature, low-voltage optical modulation in Al-doped ZnO (AZO) / $BaTiO_3$ (BTO) / Nb-doped $SrTiO_3$(110) (NSTO) multilayers by applying a bias to the TCO within a metal–oxide–semiconductor structure, inducing charge accumulation/depletion at the dielectric interface and enhancing modulation through the high-κ BTO capacitance. The multilayer has been fabricated in a plane capacitor configuration of about 100 μm lateral size by electron beam lithography (EBL). By means of spectroscopic ellipsometry we have detected a sizable variation of the optical response at an applied bias of +0.2 V at room temperature that we have ascribed to the combined effect of exponentially graded charge accumulation/depletion at the AZO/BTO and BTO/NSTO interfaces, accompanied by the Pockels effect in the BTO layer. To consider the variety of the physical effects, we have developed a complex optical model for each layer involved. We have succeeded in introducing the main bias-induced mechanisms that lie underneath the field-effect-induced variation of the refractive index in the near-infrared range up to value of more than 0.1 [1]. This study has been combined with a deep characterization of the TCO films from an electrical, morphological, and structural point of view to precisely control the optical response. Positron Annihilation Spectroscopy measurements have been coupled with other techniques (TEM, XRD, Hall) to determine the dominant defects, proved to be the VO coordinated with 2-3 V_{Zn} in the AZO films, with concentration increasing with increasing disorder [2].

These studies provide important clues to model and understand in detail the behaviour and the working mechanisms of optically active systems, with relevant applications in the field of active photonics.

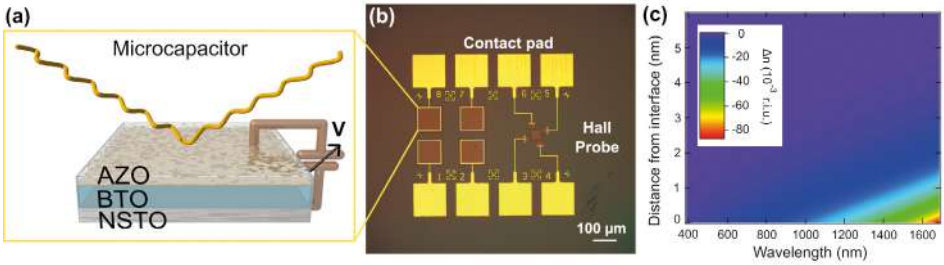

Fig. 1
(a) Sketch of the spectroscopic ellipsometry measurement configuration and (b) view under the optical microscope of the Al:ZnO/$BaTiO_3$/Nb:$SrTiO_3$ microcapacitors fabricated via EBL. (c) Variation of the refractive index Δn as a function of wavelength and distance from the Al:ZnO/$BaTiO_3$ interface. Δn is derived through the Drude-Lorentz model assuming the charge accumulation profile obtained by ellipsometry modeling. The strongest variation is evident at 1700 nm with a negative variation of about 0.1 with a charge unbalance at the interface of 0.2×10^{20} cm^{-3} at +0.2 V.

Contact persons
Stefania Benedetti (stefania.benedetti@nano.cnr.it)
Alessandro di Bona (alessandro.dibona@nano.cnr.it)

References
[1] Active optical modulation in hybrid transparent conductive oxide/electro-optic multilayers. R. Magrin Maffei, M. Magnozzi, M. Sygletou, S. Colace, S. D'Addato, A. Y. Petrov, M. Canepa, P. Torelli, A. di Bona, S. Benedetti, and F. Bisio. J. Mater. Chem. C 13, 6346 (2025). [OA]
[2] Defectivity of Al:ZnO Thin Films with Different Crystalline Order Probed by Positron Annihilation Spectroscopy. R. Magrin Maffei, M. Butterling, M. O. Liedke, S. D'Addato, A. di Bona, G. Bertoni, G. C. Gazzadi, S. Mariazzi, A. Wagner, R. S. Brusa, and S. Benedetti. Appl. Surf. Sci 665, 160240 (2024). [OA]

Projects
MUR PRIN 2022, AMONIX, project nr. 2022BTMXZT.
MUR PRIN 2022, ERACLITO, project nr. 2022ZMA4X3.

Light-responsive materials for controlled energy transfer and all-optical processing

We investigate stimuli-responsive photonic structures enabling dynamic control of light–matter interactions. Using photochromic molecules embedded in a multilayer Fabry-Perot microcavity and by modulating light-matter coupling through UV/visible irradiation, we achieve optical control over polariton-mediated energy transfer. Additionally, we develop 3D-printed optical components based on photochromic molecules embedded in UV-curable pre-polymers and patterned by digital light processing. The printed components are used for all-optical processing and logic operations.

Reversible and dynamic modulation of photonic device properties is demonstrated by integrating photochromic molecules into a multilayer Fabry-Perot microcavity [1]. The cavity incorporates two spatially-separated photoactive layers between silver mirrors (Fig. 1a), enabling controlled tuning of light–matter interactions. The donor layer, based on spiropyran (SP) dispersed in poly(methyl methacrylate) (PMMA), is almost transparent in the visible range (Fig. 1b). Upon UV irradiation, SP is converted into merocyanine (MC), while green light restores the initial state, allowing full reversible control over the active molecular concentration. This optical switching provides direct modulation of the light–matter coupling constant within the cavity. Consequently, polariton formation can be dynamically adjusted (Fig. 1c, d), enabling controlled energy transfer to a physically separated acceptor layer (BRK). Photoluminescence measurements reveal a sixfold enhancement in energy-transfer efficiency when the photoactive multilayer is placed inside the cavity compared to outside [1], demonstrating the strong influence of the cavity environment on excitonic interactions. SP photoisomerization also enables the optical control of the optomechanical coupling in a cavity [2].

In parallel, we fabricate reconfigurable optical components using 3D-printable photochromic polymers processed via digital light processing [3]. The printable materials consist of bisphenol A ethoxylate dimethacrylate (BEDMA) doped with either SP or 1,2-bis(2-methyl-1-benzothiophene-3-yl) perfluorocyclopentene (BTF6). Upon UV exposure, the SP- and BTF6-containing printed objects undergo their characteristic transitions to MC and c-BTF6 (Fig. 1e), respectively, producing vivid coloration throughout the 3D objects (Fig. 1f). These changes are fully reversible under visible-light irradiation, enabling repeated optical cycling without structural degradation. The printed structures display tunable light absorption and coloration under alternating UV and visible illumination, showing their suitability for all-optical processing and logic operations [3].

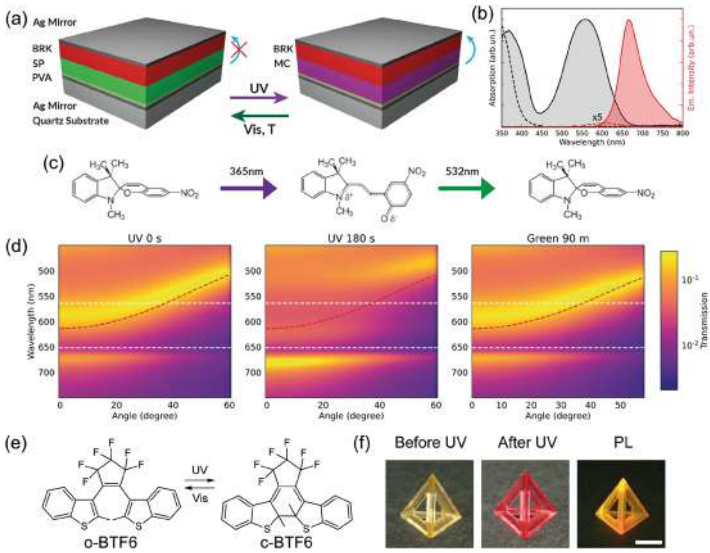

Fig. 1

(a) Schematics of the cavity before and after photochromic donor conversion. (b) Absorption spectrum of a PMMA film with SP (black dashed lines) and MC (black continuous line). Emission spectra of the SP (×5 intensity, red dashed line) and MC form (red continuous line). (c, d) Angle-resolved transmission spectra upon UV and green light exposures. The photochromic conversion from SP to MC and back to SP is also schematically displayed (c). In each colourmap, the bare cavity mode (red dashed line), the MC excitonic transition (upper white dashed line) and the BRK excitonic transition (lower white dashed line) are reported. Reproduced under the terms of the Creative Commons Attribution License from [1]. © 2024 The Authors. Published by De Gruyter. (e) Molecular structures of the BTF6 molecules in open (o-BTF6) and closed (c-BTF6) forms, respectively. (f) Photographs of 3D-printed pyramids with BTF6 upon ambient illumination before (left images) and after (middle images) the UV exposure. Right image: emission of the printed pyramids upon 365 nm excitation. Scale bar: 1 cm. Reproduced under the terms of the Creative Commons Attribution License from [3]. © 2025 The Authors. Published by Springer-Nature.

Contact persons
Luana Persano (luana.persano@nano.cnr.it)
Andrea Camposeo (andrea.camposeo@cnr.it)

References

[1] Active control of polariton-enabled long-range energy transfer. A. Cargioli et al. Nanophotonics 13, 2541-2551 (2024). [OA]
[2] Photochromic Molecules Enable Optical Control of Optomechanical Coupling in a Cavity. M. Cagnetti et al. Adv. Optical Mater. 13, 2402883 (2025). [OA]
[3] All-optical processors by 3D printable photochromic materials. F. D'Elia et al. Sci. Appl. 14, 375 (2025). [OA]

Projects

Next Generation EU PNRR, MICS, project nr. PE00000004.

Terahertz harmonic generation in micro-lasers intracavity-integrated with 2D materials plasmonic gratings

We devise innovative technological approaches in multilayer graphene or in large area topological insulator metametarials and heterostructures, to devise high-efficient non-linear micro-emitters, optically pumped by high power (2W) quantum cascade lasers (QCL) and electrically-driven integrated plasmonic lasers comprising QCL heterostructures. Our findings highlight a novel versatile pathway for monolithic, electronically-tunable coherent light emitters operating across the lacking 6-12 THz frequency band, so far inaccessible in a solid-state laser technology, and pave the way for applications in integrated photonics and on-chip frequency conversion.

Optical nonlinearity in the terahertz (THz) range represents a key technology to access high frequency spectral windows that are usually difficult to cover using conventional solid state laser technologies. Over the past decade, the non-linear optical properties of graphene have been extensively investigated, and a wide range of related applications demonstrated, ranging from optical modulators to saturable absorbers [1].

High harmonic generation (HHG) – the frequency up-conversion of an optical signal – in materials systems is governed by symmetries. This effect has been exploited in graphene, where HHG has been demonstrated, albeit only at odd multiples of the driving frequency owing to its inherent centro-symmetry. In topological insulators (TIs), unconventional HHG has been predicted, supported by the bulk and topological surface states, which are usually difficult to distinguish, relying on the ultrafast intraband dynamics, and the inversion symmetry-breaking even-order nonlinearity in the topological phase. Here, we exploit innovative technological approaches in multilayer graphene [2, 3] or in large area topological insulator metametarials [4] and heterostructures to devise high efficient non-linear micro-devices, optically pumped by quantum cascade lasers (QCLs) delivering 2W optical power, and electrically-driven integrated plasmonic lasers comprising integrated QCL heterostructures, targeting HHG in the technologically relevant Reststrahlen gap (6-12 THz) at both odd and even orders, via symmetry breaking.

We also excite plasmons confined in a multilayer graphene micro-ribbon grating within a distributed feedback terahertz quantum cascade laser that incorporates a top supercapacitor to tune the graphene Fermi energy, demonstrating third harmonic generation. Our monolithic, electrically-driven laser works in the inaccessible Reststrahlenband of its core III-V semiconductor heterostructure and shows a peak power of ~9 μW, laying the foundation of a new generation of plasmonic, non-linear light emitting sources [2].

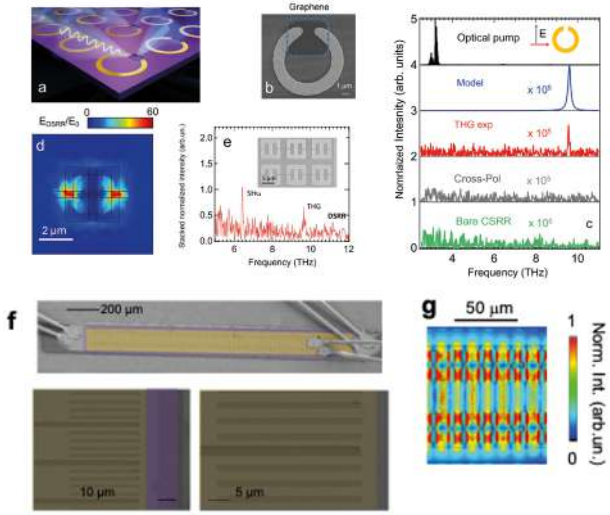

Fig. 1
(a) Schematic device concept. (b) False colour scanning electron micrograph (SEM) image of the circular split ring resonator with graphene integrated in the gap. (c) From top to bottom; black line: normalized emission spectra of THz QCL; blue line: THG efficiency; red, grey lines: emission spectrum measured on the optically pumped SLG-CSRR, after filtering the QCL pump with the Ta-filter, with the SRR array oriented parallel (red) and perpendicular (gray) to the polarization axis of the QCL; green line: emission from the optically pumped bare CSRR array sample with the SRR array oriented parallel to the polarization axis of the QCL. (d) 2D map of the simulated electric field amplification of a double SRR embedding the BiSe/InBiSe TI heterostructures. (e) Emission spectrum measured on the optically pumped SLG-CSRR. Inset: SEM image of the DSSR array. (f) SEM of a prototypical integrated QCL. (g) Electric field distribution of the graphene-integrated QCL cavity.

Contact persons
Alessandra Di Gaspare (alessandra.digaspare@nano.cnr.it)
Miriam Serena Vitiello (miriam.vitiello@nano.cnr.it)

References
[1] All in one-chip, electrolyte-gated graphene amplitude modulator, saturable absorber mirror and metrological frequency-tuner in the 2-5 THz range. A. Di Gaspare et al. Adv. Optical Mater. 10, 2200819 (2024). [OA]
[2] Electrically-driven heterostructured wire lasers with integrated graphene plasmons. A. Di Gaspare et al. Nature Nanotechnology 20, 1611–1617 (2025). [OA]
[3] Compact terahertz harmonic generation in the Reststrahlenband using a graphene-embedded metallic split ring resonator array. A. Di Gaspare et al. Nature Communications 15, 2312 (2024). [OA]
[4] Second and third harmonic generation in topological insulator-based van der Waals metamaterials. A. Di Gaspare et al. Light Sci Appl 14, 337 (2025). [OA]

Projects
H2020-FETOPEN-2018-2020, Extreme-IR, project nr. 964735.
Next Generation EU PNRR, PE4 NQSTI, SPOKE 4 PE0000023.

Tunable light emission from nanowire quantum dots

Semiconductor quantum dots (QDs) have emerged over the past decade as a pivotal solid-state platform for quantum light sources, fundamental for a wide range of quantum technology applications. Among the different geometries explored so far, QDs embedded in nanowires (NW-QDs) stand out as a promising one, offering a high degree of freedom in combining different materials, and a precise control over QD size, composition, and density. We address these challenges through the investigation of zincblende $InAs_xP_{1-x}$/InP NW-QDs and of wurtzite $GaAs_xP_{1-x}$/GaP NW-QDs. Tunable light emission from the two NW-QD systems was measured in a broad range of wavelengths up to the telecommunication bands.

Semiconductor quantum dots (QDs) are an interesting platform with possible applications in quantum information technologies based on optics, because they can be used to realize single-photon sources (SPSs). We have realized $InAs_xP_{1-x}$ QDs embedded in InP nanowires (NWs) for emission at telecom wavelengths [1]. We demonstrate the growth of pure zincblende $InAs_xP_{1-x}$ QDs in InP NWs, by employing Au-assisted vapor liquid solid growth in a chemical beam epitaxy system. We studied the growth mechanism of InP/$InAs_xP_{1-x}$ heterostructures with different compositions to control the straight growth along the ⟨100⟩ direction and to tune the emission wavelength. We successfully obtained the growth of $InAs_xP_{1-x}$ QDs with a composition in the range of x = 0.24–1.00 (Fig. 1a-b). By means of microphotoluminescence (m-PL) measurements, we demonstrate the tunability of the emission, depending on the $InAs_xP_{1-x}$ QD composition and size, remarkably observing an emission at the telecom O-band for a 10 nm thick QD with 80% of As content (Fig. 1c). Furthermore, enhanced photon extraction through optimized waveguide geometry for zincblende $InAs_xP_{1-x}$/InP NW-QDs was demonstrated.

Moreover, we have investigated an understudied material system suitable for the realization of tunable QD emission within the visible-to-near-infrared spectrum [2]. Specifically, crystal pure wurtzite GaP NWs are synthesized incorporating single $GaAs_xP_{1-x}$ QDs of various compositions (Fig. 2a, b). A great degree of control over the shape and composition of the ternary alloy QD is achieved, enabling a well-defined confinement and the tunability of the emission wavelength. This is confirmed by low temperature m-PL investigation showing that the NW emission is dominated by a narrow peak whose energy shifts according to the As content of the QD: from ~650 nm (As = 70%) to ~720 nm (As = 90%) (Fig. 2c). Our findings underscore the potential for these QDs in NWs with tailored compositions to achieve the desired light emission characteristics, thereby advancing applications in quantum optics and nanophotonics.

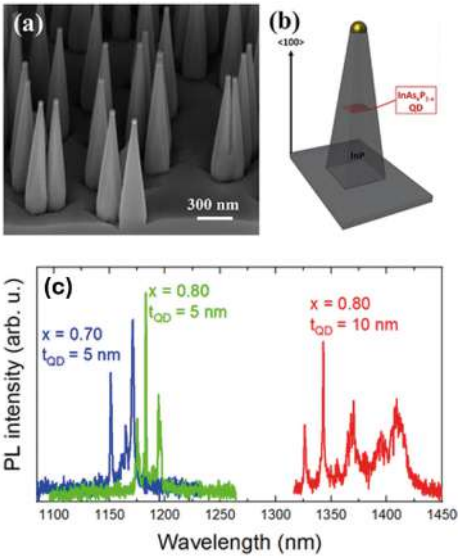

Fig. 1
Zincblende $InAs_xP_{1-x}$/InP NW-QDs. (a) SEM image of 10 nm thick $InAs_{0.88}P_{0.12}$ NWQDs. (b) Schematics of the geometry of the NW-QD. (e) μ-PL spectra at 4 K of single-QD NWs with As content of x = 0.70 and 5 nm thickness (blue), x = 0.80 and 5 nm thickness (green), and x = 0.80 and 10 nm thickness (red).

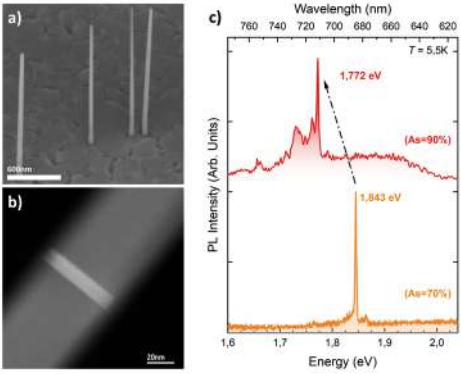

Fig. 2
Wurtzite $GaAs_xP_{1-x}$/GaP NW-QDs. (a) SEM image of the As-grown sample, (b) STEM image of a representative NWs portion embedding the QD (bright contrast). (c) Low-T m-PL spectra of two NW QDs with 90% (top) and 70% (bottom) of As content.

Contact persons
Lucia Sorba (lucia.sorba@nano.cnr.it)
Valentina Zannier (valentina.zannier@nano.cnr.it)

References
[1] Zincblende InAsxP1-x/InP Quantum Dot Nanowires for Telecom Wavelength Emission. G. Bucci, V. Zannier, F. Rossi, A. Musiał, J. Boniecki, G. Sęk, and L. Sorba. ACS Applied Materials and Interfaces 16, 26491–26499 (2024). [OA]
[2] Tunable GaAsxP1-x Quantum-Dot Emission in Wurtzite GaP Nanowires. R. A. Sorodoc, P. De Vincenzi, A. S. Sharma, G. Bucci, M. Roggi, E. Mugnaioli, L. Sorba, M. De Luca, and V. Zannier. ACS Applied Materials and Interfaces 16, 65222–65232 (2024). [OA]

Projects
Horizon Europe EIC Pathfinder, QCEED, project nr. 101185617.
Next Generation EU PNRR, PE4 NQSTI, project nr. PE0000023.
MUR PRIN 2022, GROUNDS, project nr. 20223WZ245.

Scalable technologies for quantum sensitive and large area graphene photodetectors on integrated optical platforms, for optical and quantum communications

We demonstrate scalable graphene-based THz photodetectors combining high sensitivity, fast response, and broad dynamic range. We leverage the scalability of graphene to explore its transformative potential for next-generation THz technologies, including imaging, integrated photonics, and free-space communication. Antenna-coupled multilayer and large-area CVD graphene devices, together with engineered Salisbury-screen p–n architectures, provide robust, room-temperature operation in a fully frequency-scalable platform. These detectors enable advanced THz sensing, hyperspectral imaging, and reliable free-space data transmission, highlighting graphene's promise for future THz systems.

Sensitive photodetectors showing large quantum efficiencies and broad dynamic ranges are essential components for on-chip integrated photonic quantum platforms and for probing quantum correlations in metrological sources. However, at terahertz (THz) frequencies, this is a very challenging task owing to the lack of high-absorption materials and thermal effects that impact their noise figure. We present a comprehensive study of scalable graphene-based photodetectors operating in the THz domain, targeting applications in integrated photonics, quantum technologies, and broadband sensing.

We first demonstrate antenna-coupled tunnel field-effect transistors based on multilayer graphene/hBN/bilayer graphene/hBN heterostructures, enabling multi-wavelength detection around 3 THz [1]. These devices achieve record performance, with noise equivalent power (NEP) values on the order of 10^{-12} W $Hz^{-1/2}$, nW-level minimum detectable power, and a dynamic range exceeding five orders of magnitude (Fig. 1a, b). The architecture is intrinsically frequency-scalable and suitable for probing quantum intensity correlations in nonclassical THz sources.

We then report THz photoreceivers based on large-area CVD-grown hBN/SLG/hBN stacks [2], fabricated through an industrially compatible process (Fig. 1c). Integrated with on-chip antennas, RF circuitry, and coplanar strip lines, these photo-thermoelectric detectors exhibit nanosecond response time, room-temperature responsivity of ~4 V/W, and NEP ≈4 nW $Hz^{-1/2}$ at 2.86 THz, providing a path toward multiplexed hyperspectral THz cameras and high-frequency communication links.

Finally, leveraging the same scalable graphene platform, we implement an antenna-integrated graphene Salisbury-screen p–n junction detector with optimized electromagnetic coupling (Fig. 1d). This device achieves NEP <300 pW $Hz^{-1/2}$, response time <5 ns, and a dynamic range larger than four orders of magnitude [3], reaching

the performance of exfoliated-graphene detectors (Fig. 1e) and approaching that of CMOS and micro-bolometer technologies [2, 4]. Finally, we show that SLG-based photodetectors achieve state-of-the-art performance and can be used for free-space optical communications at THz frequencies, enabling 1 Mbaud error-free data transmission [5].

Fig. 1

(a) False colour SEM image of a tunnel-field effect transistor (TFET) based on bilayer graphene. (b) Voltage responsivity (Rv) map measured as a function of the bottom and top gates of the TFET. A six-fold pattern appears, indicating a thermoelectric contribution to the photodetection. (c) AFM image of the hBN/SLG/hBN heterostructure. The inset shows the thickness profile of the heterostructure. (d) Schematic view of the antenna-coupled graphene Salisbury screen (AgSS) architecture. (e) NEP at 2.86 THz as a function of residual carrier density (n_0) for various SLG-based material platforms, showing the correlation between detector's sensitivity and material quality.

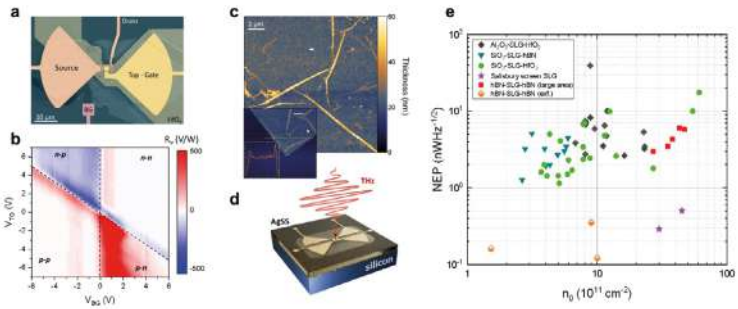

Contact persons

Leonardo Viti (leonardo.viti@nano.cnr.it)
Miriam Serena Vitiello (miriam.vitiello@nano.cnr.it)

References

[1] Quantum Sensitive, Record Dynamic Range Terahertz Tunnel Field-Effect Transistor Detectors Exploiting Multilayer Graphene/hBN/Bilayer Graphene/hBN Heterostructures. L. Viti et al. Nano Lett. 25, 6005-6012 (2025). [OA]

[2] Scalable Terahertz Room Temperature Photoreceivers Based on Large-Area Hexagonal Boron Nitride and Graphene Heterostructures. L. Viti et al. Adv. Opt. Mater. 13, 2402100 (2025). [OA]

[3] Efficient Large-Area Graphene p-n Junction Terahertz Receivers on an Integrated Optical Platform. L. Viti et al. Small Methods 9, 2500083 (2025). [OA]

[4] Engineering THz-frequency light generation, detection, and manipulation through graphene. M. S. Vitiello and L. Viti. Appl. Phys. Rev. 12, 011321 (2025). [OA]

[5] QCL-based, Cryogen-free THz Optical Wireless Communication Link. A. Sorgi et al. Laser & Photonics Reviews 19, 2301082 (2025). [OA]

Projects

Horizon Europe ERC POC, Terascan, project nr. 101157731.
Next Generation EU PNRR, PE14 RESTART, project nr. PE00000001.
Next Generation EU PNRR, PE4 NQSTI, project nr. PE00000023.
H2020-ERA-NET-QuantERA Call 2021, QATACOMB, project nr. 101017733.

Near-field quantum nanoscopy

We investigate tunable Dirac plasmon polaritons (DPPs) in topological-insulator and van der Waals metamaterials at THz frequencies. By engineering laterally coupled Bi_2Se_3 meta-elements, we tune the DPP wavevector and attenuation, achieving up to 20% momentum enhancement and >50% longer propagation. Phase-resolved near-field nanoscopy maps their dynamics in real space, while THz photocurrent imaging of hBN-encapsulated black phosphorus reveals anisotropic, deeply subwavelength polaritons tunable by gating, enabling advanced nano-optical and quantum technologies.

Collective oscillations of massless charge carriers in two-dimensional materials, known as Dirac plasmon polaritons (DPPs), offer powerful opportunities for designing nanophotonic devices with tunable optical responses [1-5]. However, controlling their dispersion at terahertz (THz) frequencies remains challenging because DPPs possess momenta far larger than free-space photons and suffer from significant attenuation.

We address this problem by revealing and tailoring DPP properties in topological-insulator (TI) metamaterials [1, 2]. Using epitaxial Bi_2Se_3, we engineer laterally coupled linear meta-elements with controlled spacing (Fig. 1a-d), enabling geometrical tuning of the DPP wavevector [1]. By launching DPPs and directly mapping their propagation with phase-resolved scattering-type near-field nanoscopy (Fig. 1a) from 2.0 to 4.6 THz, we show that reducing the coupling distance allows precise control of the polariton dispersion (Fig. 1d). In dimers and triplets with 1 µm spacing, the DPP momentum increases by up to 20%, accompanied by reduced losses and more than a 50% increase in attenuation length. These results provide design rules for future topological and quantum devices exploiting directional polariton transport.

We further extend our approach to time-domain near-field imaging, using field-resolved detection of ultrashort scattered pulses to visualize surface-polaritons in graphene [4]. This method allows direct extraction of group and phase velocities, as well as damping, through a simple normalization and modelling procedure, enabling real-time mapping of propagating modes.

Finally, we detect THz phonon-polaritons in hBN-encapsulated black-phosphorus field-effect transistors using THz near-field photocurrent nanoscopy [6]. The technique reveals deeply subwavelength polaritons ($\lambda_p \approx \lambda_0/76$) with dispersion tunable via electrostatic gating (Fig. 1d, f). Owing to the anisotropic dielectric response of black phosphorus, polariton propagation differs along the armchair and zigzag axes, enabling directional, highly confined THz light control.

Together, these advances establish a versatile platform for tunable THz polaritonics and phase-sensitive near-field imaging, opening new perspectives for sensing, nonlinear optics, and quantum nanophotonics.

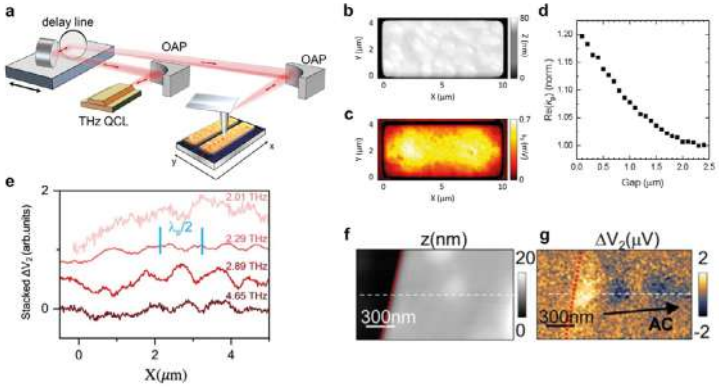

Fig. 1

(a) Schematic of the THz s-SNOM setup in detector-less configuration. The output THz radiation from the QCL is collimated by an off-axis parabolic (OAP) mirror. The optical path length is set by a delay line, while the metallic tip couples the THz field on the sample under test. (b, c) Topography and self-mixing signal (third harmonic –s_3) acquired on a rectangular Bi_2Se_3 resonator. s_3 oscillations indicate the presence of surface modes. (d) Simulated increase in plasmon polariton momentum as a function of the gap between two adjacent Bi_2Se_3 resonators. (e) Near-field photovoltage profiles in a black phosphorus p-n junction, as a function of the coordinate x, defined as the distance from the flake edge along the junction line. (f, g) Topography z (grey scale) and near-field photo-voltage ΔV_2 oscillations (colour scale) measured along the junction parallel to the armchair direction (black arrow).

Contact persons
Leonardo Viti (leonardo.viti@nano.cnr.it)
Miriam Serena Vitiello (miriam.vitiello@nano.cnr.it)

References

[1] Tracing terahertz plasmon polaritons with a tunable-by-design dispersion in topological insulator metaelements. L. Viti et al. Light: Science & Applications 14, 288 (2025). [OA]
[2] Holographic Nano-Imaging of Terahertz Dirac Plasmon Polaritons in Topological Insulator Antenna Resonators. V. Pistore et al. Small 20, 2308116 (2024). [OA]
[3] Terahertz Plasmon Polaritons in Large Area Bi2Se3 Topological Insulators. V. Pistore et al. Advanced Optical Materials 12, 2301673 (2024). [OA]
[4] Spacetime Imaging of Group and Phase Velocities of Terahertz Surface Plasmon Polaritons in Graphene. S. Anglhuber et al. Nano Letters 25, 2125-2132 (2025). [OA]
[5] Terahertz near-field microscopy of metallic circular split ring resonators with graphene in the gap. C. Schiattarella et al. Scientific Reports 14, 16227 (2025). [OA]
[6] Near-field detection of gate-tunable anisotropic plasmon polaritons in black phosphorus at terahertz frequencies. E. A. A. Pogna et al. Nature Communications 15, 2373 (2024). [OA]

Projects

Horizon Europe ERC POC, STAR, project nr. 101081567.
Next Generation EU PNRR, PE4 NQSTI, project nr. PE0000023.
Fondazione Internazionale Premio Balzan, Optoelectronics and nano-photonics in two-dimensional nanomaterial heterostructures.

Metasurface-based beam steering systems

Metasurfaces, that means arrangements of subwavelength scatterers, are powerful tools for shaping the flow of light at will within extremely compact footprints. A relevant application field is that of optical beam scanning, declined in terrestrial applications (e.g., automotive LIDARS), and flight- or space-based ones (e.g., satellite optical communication systems, drone-borne optical crop monitoring). Here, we report about our research on reconfigurable pixel arrays based on optically tunable optical scatterers, paving the way for efficient and polarization-independent nonmechanical beam steering.

Our research focuses on designing and optimizing tunable reflective metasurfaces for high-speed, dynamic beam steering at the optical telecom wavelength of 1550 nm. The core innovation lies in integrating GeSbTe (GST) as a phase-change material (PCM) into a multi-layered metal/PCM/metal pixel architecture (Fig. 1a).

This structure is engineered to achieve pure phase control while maintaining high reflectance and minimizing loss amplitude modulation. To this end, a tailored optimization algorithm utilizing Rigorous Coupled Wave Analysis (RCWA) was employed. The optimization maps (Fig. 1b) highlight the optimal geometric parameters that maximize reflectance in both states (R_A and R_C) while precisely achieving the target phase shift ($\Delta\phi=\pi$), confirming the feasibility of a low-loss, phase-only modulation pixel. This result addresses a critical limitation of previous dynamic metasurfaces, which often suffer from significant energy loss and crosstalk between amplitude and phase. The dynamic capability of the device is further highlighted by the fact that GST allows for intermediate crystallization states. By incorporating these intermediate states, the proposed beam steerer architecture achieves ternary modulation, which, as demonstrated by Finite Element Method (FEM) simulations of the far-field pattern, results in preferential beam redirection with significantly reduced sidelobes (Fig. 1c).

The precise mechanism of light deflection is visually confirmed by the electromagnetic field map (Fig. 1d). This performance is coupled with a key technological advantage: the submicrometric pixel size overcomes the limitations of conventional systems like LCOS-based Spatial Light Modulators (SLMs), ultimately allowing for a wider angular range for beam steering. Finally, the practical viability of the device was established through extensive technical analyses paving the way for realizing high-speed (up to 50 Hz frame rate), low-energy, and finely controllable optical beam steering devices.

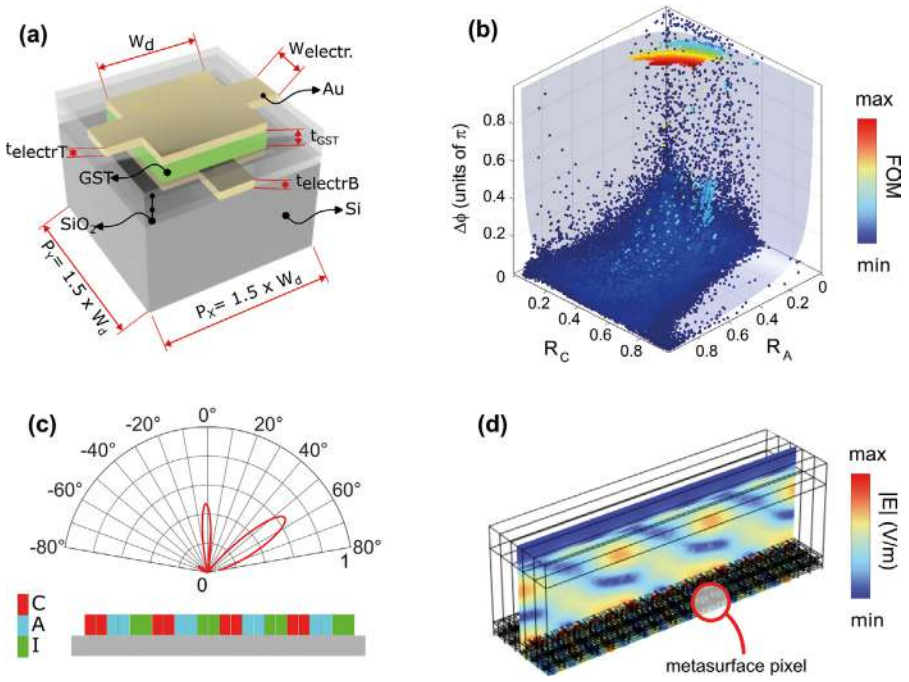

Fig. 1
(a) Three-dimensional schematic of the metasurface unit cell with materials and key geometric parameters. The geometrical parameters are optimized by a numerical routine to simultaneously maximise the reflectance in amorphous state (R_A), the reflectance in crystalline state (R_C), and the light phase shift $\Delta\phi$ (b) Result of the random-start multiobjective optimization. Each point corresponds to the outcome of a single optimization run. The red points correspond to the runs that yielded the best overall performance in terms of the figure of merit (FOM). (c) Far-field polar plot showing the result of the ternary phase modulation (i.e., including an additional intermediate state "I" to the Amorphous and Crystalline pixels). The coloured bar below represents the spatial arrangement of the metasurface pixels corresponding to the three distinct phase states. (d) Three-dimensional visualization of the electric field distribution diffracted in the near field of the metasurface structure.

Contact persons
Simone Zanotto (simone.zanotto@nano.cnr.it)

References
[1] Design of GST Phase Only Pixel Metasurfaces for Beam Steering at Optical Telecom Wavelength. G. E. Lio and S. Zanotto. Discov Mater 5, 265 (2025). [OA]

Projects
Bando Regione Toscana 2023 - Progetti ALTA FORMAZIONE, MELA, CUP: B53C23003180009.

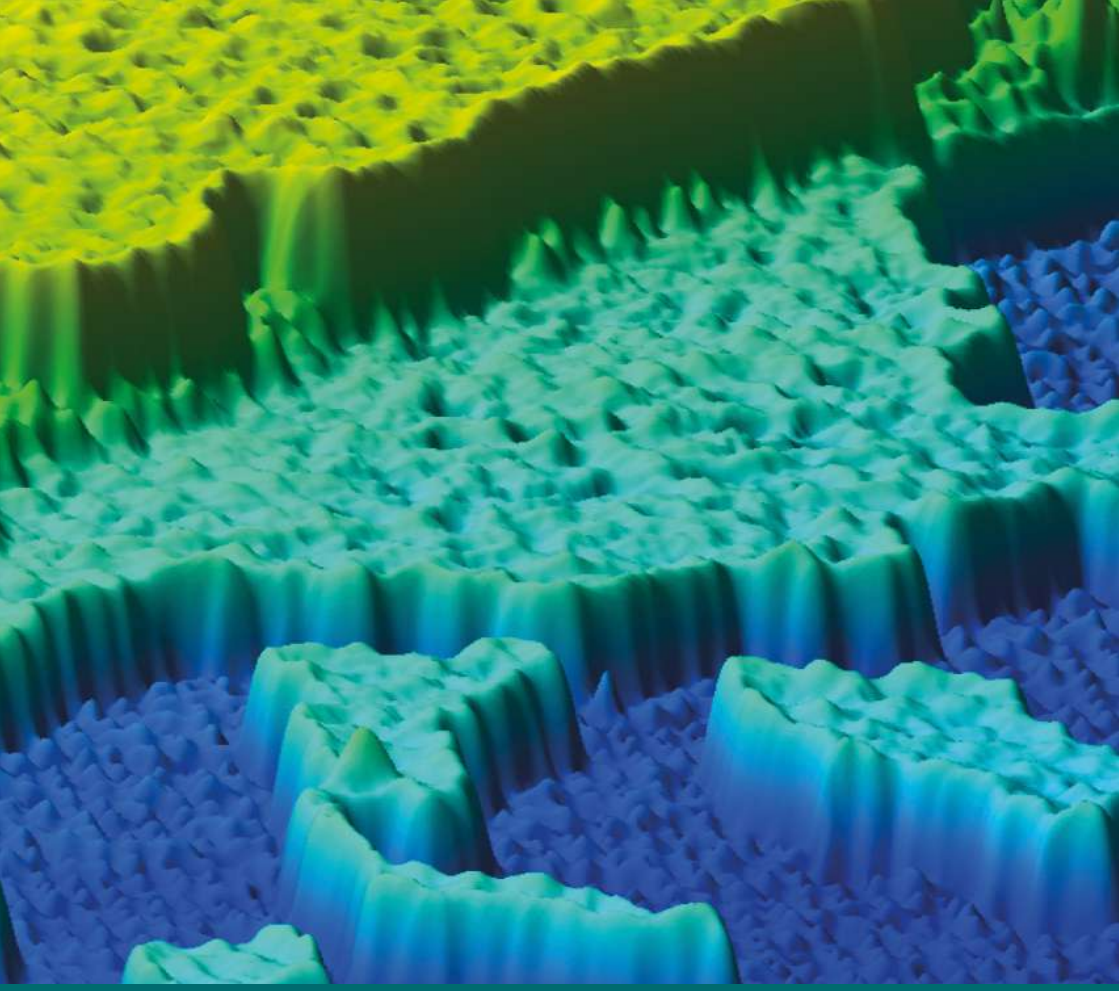

Highlights - Solid-state quantum technology

Research in solid-state quantum technology at Cnr Nano focuses on the fabrication, characterization, and investigation of novel quantum **nanodevices both for fundamental science and for applications**. Joint experimental and theoretical activity is devoted to the study of quantum systems and phenomena, and aims at developing novel concepts and ideas, with potential impact on future applications. Advanced fabrication techniques, low-temperature measurements, and theoretical approaches are developed along **the following main research lines**.

Superconducting electronics. Current research in superconducting electronics is advancing scalable quantum technologies by integrating hybrid nanostructures and 2D materials. Key developments include planar InSb nanoflag Josephson junctions for precise supercurrent control and van der Waals graphene platforms for ballistic transport and synthetic quantum phase simulation. Moreover, thermal and signal efficiencies are being optimized through the bipolar thermoelectric effect. To overcome scaling bottlenecks, the InAs-on-insulator platform provides a high-density architecture for ferroelectric JoFETs and photonic heat transport. Furthermore, nonreciprocal systems like tunable Josephson diodes are paving the way for low-dissipation logic and quantum spintronics. Together, these innovations establish a versatile framework for next-generation hybrid circuits and high-efficiency quantum simulators.

Heat management and thermoelectricity in hybrid superconducting systems. Research into superconducting hybrid nanodevices is revolutionizing cryogenic thermal management by exploiting, for example, the bipolar thermoelectric effect and symmetry breaking to control nanoscale heat flow. Using the Graphene/Insulator/Superconductor platform, we have leveraged Seebeck and Peltier effects to achieve the first demonstrated net electron-cooling in graphene. Furthermore, utilizing

Abrikosov vortices in the quantum limit provides a high figure of merit for sub-Kelvin energy conversion. For scalable integration, the InAs-on-insulator architecture introduces gate-controlled photonic heat transport, addressing thermal waste in high-density Josephson electronics. By integrating these effects into multi-terminal systems researchers can utilize nonreciprocal Josephson diodes and passive detectors to create efficient, low-dissipation quantum logic circuits essential for future computing.

Spin-based quantum devices. We advance spin-based quantum devices by integrating molecular spin triangles into hybrid superconducting circuits for nanoscale control via spin-electric transitions. A generalized exchange qubit framework, with spins embedded in planar microwave resonators, enables high-precision magnetic field sensors and single-photon switches through "perfect absorption" points. This ultrastrong spin–resonator coupling highlights molecular complexes as versatile, high-performance components for next-generation hybrid quantum architectures.

Quantum information, thermodynamics, and metrology. Our work integrates quantum information, thermodynamics, and metrology through advanced photonic platforms. We engineer high-power, broadband harmonic frequency combs in quantum cascade lasers, a key tool for precision quantum technologies from optical to terahertz regimes. Theoretically, we explore quantum thermal machines, cooling, batteries, and work fluctuations for quantum computing, alongside foundational work in quantum metrology and noise. This synergy of cutting-edge theoretical research and novel light-source development underscores our leading international role in quantum science and technology.

[OA] *in the References indicates an Open Access publication.*

Heat management in hybrid graphene/ superconductor devices

We address charge and heat transport in graphene/insulator/superconductor tunnel junctions to advance cryogenic superconducting technologies. Theoretically, we demonstrated thermal-gradient currents arising from a dissipative term, a conventional linear thermoelectric response, and a minor nonlinear contribution from particle–hole symmetry breaking. The second term dominates, enabling Peltier and Seebeck effects. Experimentally, we used superconducting tunnel contacts to tune graphene electron temperature relative to lattice temperature and we demonstrated its first net electron-cooling. Our results establish GIS devices as a key platform for cryogenic thermoelectric control for quantum technology.

Controlling charge and heat transport at the nanoscale and cryogenic temperatures is essential for advancing superconducting quantum technologies. Thanks to its tunable electronic and thermal properties, graphene offers a versatile platform for hybrid superconducting devices. Here, we theoretically and experimentally investigate thermal transport and thermoelectric generation in graphene/insulator/superconductor (GIS) tunnel junctions under temperature gradients and voltage bias.

Our theoretical studies demonstrate that, under a thermal gradient, charge transport of the GIS system is determined by three contributions [1]: (i) the dissipative term, (ii) the conventional thermoelectric effect arising from electron–hole asymmetry, and (iii) the non-linear thermoelectric component due to spontaneous particle-hole symmetry breaking. The latter is generally negligible, thus providing a limited correction to the behaviour of the system. Instead, the other components dominate depending on the electronic configuration of graphene and the temperature distributions. Interestingly, in the thermoelectric regime, the GIS junction supports both a Peltier current in short-circuit conditions and a Seebeck voltage in open-circuit operation.

Experimentally, we introduce innovative thermal devices capable of modulating the electron temperature in graphene by using superconducting tunnel contacts, which act as coolers and thermometers [2]. These devices can refrigerate or induce a net cooling ($T_G < T_b$) of the graphene electrons by a simple voltage bias in a wide range of T_b (250 – 450 mK). By modeling all the main thermal exchange mechanisms, we extracted a top graphene cooling of ~15.5 mK at T_b ~448 mK, which is the first experimental demonstration of electrons cooling in graphene-based devices. Our theoretical and experimental results identify GIS junctions as a promising platform for controlled thermoelectric and thermal management at cryogenic temperatures, with potential applications in quantum caloritronics, cold-electron bolometers, superconducting logic, and heat engines.

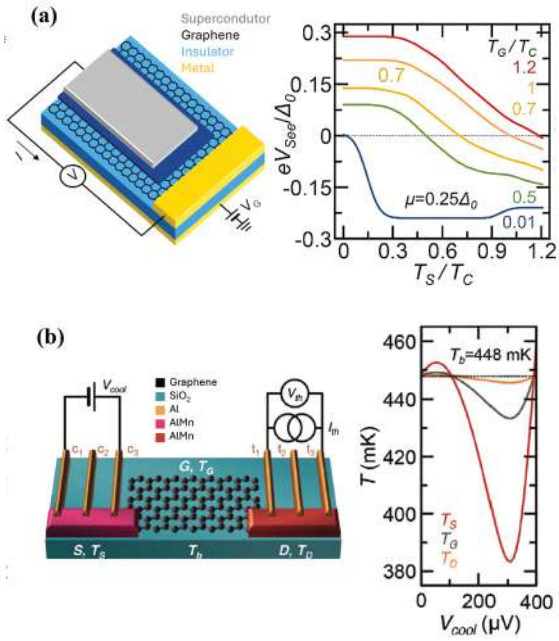

Fig. 1

(a) Sketch of the GIS thermoelectric tunnel junction. The current (I) vs voltage (V) characteristic depends on the electronic temperature of the superconductor (T_S) and of the graphene (T_G) at a given value of the electro-chemical potential (μ) defined by the gate voltage (V_G) applied to the back-gate electrode. Seebeck voltage (V_{See}) vs the T_S calculated at $\mu = 0.25\Delta_0$, with Δ_0 the superconductor gap [1]. (b) Schematic representation of the thermal transistor. By voltage biasing (V_{cool}) a couple of superconducting Al tunnel coolers (c_1 and c_3), the electronic temperature (T_S) of the $Al_{0.98}Mn_{0.02}$ source electrode (S) is decreased/increased relative to the substrate phonon temperature (T_b). The temperature (T_D) of the $Al_{0.98}Mn_{0.02}$ drain electrode (D) is measured by current biasing (I_{th}) a couple of superconducting tunnel thermometers (t_1 and t_3) while recording the voltage drop (V_{th}). The change of the graphene electronic temperature (T_G) is reflected in the modulation of T_D. Electronic temperatures T_D, T_G, and T_S extracted from the experimental data at T_b = 448 mK by properly modelling the predominant thermal exchange processes in the structure.

Contact persons
Federica Bianco (federica.bianco@cnr.it)

References

[1] Coexistence of linear and non-linear thermoelectricity in graphene-superconductor tunnel junctions. F. Bianco, D. Zhang, and F. Paolucci. J. Appl. Phys. 136, 154901 (2024). [OA]
[2] Active Electron Cooling of Graphene. F. Paolucci, F. Bianco, F. Giazotto, and S. Roddaro. Adv. Funct. Mater. 35, 2418456 (2025).

Projects

MUR PRIN 2022, EQUATE, project nr. 2022Z7RHRS.

Bipolar thermoelectricity and exotic states in superconducting devices

The bipolar thermoelectric effect, resulting from spontaneous symmetry breaking of electron–hole symmetry under thermal gradients, has been demonstrated in our laboratories. We studied this phenomenon in superconducting single-electron transistors and utilised it for patenting a passive thermoelectric detector. We applied it also in low-temperature thermal diodes and heat-pipe devices. We identified that Abrikosov vortices, in the quantum limit, produce millivolt-per-kelvin thermovoltages and ZT ≈ 3 at sub-Kelvin temperatures. Finally, we suggest the realisation of Cooper quartets in double quantum dots, creating a new platform for charge-4e superconductivity and correlated Andreev states.

The recent discovery of the bipolar thermoelectric effect, arising from the spontaneous violation of electron-hole symmetry under a thermal gradient, has been comprehensively investigated and integrated into novel experimental settings. Specifically, in the superconducting single-electron transistor [1], we have demonstrated the ability to modulate the bipolar thermoelectric properties via gating. Furthermore, we have engineered and secured a patent for an innovative passive thermoelectric detector predicated on the above bipolar thermoelectric effect [2]. We further illustrate the efficient exploitation of this effect in the development of thermal management devices, heat pipes, and thermal diodes, tailored for low-temperature superconducting quantum technologies [3].

Our investigation into the thermoelectric response of Abrikosov vortices in type-II superconductors under quantum-limit conditions revealed a pronounced thermoelectric effect attributable to particle-hole asymmetry within vortex-bound states, forecasting thermovoltages on the order of several millivolts per Kelvin at cryogenic temperatures. These findings suggest ZT values up to 3, indicating significant promise for applications in highly sensitive low-temperature thermocouples or localized single-photon bolometers [4].

Additionally, we report, for the first time, the realization of a quantum configuration corresponding to Cooper quartets—namely, correlated four-electron bound states—in a double quantum dot device coupled to superconducting electrodes. An effective attractive interdot interaction stabilizes this configuration and gives rise to a previously unobserved ground state, characterized by a coherent quantum superposition of the vacuum and four-electron occupation states [5].

The findings disclose a distinct quartet resonance with minimal-pair correlations, thereby establishing a robust solid-state framework for the exploration of charge-4e superconductivity and strongly correlated Andreev matter, with significant potential for quantum technological applications.

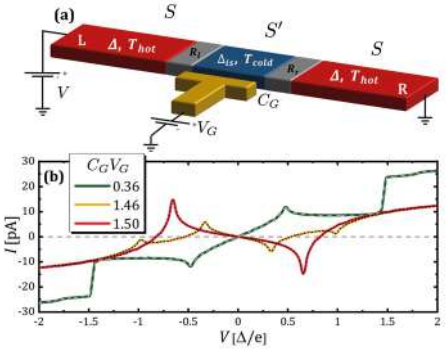

Fig. 1
(a) Sketch of the SIS'IS single-electron transistor to gate control the bipolar thermoelectric effect. (b) Current-voltage characteristics of the gate-tunable bipolar thermoelectric transistor [1].

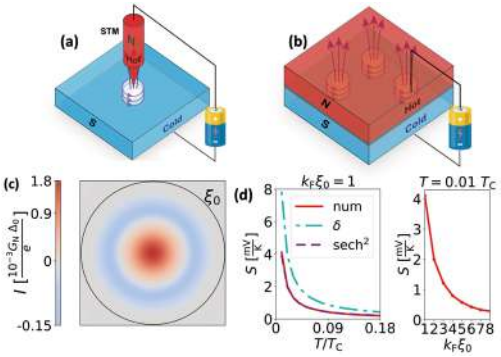

Fig. 2
(a) A heated STM tip can be used to measure the localized thermoelectric response in the cold Abrikosov vortex core. (b) Heated SIN junction to measure thermoelectric response of Abrikosov vortex lattice. (c) Thermoelectric response scanning the Abrikosov vortex with a heated STM tip. (d) Seebeck coefficient plotted versus normalized temperature (left plot) or electron density (right plot) of a heated SIN [4].

Contact persons
Alessandro Braggio (alessandro.braggio@nano.cnr.it)
Francesco Giazotto (francesco.giazotto@cnr.it)

References
[1] Bipolar thermoelectric superconducting single-electron transistor. S. Battisti, G. De Simoni, L. Chirolli, A. Braggio, and F. Giazotto. Phys. Rev. Research 6, L012022 (2024). [OA]
[2] Thermoelectric Single-Photon Detection Through Superconducting Tunnel Junctions. F. Paolucci, G. Germanese, A. Braggio, and F. Giazotto. J. Low. Temp. Phys. 214, 86 (2024).
[3] Tunable thermoelectric superconducting heat pipe and diode. F. Antola, A. Braggio, G. De Simoni, and F. Giazotto. Supercond. Sci. Technol. 37, 115023 (2024). [OA]
[4] Giant Thermoelectric Response of Fluxons in Superconductors. A. N. Singh, B. Bhandari, A. Braggio, F. Giazotto, and A. N. Jordan. Phys. Rev. Lett. 133, 256002 (2024).
[5] Cooper quartets in interacting hybrid superconducting systems. L. Chirolli, A. Braggio, and F. Giazotto. Phys. Rev. Research 6, 033171 (2024). [OA]

Projects
Royal Society (UK), International Exchanges between the UK and Italy, IEC R2 192166.
MUR PRIN 2022, NEThEQS, project nr. 2022B9P8LN.
Next Generation EU PNRR, PE4 NQSTI, project nr. PE0000023.
H2020-EU.1.2.1. - FET Open, SUPERGATE, project nr. 964398.
HORIZON-EIC-2021-TRANSITIONOPEN-01, SPECTRUM, project nr. 101057977.

Quantum thermoelectricity and heat transport in superconducting and topological nanodevices

Superconducting hybrid nanodevices, with interplay between quantum and superconducting correlations, host many phenomena, including, quite unexpectedly, strong thermoelectric responses and exotic thermal properties. Topological materials further enrich this physics. We concentrate on the thermoelectric and thermal effects in multi-terminal superconducting hybrid systems. Further, we characterize the thermoelectric effects on electrical current and current noise in different systems: superconducting nanowires, topological insulators, and quantum Hall edge states. Finally, we analyse heat transport within quantum Hall systems and Andreev interferometric setups.

Quantum thermoelectricity and heat transport investigate heat manipulation and, eventually, its conversion into electrical energy in nanoscale devices where quantum effects become dominant. This knowledge is essential to explore the intricate boundary between quantum dynamics and thermodynamics, commonly referred to as quantum thermodynamics. However, it also has practical implications for the whole field of quantum technologies, where careful heat manipulation is required to reduce unwanted dephasing and decoherence and to optimize nanodevice performance. Within this field, superconducting hybrid nanodevices exhibit particularly rich thermoelectric and thermal properties, especially when superconductivity is combined with topological systems (see [1] for a recent review).

We explore thermoelectric effects on current and noise in several systems, including superconducting wires and interacting quantum Hall edge states. For example, we study nonlocal thermoelectricity in a superconducting wire subject to spin-orbit coupling and a magnetic field with a relative orientation θ between them, finding a strong dependence on θ that corresponds to the emergence of Bogoliubov-Fermi points [2]. We investigate the unique properties of noise in multi-terminal hybrid normal-superconducting systems in the thermal out-of-equilibrium regime, i.e., when temperature biases are present (ΔT-noise) [3]. We show that the non-local thermoelectrical effect can be used to detect heat exchange and non-equilibrium physics in interacting quantum Hall edge states (see Fig. 1) [4].

We address heat transport in a quantum Hall and interferometric setup. We show that heat-charge separation can reach 100% efficiency in a hybrid superconducting quantum Hall setup [5], and we propose an electronic refrigerator based on a ballistic Andreev interferometer (see Fig. 2) that can achieve a maximum cooling power per channel up to five orders of magnitude larger than that of conventional normal metal–insulator–superconductor coolers [6].

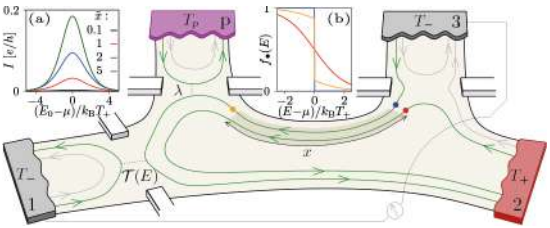

Fig. 1
Edge channels (ECs) in the upper border interact along the distance *x* before a scatterer of transmission probability *T(E)* enables a thermoelectric response between terminals 1 and 3 as a detector of the heat exchanged between two channels. Inset (a): thermoelectric current for interacting regions of different lengths when $T(E)=\theta(E-E_0)$. Inset (b): the electron distribution of ECs before and after the interacting region, as indicated by coloured dots on the main scheme.

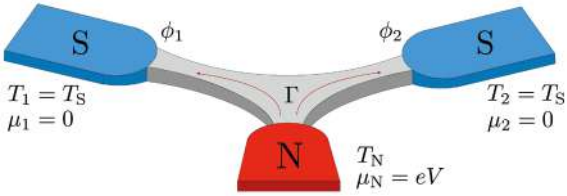

Fig. 2
Sketch of the Andreev interferometer. The normal (N) terminal, depicted in red, is located on the bottom, while the superconducting (S) terminals, in blue, are positioned on the top right and top left. A phase difference $\phi=\phi_2-\phi_1$ is established between the two superconductors. A beam splitter, in gray, couples the N terminal to the S terminals.

Contact persons
Alessandro Braggio (alessandro.braggio@nano.cnr.it)
Fabio Taddei (fabio.taddei@nano.cnr.it)

References

[1] Thermoelectric Processes of Quantum Normal-Superconductor Interfaces. L. Arrachea, A. Braggio, P. Burset, E. J. H. Lee, A. Levy Yeyati, and R. Sánchez. Ann. Phys. (Berl.) 537, e00197 (2025). [OA]
[2] Nonlocal thermoelectricity in quantum wires as a signature of Bogoliubov-Fermi points. J. Herrera Mateos, L. Tosi, A. Braggio, F. Taddei, and L. Arrachea. Phys. Rev. B 110, 075415 (2024).
[3] ΔT-noise in multiterminal hybrid systems. L. Pierattelli, F. Taddei, and A. Braggio. Phys. Rev. Research 7, 023321 (2025). [OA]
[4] Nonlocal thermoelectric detection of interaction and correlations in edge states. A. Braggio, M. Carrega, B. Sothmann, and R. Sánchez. Phys. Rev. Research 6, L012049 (2024). [OA]
[5] Heat-charge separation in a hybrid superconducting quantum Hall setup. C. Panu, F. Taddei, M. Polini, and A. Yacoby. Phys. Rev. B 110, L161407 (2024).
[6] High-performance Andreev interferometer-based electronic coolers. F. Cioni and F. Taddei. Phys. Rev. B 112, 035402 (2025).

Projects

Royal Society (UK), International Exchanges between the UK and Italy, IEC R2 192166 & IEC R2 212041.
MUR PRIN 2022, NEThEQS, project nr. 2022B9P8LN.

Quantum thermodynamics and quantum information

In the context of quantum thermodynamics, our research has focused on quantum thermal machines, quantum cooling, the preparation of quantum registers, quantum batteries, and the measurement of work fluctuations, as well as their applications in quantum computing. In the area of quantum information, we have concentrated on quantum metrology, noise characterization, and the formal aspects of the theory. Together, these activities demonstrate the intense research efforts of our institute in cutting-edge theoretical research in the field of quantum science and technology and highlights its leading role at the international level.

One of the most crucial requirements for effective quantum computation is the ability to prepare pure qubit states with extremely high fidelity. The dynamic cooling technique (Fig. 1) was so far thought to not scale effectively with number of qubits. We established that the scaling is in fact more advantageous than previously thought and demonstrated that on a real quantum hardware [1]. We then took a completely different approach to cooling, namely "cooperative quantum information erasure" [2]. By optimizing this method, we demonstrated record fidelities of $F \approx 0.999$ with up to 5k qubits on a real quantum hardware. The work fluctuation theorem for open systems, an important result in quantum thermodynamics, is still awaiting a fully-fledged experimental validation. We paved the way towards this by combining theoretical methods and demonstration on a real quantum hardware [3].

We addressed is the statistical characterization of how Markovian noise degrades entanglement in quantum systems [4, 5]. In both studies, we used this through the Positive Partial Transpose Time (PPTT), a measure of how long entanglement survives. The first work analyzes randomly sampled Lindbladians acting on qubits and qutrits, showing that stronger Hamiltonian contributions accelerate entanglement loss and that, for large ratios of unitary to dissipative terms, PPTT values converge to a universal limiting distribution. It also reveals how entanglement in many-body memories decays more slowly as system size grows. The second work extends the approach to composite systems up to dimension 8, comparing global, independent local, and correlated local noise. It demonstrates that global noise consistently preserves entanglement longer, while independent local noise leads to the fastest degradation, and introduces an efficient numerical scheme for reconstructing PPTT distributions.

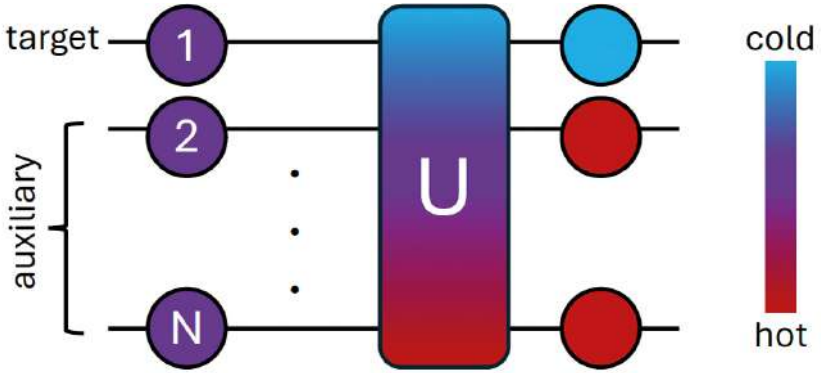

Fig. 1
Dynamic cooling of N identical qubits. Here the target qubit is cooled at the expense of heating up the auxiliary qubits via the application of the global unitary operator U.

Contact persons
Michele Campisi (michele.campisi@nano.cnr.it)
Vittorio Giovannetti (vittorio.giovannetti@sns.it)

References

[1] Dynamic Cooling on Contemporary Quantum Computers. L. Bassman Oftelie, A. De Pasquale, and M. Campisi. PRX Quantum 5, 030309 (2024). [OA]
[2] Collective preparation of large quantum registers with high fidelity. L. Buffoni and M. Campisi. Quantum Science and Technology 10, 025053 (2025). [OA]
[3] Measurement of the work statistics of an open quantum system using a quantum computer. L. Bassman Oftelie and M. Campisi. Quantum Science and Technology 10, 025045 (2025). [OA]
[4] Entanglement Degradation in the Presence of Markovian Noise: a Statistical Analysis. N. Cerrato, G. De Palma, and V. Giovannetti. Physical Review A 111, 012407 (2025).
[5] Statistical characterization of entanglement degradation under Markovian noise in composite quantum systems. N. Cerrato, S. Succi, G. De Palma, and V. Giovannetti. Physical Review A 112, 022219 (2025).

Projects

HORIZON-MSCA-2021-PF-01, QC4QT, project nr. 101063316.

InAs-on-Insulator (InAsOI): a versatile platform for hybrid superconducting electronics and cryogenic coherent caloritronics

InAs-on-Insulator represents the superconducting equivalent of Silicon-on-Insulator technology, specifically engineered to scale Josephson electronics. By combining a superconducting-proximitized InAs epilayer with an insulating buffer, this platform provides electrical decoupling for the high-density integration of planar ferroelectric Josephson field-effect transistors. InAsOI effectively resolves the critical quantum cabling bottleneck through efficient supercurrent time-division multiplexing. Finally, it redefines cryogenic thermal waste management via gate-controlled photonic heat transport, providing a versatile, scalable tool for next-generation hybrid superconducting circuits.

Indium Arsenide on Insulator (InAsOI) [1, 2] is a heterostructure introduced as a pioneering platform for the development of hybrid semiconductor-superconductor electronics. This material consists of a semiconducting Indium Arsenide (InAs) epilayer grown onto an Indium Aluminum Arsenide (InAlAs) metamorphic buffer (see Fig. 1a). The InAlAs buffer acts as a cryogenic electrical insulator for temperatures below 70 K, effectively enabling the electrical decoupling of adjacent surface-exposed devices. This architecture offers key advantages over conventional InAs-based platforms, with the high critical current density and voltage being particularly relevant. The characteristics of InAsOI make it an ideal foundation for fabricating gate-tunable devices, i.e., a Josephson Field Effect Transistor (JoFET), where the use of high-permittivity (high-k) [3] gate dielectrics, such as Hafnium Dioxide (HfO_2), allows for efficient electrostatic control of the superconducting properties. The ON/OFF switching functionality of these devices has enabled the realisation of 1-input-8-output superconducting demultiplexers [4] operating at 50 mK in the DC-to-VHF frequency range and with near-zero insertion loss in the superconducting (ON) state (Fig. 2). Moreover, JoFETs fabricated with HfO_2 demonstrated a ferroelectric behaviour (Fe-JoFET) at sub-Kelvin temperatures, showing a hysteretic critical current vs. gate voltage characteristic. InAsOI is also highly suitable for caloritronic [5] applications, primarily due to its outstanding thermal properties at cryogenic temperatures. Moreover, such a weak coupling, combined with electrical gate control, enabled the realisation of a groundbreaking semiconductor-superconductor photonic field-effect heat transistor (Fig. 1 b, c, d) operating in a non-galvanic (radiative) configuration over macroscopic distance (i.e., up to 1 mm). The device achieved a record temperature modulation, a value exceeding previous electrostatic modulations by more than an order of magnitude.

Fig. 1
Cross-section of an InAsOI-based JoFET. The shaded region is the graded metamorphic buffer hosting the InAs epilayer (green). An insulating layer (yellow) separates the Al gate electrode (grey) from the conduction layer, proximitized by Al superconducting contacts. b) Circuit schematic with SEM images (5 mm scale bar) of a photonic heat-transport caloritronic device on the InAsOI platform, including wiring and measurement setup. Red and blue: hot and cold resistors with Josephson thermometers; green: a gate-tunable photonic heat

modulator formed by two parallel JoFETs. Hot and cold resistors are non-galvanically connected via two capacitors. Red and blue wiring denote the respective reservoir setups. c, d) 3D renderings of the hot/cold resistors with Josephson thermometers and of a single JoFET.

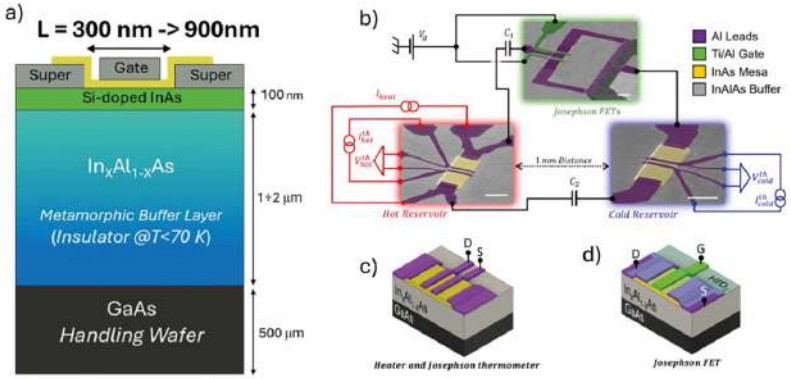

Fig. 2
a) Schematic diagram of the superconducting 1I8O demultiplexer. b) False-colour optical microscope image of the superconducting 1->8 demultiplexer, highlighting the chosen superconducting path and the gate control configuration. c) V-I characteristics of all the demultiplexer signal lines with the gate configuration shown in (b). d) Line resistances (left) and normalized line resistances (right) of all the 1I8O signal lines with the gate configuration shown in (b).

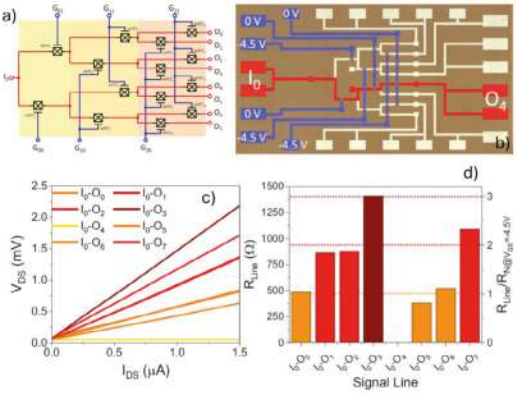

Contact persons
Giorgio De Simoni (giorgio.desimoni@nano.cnr.it)
Francesco Giazotto (francesco.giazotto@cnr.it)

References

[1] InAs on Insulator: A New Platform for Cryogenic Hybrid Superconducting Electronics. A. Paghi et al. Adv. Funct. Mater. 35, 2416957 (2025). [OA]
[2] Structural and Transport Properties of Thin InAs Layers Grown on InxAl1−xAs Metamorphic Buffers. G. Senesi et al. Nanomaterials 15, 173 (2025). [OA]
[3] Cryogenic behavior of high-permittivity gate dielectrics: The impact of atomic layer deposition temperature and the lithographic patterning method. A. Paghi et al. J. Appl. Phys. 28, 044103 (2025). [OA]
[4] Supercurrent time division multiplexing with solid-state integrated hybrid superconducting electronics. A. Paghi et al. Nat. Commun. 16, 8442 (2025). [OA]
[5] Extremely weak sub-kelvin electron–phonon coupling in InAs on Insulator. S. Battisti et al. Appl. Phys. Lett. 11, 202601 (2024). [OA]

Exploring hybrid spins-superconducting circuits for quantum technologies

We report our recent developments on the integration of spins into hybrid quantum circuits. We first consider molecular spin qubits embedded into planar superconducting microwave resonators. We show that such hybrid circuits can be used as sensors for magnetic fields or tailored to obtain points of Perfect Absorption at single microwave photon level. We also consider the ultrastrong coupling regime between spin waves and superconducting resonators. Here, the temperature dependence of the coupling strength and the mode frequencies can be related to the interplay between spin waves and Meissner currents.

We investigate molecular spins embedded into planar microwave (MW) superconducting resonators at low temperature. In the first experiment, the spins are driven by a MW pulse sequence, while a radiofrequency (RF) coil applies the external AC magnetic field to be probed, as in Fig. 1.a [1]. Using Dynamical Decoupling (DD) protocols (e.g., Carr Purcell Meiboom Gill, CPn, being n the number of π pulses), the amplitude of the AC field can be inferred with sensitivities up to $S \approx nT/\sqrt{Hz}$, depending on n and on the interpulse delay, τ (Fig. 1b). In the second experiment, the spins are strongly coupled to the resonator at mK temperature and in the single MW photon regime, as in Fig. 1.c,d [2]. Here, points of Perfect Absorption (PA), with zero reflection (no outcoming photon), are observed in the spin-photon polaritons before and after resonance (Fig. 1d). This is due to the recovery of the balance between radiative and non-radiative losses mediated by the resonator-spins detuning. We further show that realizing PA corresponds to tailor Hermitian subspaces into the system [2] and that PA can be still recovered even in the weak spin-photon coupling regime [2]. These results hold potential for applications in single MW photon switches or for quantum sensing.

Next, we study the interplay between magnetism and superconductivity, more specifically the coupling effects arising from the electromagnetic proximity with an insulating magnetic film [3]. To this end, we focus on a bilayer composed of an Yttrium Iron Garnet film (YIG), exhibiting low-damping magnon excitations, and a high-Tc Yttrium Barium Copper Oxide (YBCO) superconducting MW resonator (Fig. 2a, b). Transmission spectra acquired upon cooling show a progressive increase in the magnon–photon coupling (g; $g/g(0)$), reaching up to about 2 GHz, and a simultaneous shift of the magnon–photon polaritons (δ; $\delta/\delta(0)$) These trends agree well with the shift of the frequency of the resonator (ω_C; $\omega_C/\omega_C(0)$) as a function of temperature, and can be ultimately attributed to the interplay between spin waves and Meissner currents (Fig. 2c). These results shed light on the evolution of hybrid superconducting–magnetic systems in the ultrastrong coupling regime, opening a path toward the observation of novel effects at experimentally accessible coupling strengths.

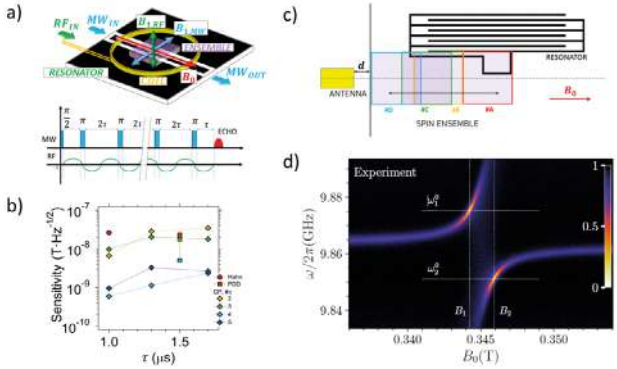

Fig. 1

Left: Quantum sensing of magnetic fields [1]. a) MW resonator (black), spin ensemble (purple) and RF coil (orange) along with a quantum sensing protocol used. b) Sensitivity obtained for different protocols, τ, n. Right: Perfect Absorption (PA) of single MW photons [2]. c) resonator with different sample positions (#A-#D). d) Reflection map showing spin-photon polaritons with the two PA dips.

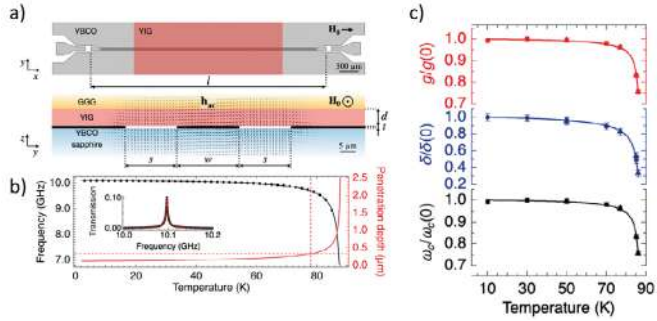

Fig. 2

The YBCO/YIG bilayer used. b) Temperature dependence of the frequency and the penetration depth for the YBCO resonator in zero field. c) Trends found for g, δ and ω_c in the YBCO/YIG bilayer, suggesting interplay between superconductor and magnon modes.

Contact persons

Marco Affronte (marco.affronte@unimore.it)
Alberto Ghirri (alberto.ghirri@nano.cnr.it)

References

[1] Quantum sensing of magnetic fields with molecular spins. C. Bonizzoni et al. npj Quantum Inf. 10, 41 (2024). [OA]

[2] Observation of Perfect Absorption in Hyperfine Levels of Molecular Spins with Hermitian Subspaces. C. Bonizzoni et al. Nat. Commun (2025). DOI: https://doi.org/10.1038/s41467-025-67163-z. [OA]

[3] Interplay between magnetism and superconductivity in a hybrid magnon-photon bilayer system. A. Ghirri et al. Phys. Rev. Applied 22, 034004 (2024).

Projects

Next Generation EU PNRR, SMILE-SQUIP, project nr. PE00000023.

InSb nanoflag-based Josephson junctions as a platform for quantum technologies

Planar Josephson junctions (JJs) based on InSb nanoflags have recently emerged as an intriguing platform in superconducting electronics. We apply Scanning Gate Microscopy (SGM) to such devices, demonstrating the possibility of manipulating the supercurrent flow across the junction at a local level. Furthermore, knowledge of the current-phase relationship (CPR) of such hybrid junctions is crucial for their applications. For this purpose, we have investigated superconducting quantum interference devices (SQUIDs) employing InSb nanoflag JJs. By measuring interference patterns in both symmetric and asymmetric SQUID configurations, we extract unprecedented details of the CPRs of these junctions.

SQUIDs are one of the most important classes of devices in quantum technologies. The fundamental component of a SQUID is the JJ, which is created by sandwiching a normal (non-superconducting) material between two superconducting electrodes. When two JJs are connected in parallel, a SQUID is formed. This type of device is the most sensitive magnetometer, with crucial applications in superconducting electronics. Furthermore, SQUIDs have been explored to investigate a fundamental property of JJs: their CPR. This key quantity is challenging to test directly in experiments.

Figure 1a shows a microscopy image of a symmetric SQUID based on InSb nanoflags, in which the two JJs are nominally identical. Applying a magnetic field perpendicular to the plane of the SQUID, an interference pattern is observed in the supercurrent, which is periodic with the number of superconducting flux quanta enclosed in the SQUID loop. This is shown in Fig. 1b. Superimposed on the experimental data is the result of a simulation, from which we can directly extract the CPR of the JJs. Our results demonstrate the skewness of the CPR, showing significant contributions from higher harmonics [1].

Mapping supercurrent profiles with SGM on JJs has been theoretically proposed recently [Phys. Rev. B 106, 035432 (2022)]. We performed the first experimental demonstration of SGM on JJs. The experimental setup is reported in Fig. 2a: when the charged tip of the SGM is placed close to the semiconducting (normal) region of the JJ, it modifies the local carrier concentration. Then, the tip has been scanned across the JJ. For each point, we have measured the supercurrent of the device. The results are reported in Fig. 2b. The map shows a clear reduction of the supercurrent of the device, once the tip is placed close to the location of the JJ, indicating the local nature of the tip-device interaction. In Fig. 2c, we report the results of a numerical simulation, which reliably reflects all features observed in the experiment. Our results raise the perspective of locally imaging and manipulating the supercurrent flow [2].

Fig. 1
(a) Top-view scanning electron microscopy image of a symmetric SQUID. (b) Magnetic field response of the symmetric SQUID. Colour map of the differential resistance as a function of current bias and the applied magnetic field. Overlay: Critical current from theoretical model.

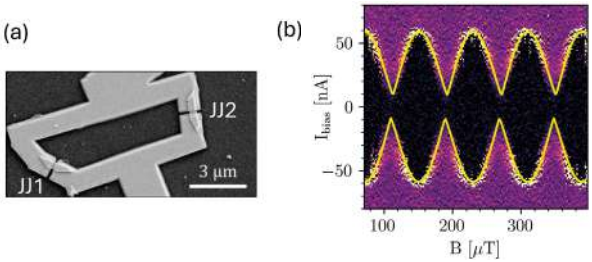

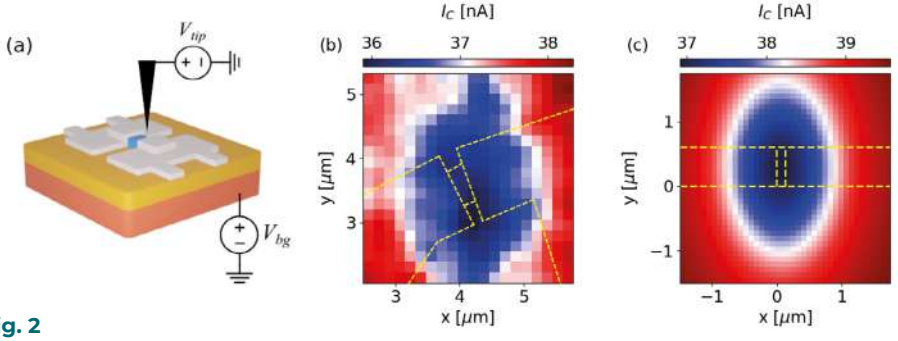

Fig. 2
(a) Graphical representation of a Scanning Gate Microscopy experiment. The light blue section corresponds to the exposed semiconducting region of the nanoflag. (b) SGM map measurement: critical current map as a function of the position of the tip. (c) Numerical simulation of the tip-induced critical current modulation map. In (b) and (c), the device outline is indicated by the dashed yellow lines.

Contact persons
Stefan Heun (stefan.heun@nano.cnr.it)
Lucia Sorba (lucia.sorba@nano.cnr.it)

References

[1] Unveiling the current-phase relationship of InSb nanoflag Josephson junctions using a NanoSQUID magnetometer. A. Chieppa, G. Shukla, S. Traverso, G. Bucci, V. Zannier, S. Fracassi, N. Traverso Ziani, M. Sassetti, M. Carrega, F. Beltram, F. Giazotto, L. Sorba, and S. Heun. Nano Letters 25, 14412 (2025). [OA]
[2] Supercurrent modulation in InSb nanoflag-based Josephson junctions by scanning gate microscopy. A. Lombardi, G. Shukla, G. Bucci, S. Salimian, V. Zannier, S. Traverso, S. Fracassi, N. Traverso Ziani, M. Sassetti, M. Carrega, F. Beltram, L. Sorba, and S. Heun. Commun Mater 6, 272 (2025). [OA]
[3] Side-gate modulation of supercurrent in InSb nanoflag-based Josephson junctions. B. Turini, S. Salimian, M. Carrega, F. Paolucci, V. Zannier, L. Sorba, and S. Heun. Phys. Status Solidi B 262, 2400534 (2025). [OA]

Projects

MUR PRIN 2022, TopoFlag, project nr. 2022PH852L.
Next Generation EU PNRR, PE4 NQSTI, project nr. PE0000023.

Engineering graphene-based devices as solid-state quantum simulators and quantum Hall superconductors

Two-dimensional materials (2DMs) offer novel degrees of freedom that can be leveraged to advance the field of quantum technologies. We focus on ultra-clean field-effect devices based on van der Waals (vdW) engineering of CVD graphene, resulting in ballistic electronic transport over several micrometers and quantum Hall (QH) states at low magnetic fields. On the one hand, these devices realize solid-state quantum simulators, where different terms of the Hamiltonian can be tuned by acting on the twist angle and in situ on the field-effect. On the other hand, synthetic phases combining QH and superconductivity emerge when coupled to 3D superconducting leads.

Quantum technologies based on 2DMs demand a combination of scalability, low electronic disorder, and tunability. To fulfill these requirements, we develop vdW techniques enabling high-quality devices based on CVD graphene (Fig. 1a), such as direct pick-up mediated by hexagonal boron nitride (hBN) [1]. With this approach we obtain ballistic transport limited by the device channel size (Fig. 1a, bottom inset).

We employ multilayers with rotational mismatch (so-called twist) to program different Hamiltonian terms. In the trilayer shown in Fig. 1b, the interlayer hopping is active only for the two bottom layers, while it is suppressed by large-angle twisting within the top ones [2]. This configuration produces a monolayer (MLG) decoupled from a Bernal bilayer (BLG), as demonstrated by quantum transport (Fig. 1c), which reveals independent sets of Landau levels and a built-in BLG band gap (~10 meV). This gap stems from the proximal MLG, inducing different on-site energies on the bottom layers (diagonal terms in BLG Hamiltonian). Further control can be offered by adjustments in twist angle, layer number, and encapsulating material.

The hBN-graphene platform is also suited for the fabrication of ballistic Josephson junctions (JJs, see Fig. 2a) [3], comprising superconducting contacts with a large critical field such as Nb [4]. These JJs carry gate-tunable supercurrents, which survive to perpendicular magnetic fields inducing the QH effect. Fig. 2b shows the coexistence of QH states (indicated by the filling factor ν on the top axis) and superconducting pockets (dark spots with suppressed zero-bias resistance). The supercurrent is prominent at transitions between QH plateaus and shows quasi-periodic quantum interference as a function of the magnetic flux (Fig. 2c). This behaviour is understood based on the physics of a proximitized percolative phase, with a subtle interplay of applied electromagnetic fields and doping at the graphene-Nb interface [3]. These findings contribute to the quest for proximitized QH phases as potential hardware for fault-tolerant quantum computers.

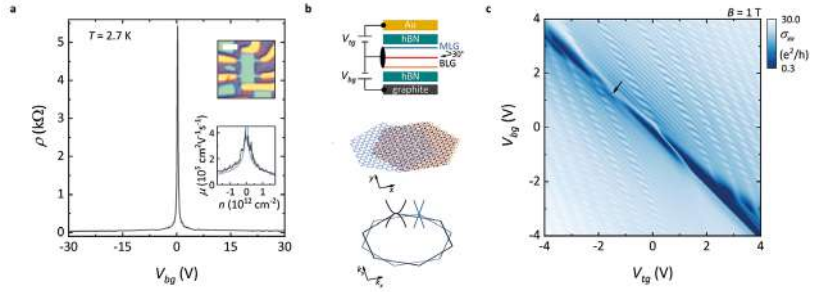

Fig. 1

(a) Resistivity as function of back-gate voltage, measured in CVD graphene (top inset, scale bar is 2 μm). Bottom inset: mobility as a function of carrier density. (b) Sketch of a twisted MLG-BLG device (top), with corresponding real-space (middle) and k-space configurations (bottom). (c) Longitudinal conductivity as a function of gate voltages at B = 1 T; the black arrow indicates closing of the BLG gap. Panel a is adapted from [1], panels b-c are adapted from [2].

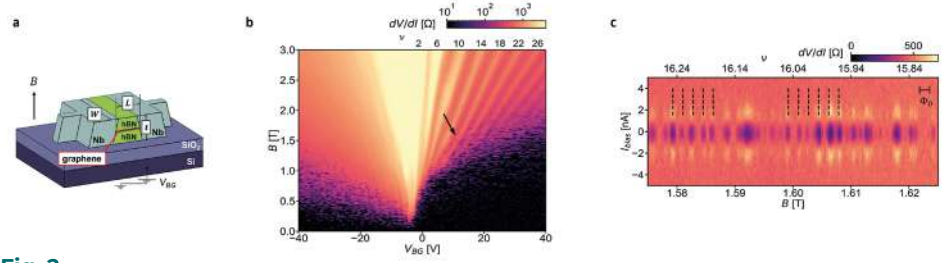

Fig. 2

(a) Sketch of a Nb-contacted graphene JJ (W = 3 μm, L = 0.4 μm, t = 60 nm). (b) dV/dI at zero dc bias, as a function of back-gate voltage and magnetic field. (c) dV/dI as a function of magnetic field and dc bias, in the vicinity of the pocket indicated by a black arrow in panel b. The dashed black lines correspond to a periodicity of $\Phi_0 = h/2e$. All panels are adapted from [3]; T = 40 mK.

Contact persons

Sergio Pezzini (sergio.pezzini@nano.cnr.it)
Stefan Heun (stefan.heun@nano.cnr.it)

References

[1] Decoupled High-Mobility Graphene on Cu(111)/Sapphire via Chemical Vapor Deposition. Z. M. Gebeyehu et al. Advanced Materials 36, 2404590 (2024). [OA]

[2] Built-in Bernal gap in large-angle-twisted monolayer-bilayer graphene. A. Boschi et al. Communications Physics 7, 391 (2024). [OA]

[3] Quasi-Φ_0-Periodic Supercurrent at Quantum Hall Transitions. I. Villani et al. ACS Nano 19, 27370-27378 (2025). [OA]

[4] Vortex Arrays and Strong Proximity Coupling in Nb/Au Bilayer. W. Li et al. Applied Physics Letters 127, 194003 (2025). [OA]

Projects

Next Generation EU PNRR, PE4 NQSTI, PRO, project nr. PE0000023.

Diode effects and energy conversion in advanced superconducting junctions

In recent years, extensive research has explored nonreciprocal and diode-like phenomena in superconducting systems, with particular emphasis on Josephson junctions and hybrid devices. These studies reveal how tailored geometries, biharmonic current drives, and multi-loop configurations enable the realization of tunable Josephson diodes, nonreciprocal SQUIDs, and supercurrent rectifiers. Such advancements represent a significant step toward the development of superconducting nanoelectronics and quantum spintronics, offering promising applications in low-dissipation logic circuits and efficient energy-conversion technologies.

Non-reciprocity lies at the core of numerous technological applications. It is essential in devices such as p–n junction diodes, where current flows preferentially in one direction, enabling rectification and signal processing. Beyond electronics, non-reciprocity plays a fundamental role in thermoelectric phenomena, where directional asymmetry in transport processes underpins energy conversion between heat and electricity.

Recently, superconducting junction devices have achieved remarkable progress in realizing non-reciprocal superconductivity, despite the intrinsic reluctance of conventional BCS superconductors to exhibit such behaviour due to their inherent electron–hole symmetry. Non-reciprocity in superconductors has now been demonstrated in multiple architectures. For instance, Josephson junctions can host asymmetric supercurrents, forming the basis of superconducting diodes enabled by the simultaneous breaking of inversion and time-reversal symmetries through back-action schemes [1], biharmonic current drives [2] (Fig. 1), asymmetric supercurrent interferometers [3, 4], and current crowding effects [5]. Beyond supercurrent diodes, non-reciprocity has also been realized in spin-selective quasiparticle tunnel junctions, leading to the development of quasiparticle diodes [patent WO2023002513A1]. Remarkably, these devices exhibit giant thermoelectric effects, efficiently converting heat into electrical power [6], paving the way for the first superconducting spintronics heat engine (Fig. 2).

This principle is essential for enhancing device efficiency and also serves as a foundation for designing advanced systems that leverage broken symmetry to enable functionalities such as thermal management and energy harvesting. Moreover, it provides fundamental tools to probe unconventional superconducting states, such as helical and topological phases, thereby opening new pathways for emerging quantum technologies.

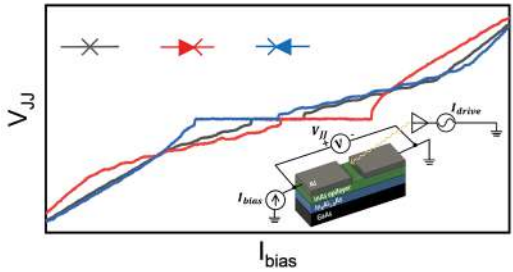

Fig. 1
IV curves under applied biharmonic drive signal ($I_{drive}=I_1 \sin(\omega t)+ I_2 \sin(2\omega t+\theta)$, with $\omega/2\pi$=1.35 GHz) at different phase shifts (θ=0,π/2,-π/2 for gray, red and blue curves, respectively). Diode symbols represent no diode (gray), positive diode (red), and negative diode (blue), showing that the polarity of the diode can be tuned by θ. Bottom: schematic structure of the device and conceptual sketch of the setup.

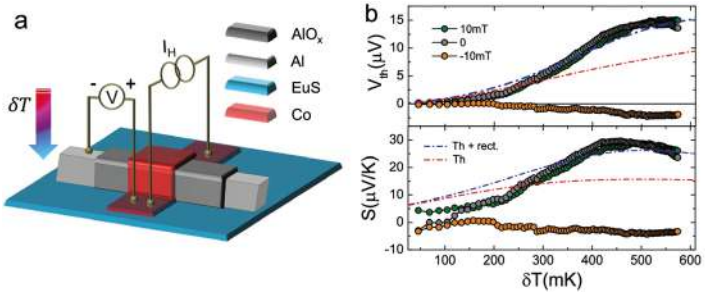

Fig. 2
(a) Scheme of the electric circuit used to quantify the thermoelectric response of the superconducting spintronic heat engine, with the temperature difference obtained via a Joule heating current flowing through the Co strip. (b) Thermovoltage (top) and Seebeck coefficient (S, bottom) vs the junction temperature gradient at selected magnetic field values and measured at T_{bath} = 100 mK. Dash-dotted lines represent the fits to the data considering thermoelectricity with (blue) and without (red) additional rectification effects.

Contact persons
Elia Strambini (elia.strambini@cnr.it)
Francesco Giazotto (francesco.giazotto@cnr.it)

References

[1] Back-action supercurrent rectifiers. D. Margineda et al. Commun. Phys. 8, 1–7 (2025). [OA]
[2] Biharmonic-Drive Tunable Josephson Diode. L. Borgongino et al. Nano Lett. 25, 14451–14458 (2025). [OA]
[3] Double loop dc-SQUID as a tunable Josephson diode. A. Greco et al. Appl. Phys. Lett. 125, 072601 (2024). [OA]
[4] Diode effect in the Fraunhofer pattern of disordered planar Josephson junctions. L. Chirolli et al. Communications Physics 8, 483 (2025). [OA]
[5] Streamline-controlled rectification of supercurrent in thin-film asymmetric weak links. F. Antola et al. Phys. Rev. Appl. 24, 064003 (2025).
[6] Superconducting spintronic heat engine. C. I. L. de Araujo et al. Nat. Commun. 15, 4823 (2024). [OA]

Probing spin-electric transitions in a molecular exchange qubit

Electric fields represent an ideal means for controlling spins at the nanoscale. Here we perform low-temperature magnetic far-IR spectroscopy on a molecular spin triangle (Fe_3) and provide the first experimental evidence of spin-electric transitions in polynuclear complexes. Based on spin Hamiltonian simulations of the spectra, we identify the observed transitions and estimate the value of the spin-electric coupling. Finally, we introduce the concept of generalized exchange qubit, which applies to a wide class of molecular spin triangles, and includes the scalar chirality and the partial spin sum qubits as special cases.

Manipulation of the electron spin magnetization is traditionally achieved with resonant spectroscopy techniques, such as electron paramagnetic resonance, where transitions between Zeeman levels are induced by the magnetic field component of the electromagnetic field. Multispin systems offer the possibility of going beyond this consolidated paradigm, and of using electric fields to access protected degrees of freedom, such as the scalar chirality or the partial spin sum. Here we access these degrees of freedom in a Fe_3 molecular nanomagnet through magnetic far-infrared spectroscopy and provide the first direct evidence of spin-electric transitions in polynuclear magnetic molecules [1]. The simulation of the spectra – carried out through a spin-Hamiltonian approach – allows us to assess the presence of both magnetic- and electric-dipole induced transitions, and to estimate the value of the spin-electric coupling. The analysis of the eigenstates shows that the Fe_3 molecule can be regarded as a generalized exchange qubit, corresponding to a hybrid between the spin-chirality and the partial-spin sum qubits.

These experimental signatures of spin-electric transitions represent a significant step towards an all-electric manipulation of the molecular spin. Pulsed excitation experiments in the THz regime will be required to measure the relaxation and coherence times of the molecular exchange qubit. The use of a quasi-optical setup and of samples formed by equally-oriented molecules will also allow to exploit the light polarization as a means to selectively address electric and magnetic-dipole transitions, and to identify the physical origin of the zero-field splitting in the ground multiplet of the spin triangles, a debated issue with significant implications on the coherence properties of the spin qubit [arXiv:2510.03099 (2025)].

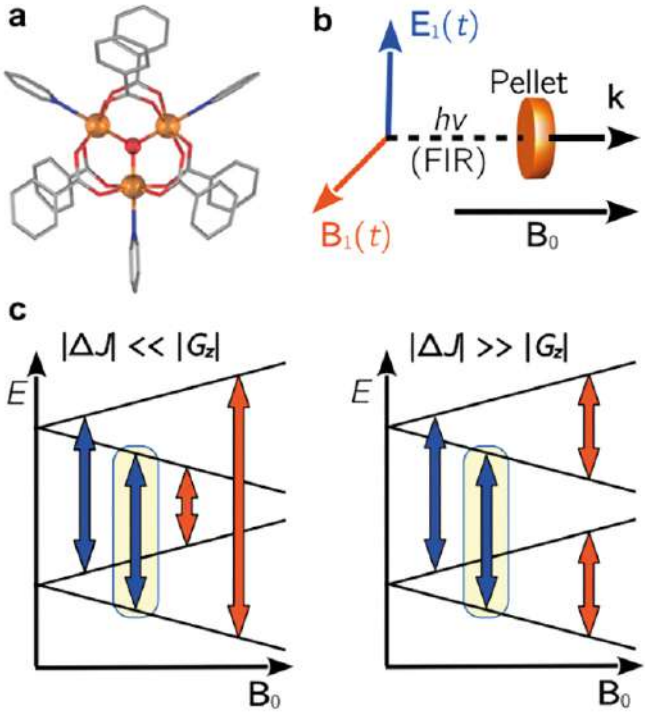

Fig. 1
(a) Schematic structure of the Fe_3 spin triangle. The orange spheres indicate Fe^{III} ions and the red sphere indicates the central oxide bridge that constitutes the main superexchange pathway. Benzoato and pyridine ligands are plotted as sticks for clarity. (b) Sketch of the experimental setup, showing the far-IR (FIR) beam's Poynting vector (k), and of the electric and magnetic field components ($E_1(t)$ and $B_1(t)$, respectively) with respect to the sample pellet and the magnetic field (Faraday geometry). (c) Schematic view of the transitions, within the ground-state quadruplet of the spin triangle, for a magnetic field B_0 oriented along the main symmetry axis of the molecule. Orange and blue arrows correspond to magnetic- and electric-dipole transitions, respectively. Highlighted in yellow is the transition between the ground (|0>) and the second excited state (|1>) states that define the exchange qubit.

Contact persons
Filippo Troiani (filippo.troiani@nano.cnr.it)

References

[1] Probing spin-electric transitions in a molecular exchange qubit. F. le Mardelé, I. Mohelský, J. Wyzula, M. Orlita, P. Turek, F. Troiani, and A. K. Boudalis. Nature Communications 16, 1198 (2025). [OA]

Metrological terahertz quantum sources

Optical frequency combs (OFCs) are emerging as key high-precision tools for the development of quantum technology platforms. These include potential applications for optical and quantum communication, computation, information, sensing, and metrology and can extend from the near-infrared with micro-resonator combs, up to the technologically attractive terahertz (THz) frequency range, with powerful and miniaturized quantum cascade laser (QCL) FCs. Here, and by design, we devise a strategy to obtain broadband harmonic frequency comb (HFC) emission of a pre-defined order in a QCL with record optical power/mode.

OFCs, which establish a rigid phase-coherent link between the microwave and optical domains of the electromagnetic spectrum, are emerging as key high-precision tools for the development of quantum technology platforms. These include potential applications for communication, computation, information, sensing, and metrology and can extend from the near-infrared with micro-resonator combs, up to the technologically attractive THz frequency range, with powerful and miniaturized QCL FCs.

The recently discovered ability of the QCLs to produce a harmonic FC (HFC)—a FC with large intermodal spacings—has attracted new interest in these devices for both applications and fundamental physics, particularly for the generation of THz tones of high spectral purity for high data rate wireless communication networks, for radio frequency arbitrary waveform synthesis, and for the development of quantum key distributions. The controlled generation of harmonic states of a specific order remains, however, elusive in THz QCLs. Here, and by design, we devise a strategy to obtain broadband HFC emission of a pre-defined order in a QCL. By patterning regularly spaced metallic defects or graphene scatters on the top surface of a double-metal Fabry–Perot QCL, we demonstrate harmonic comb emission with modes spaced by a (n+1) free spectral range and with an optical power/mode > 300 uW.
The devices quantum sources are employed in a transportable THz free space optical communication system implementing a binary on-off keying modulation scheme with Manchester encoding, paving the way for the deployment of optical wireless communication systems exploiting the 2–4 THz frequency range.

Finally, we perform a comparative study of the thermal and electronic properties of Fabry–Perot and micro-ring THz HFC QCLs, using micro-probe band-to-band photoluminescence. By monitoring the lattice temperature and the electron cooling above the threshold for stimulated emission, we extract the device thermal resistances and the internal quantum efficiencies, highlighting the key role of the resonator architecture.

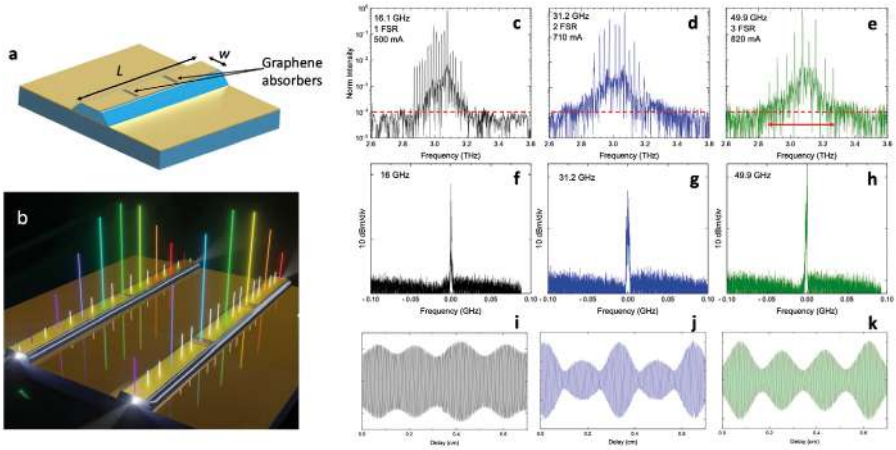

Fig. 1

(a) False colour scanning electron micrograph (SEM) image of a tunnel-field effect transistor (TFET) based on bilayer graphene. (b) Voltage responsivity (R_V) map measured as a function of the bottom and top gates of the TFET. A six-fold pattern appears, indicating a thermoelectric contribution to the photodetection. (c-e) Fourier transform infrared (FTIR) emission spectra of the reference device without any top surface patterned scatters (c), and of the QCL with 1 and 2 top surface graphene scatters (d, e). The red-dashed lines mark the noise level. (f–h) Intermode beat note of the reference laser (f) and of the device with n = 1 (g) and n = 2 (h), collected with an RF spectrum analyzer, under the same condition of the corresponding spectra. (i, j) Corresponding interferograms (IFG) of the spectra in panel c (i), d (j), and e (k).

Contact persons

Miriam Serena Vitiello (miriam.vitiello@nano.cnr.it)

References

[1] Quantum cascade laser: 30 years of discoveries. M. S. Vitiello et al. Nanophotonics 14, 3353 (2025). [OA]

[2] Experimental analysis of the thermal management and internal quantum efficiency of terahertz quantum cascade laser harmonic frequency combs. M. A. J. Guerrero et al. Nanophotonics 14, 4249 (2025). [OA]

[3] Harmonic quantum cascade laser terahertz frequency combs enabled by multilayer graphene top-cavity scatters. M. A. J. Guerrero et al. Nanophotonics 13, 1835 (2024). [OA]

[4] Theoretical model of passive mode-locking in terahertz quantum cascade lasers with distributed saturable absorbers. L. Seitner et al. Nanophotonics 13, 1823 (2024). [OA]

[5] Sculpting harmonic comb states in terahertz quantum cascade lasers by controlled engineering. E. Riccardi et al. Laser & Photonics Reviews 19, 2301082 (2024). [OA]

Projects

HORIZON-CL4-2021-DIGITAL-EMERGING-01, Muquabis, project nr. 101070546.
H2020-ERA-NET-QuantERA Call 2021, QATACOMB, project nr. 731473 and 101017733.
Horizon Europe ERC POC, TERASCAN, project nr. 101157731
Next Generation EU PNRR, PE4 NQSTI, project nr. PE0000023.

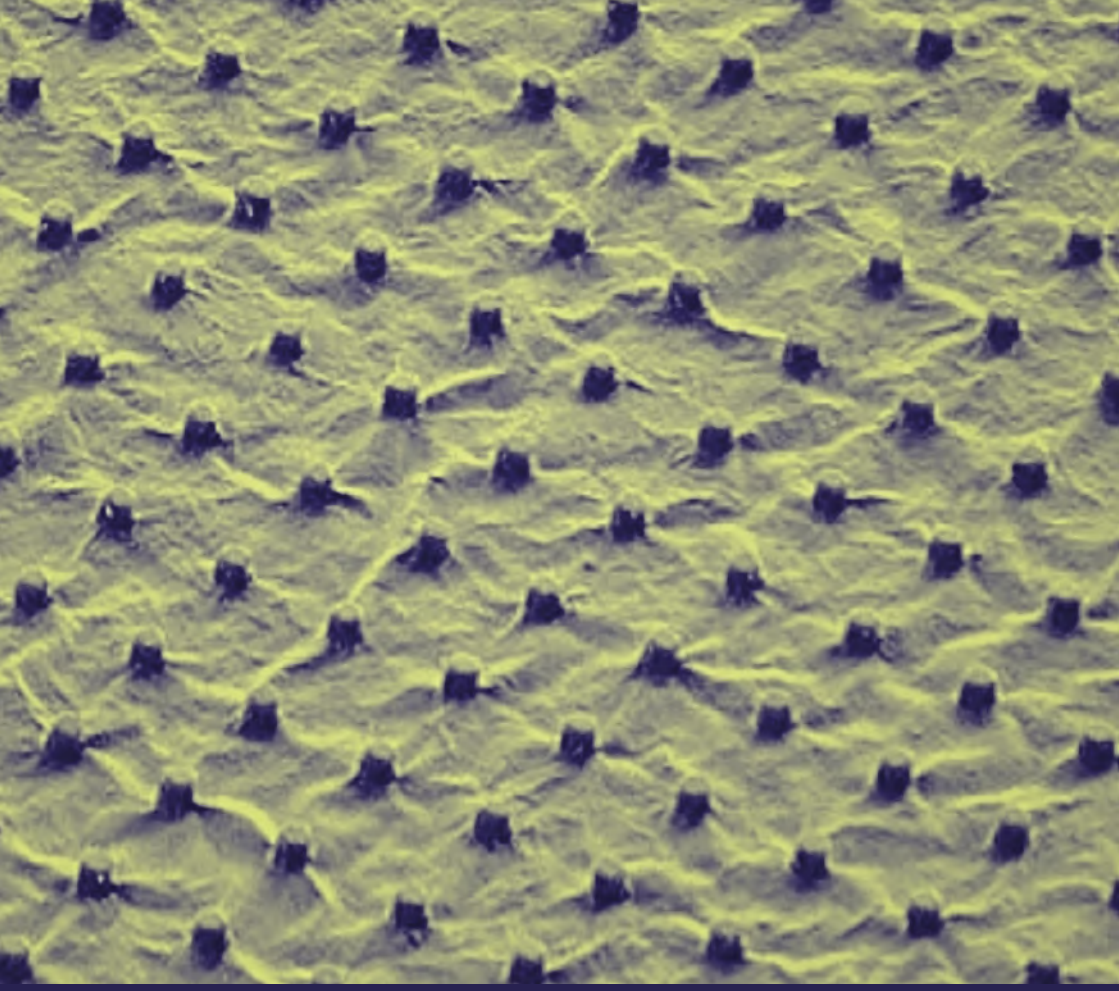

Highlights
-
Surfaces and interfaces: nanofabrication, imaging, and spectroscopy

"Surfaces and Interfaces: nanofabrication, imaging, and spectroscopy" focuses on advanced materials and devices for the green and circular economy, spanning energy harvesting, sensing, electronics, and bio-related interdisciplinary applications. The investigated materials and systems are the result of the combined synergy of theoretical and experimental efforts to design and develop advanced materials. Properties and device functionalities are predicted by first principle methods, realized through advanced deposition and nanofabrication methods and investigated using state-of-the-art spectroscopies and microscopies in on-site laboratories and through collaborations at important large-scale facilities. An important contribution to the advancement of properties and imaging comes from the use of Artificial Intelligence and machine learning to obtain rapid, cost-effective, high-throughput, and statistically significant analysis.

A great effort has been made to overcome fundamental limits in **nanoscale imaging and spectroscopy**, essential for discovering and understanding new material properties. A key demonstration was the first experimental realization of orbital-angular-momentum-resolved electron energy-loss spectroscopy in transmission electron microscope performed with the use of custom-designed electrostatic sorter. This method unlocks symmetry-resolved spectroscopy, paving the way for atomic-scale mapping of orbital and magnetic properties. A second aspect is the overcome of the limits of TEM investigation, exploiting artificial intelligence and numerical simulations. The latter have been implemented to overcome resolution limits imposed by lens aberrations, without requiring costly hardware correctors. Another important aspect is the use of advanced spectroscopies for the study of dynamics of materials, investigating for example the ultrafast electronic and atomic structural evolution following photoexcitation, which are essential for the rational optimization of the efficiency of materials for photocatalytic and energy conversion applications.

AI-assisted workflows have an increasing importance for material science. They automate the analysis of TEM data, from image processing to crystallographic mapping and strain analysis, reducing multi-day manual processes to minutes and enabling predictive multiphysics simulations of device behaviour with impact on transport and qubit-relevant properties. Machine learning has also been applied using a custom workflow to automatically study droplet microfluidics, in channels fabricated by digital light processing. This provides critical insights for optimizing microchip design for applications in cellular transport and tissue engineering.

One of the core activities of this section is the design and synthesis of **novel functional materials** for high-impact applications, from next-generation electronics to sustainable and biomedical technologies. One route has addressed the dual challenge of developing advanced magnetic nanostructures while adhering to the ecological principles of the circular economy and waste reduction by exploiting films of organic radicals via a sustainable fabrication process, easily selectively removed using only distilled water, restoring substrates to pristine condition for reuse. In the same direction, high-performance biodegradable piezoelectric devices made by natural cellulose nanocrystals achieved record-setting performance and their biocompatibility opens pathways for implantable, self-powered medical devices.

2D Materials like graphene intercalated with metals like platinum or gallium led to the formation of elusive phases predicted to be 2D superconductor, a significant target in materials science for sensing and energy storage. Besides graphitic nanodiamonds have been investigated for humidity-resistant low-friction coatings, demonstrating to promote a stable tribolayer that maintains high performance even in humid, ambient conditions.

[OA] *in the References indicates an Open Access publication.*

Demonstration of angular-momentum-resolved electron energy-loss spectroscopy

We report the first experimental realization of orbital–angular-momentum-resolved electron energy-loss spectroscopy (OAM-EELS) in a single acquisition by integrating an electrostatic OAM sorter into a transmission electron microscope. In hexagonal boron nitride, we resolve the π* and σ* transitions at the B K-edge, identifying their distinct OAM signatures in accordance with dipole selection rules. This method enables symmetry-resolved spectroscopy and paves the way for orbital and magnetic studies at the atomic scale.

Rotational symmetry plays a fundamental role in determining selection rules for atomic transitions probed by electron energy-loss spectroscopy (EELS). We demonstrate the first experimental realization of orbital-angular-momentum-resolved EELS (OAM-EELS) using a transmission electron microscope equipped with a custom-designed electrostatic OAM sorter. The experiment focuses on the B K-edge of hexagonal boron nitride (h-BN), characterized by π* and σ* antibonding orbitals with distinct angular momentum projections m.

The experimental configuration utilizes electrostatic phase elements performing a log-polar conformal transformation, converting OAM phase into a measurable linear coordinate. A 300 kV TEM with convergence semi-angle of 5.4 mrad was employed to minimize angular aberrations. The resulting 2D spectrum encodes energy-loss and OAM information simultaneously. Intrinsic OAM spectral components were retrieved through deconvolution of the point spread function derived from the zero-loss peak and model-based multiple linear least squares fitting (Fig. 1).

The extracted spectrum reveals distinct profiles for π* and σ* transitions with onset at ~192 eV and ~198 eV, respectively. The π* feature centres at 0 ħ, while σ* shows maxima at ±1 ħ, consistent with dipole selection rules. Comparison with multislice simulations confirms the delocalization role in broadening experimental OAM spectra. Monte Carlo modeling demonstrates that off-axis atomic excitations contribute incoherently, leading to intrinsic spread beyond expected discrete values.

Our analysis shows that observed OAM broadening stems principally from intrinsic delocalization of inelastic scattering. This technique enables post-selection of specific angular momentum channels, offering unprecedented access to symmetry-resolved spectroscopy at the nanoscale. Applications extend to orbital mapping, magnetic dichroism experiments, and multipolar transition analysis, potentially transforming our ability to interrogate local electronic structure with atomic resolution.

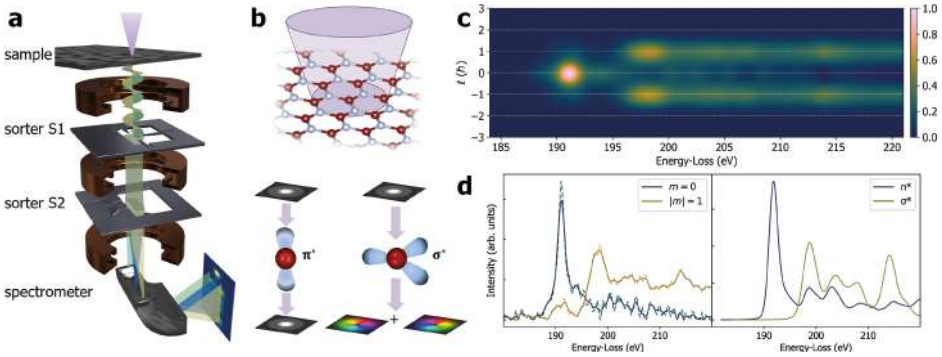

Fig. 1
(a) Experimental setup for OAM-EELS double dispersion. (b) Sketch of electron beam illumination on h-BN (top) and the electron wavefunction after single scattering on boron (bottom). (c) Experimental OAM-EELS after model-based fitting to remove de-localization and point spread function of the sorter. (d) Experimental EEL spectra (left) and corresponding theoretical spectra from ab-initio DFT (right).

Contact persons
Giovanni Bertoni (giovanni.bertoni@nano.cnr.it)
Vincenzo Grillo (vincenzo.grillo@nano.cnr.it)

References
[1] Demonstration of angular-momentum-resolved electron energy-loss spectroscopy. A. H. Tavabi, P. Rosi, G. Bertoni, E. Rotunno, L. Belsito, A. Roncaglia, S. Frabboni, G. C. Gazzadi, E. Karimi, P. Tiemeijer, R. E. Dunin-Borkowski, and V. Grillo. Nature Communications 16, 1067 (2025). [OA]
[2] Three-dimensional Stacking of Phase Plates for Advanced Electron Beam Shaping. G. Ruffato, M. Beleggia, A. H. Tavabi, E. Rotunno, L. Viani, P. Rosi, P. H. Kavkani, C. Chiari, S. Frabboni, G. C. Gazzadi, G. Pozzi, G. Bertoni, P. Tiemeijer, R. E. Dunin-Borkowski, and V. Grillo. Microscopy and Microanalysis 31, ozae108 (2025). [OA]

Projects

HORIZON-INFRA-2022-TECH-01, IMPRESS, project nr. 101094299.
H2020-INFRAIA-2018-2020, ESTEEM3, project nr. 823717.
H2020-FETOPEN-2016-2017, Q-SORT, project nr. 766970.
H2020-FETOPEN-2018-2020, SMART-electron, project nr. 964591.
Next Generation EU PNRR, iENTRANCE@ENL, project nr. IR0000027.

Achieving chemical recognition, recycling, and circularity with radical nanostructures

In this work, we investigated 3D magnetic nanostructures composed of 4,4'-dicyano-2,2′-biphenylene-fused tetrazolinyl (BFTZ) - an organic radical, chemically stable and thermodynamically robust, that allows thin film processing and growth on interdigitated Au-SiO_2 hybrid substrates. We demonstrated the ability to: (1) grow radical nanostructures that retain their magnetic properties, (2) adjust their morphology and size, (3) selectively remove nanostructures from specific substrate regions using distilled water, and (4) return substrates to their pristine conditions, making them reusable after washing, in line with the principles of circular economy.

The rapid proliferation of electronic devices has led to a critical surge in global electronic waste, creating an urgent need for sustainable materials and manufacturing processes. Simultaneously, the field of 3D nanomagnetism is advancing spin-based technologies, but it relies heavily on inorganic materials, leaving organic molecules almost underexplored despite their potential for flexibility and low cost. This work addresses the dual challenge of developing advanced 3D magnetic nanostructures while adhering to the ecological principles of the circular economy and waste reduction. In a joint theoretical-experimental work in collaboration with University of Tübingen, we fabricated 3D nanostructures using a stable organic radical (4,4'-dicyano-BFTZ) deposited on interdigitated Au-SiO_2 hybrid substrates. Our study, which combines X-ray photoemission spectroscopy, classical molecular dynamics (MD), and simulations from first principles, demonstrates that the morphology of these structures can be precisely tuned through chemical recognition of the substrate (Fig. 1): radicals grow as vertical nanorods on silicon dioxide (driven by physisorption) and as uniform films or pillars on gold (driven by chemisorption). Crucially, the radicals retain their magnetic properties in these assemblies. In designing and carrying out the fabrication process, we established a green recycling protocol, proving that distilled water can selectively remove the nanostructures—cleaning gold regions faster due to a catalytic effect—and restore the substrates to their pristine condition for reuse without damage. We demonstrated the possibility of merging high-tech organic spintronics with sustainability through the replacement of toxic chemicals and single-use components with a "green" fabrication cycle. This allows for the preservation of expensive micro-patterned substrates and offers a new degree of control over magnetic nanostructure growth via substrate roughness and chemical composition.

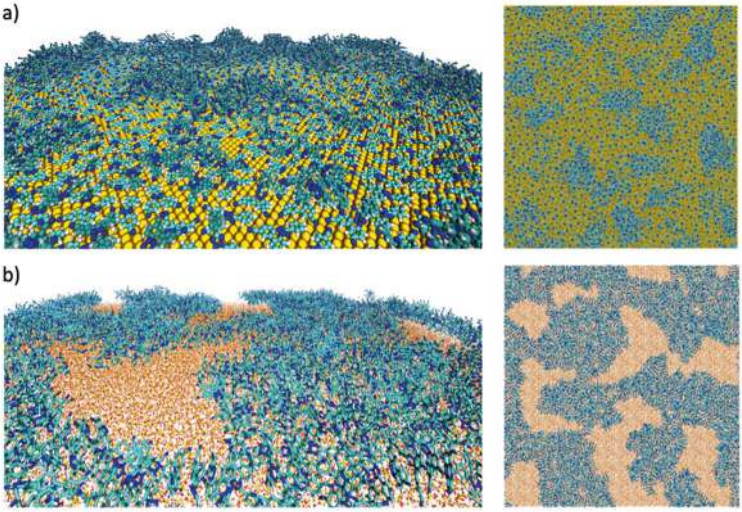

Fig. 1
Side (left) and top (right) view of the final snapshots of the MD simulations relative to the deposition of 4,4'-dicyano-BFTZ radical on (a) Au(111) and (b) a-SiO_2 substrates. Adapted from [1].

Contact persons
Arrigo Calzolari (arrigo.calzolari@nano.cnr.it)

References
[1] Achieving Chemical Recognition, Recycling, and Circularity with Radical Nanostructures. A. Das, E. M. Nowik-Boltyk, T. Junghoefer, E. Nadler, F. Gity, P. K. Hurley, Z. Yang, A. Rajca, F. Tavanti, A. Calzolari, and M. B. Casu. Adv. Funct. Mater. 35, 04323 (2025). [OA]

Managing of complex fluids by light-based additive manufacturing

Droplet microfluidics is widely used in nanomaterial synthesis, photonics, drug delivery, and regenerative medicine. Advances in artificial intelligence and additive manufacturing enable improved flow simulation, droplet monitoring, and device design [1]. We study water-in-oil droplets in various flow-focusing microchannel geometries fabricated by digital light processing. Machine learning analyzes droplet deformation, size, and structure relative to geometry and flow conditions, offering insights for microchip design and other flow parameters. The findings yield valuable insight for the development of microchips for use in cellular transport and tissue engineering.

A flow-focusing microfluidic junction was engineered to generate water-in-oil (W/O) emulsion droplets and coupled to expansion channels with opening angles (α) of 30°, 45°, 60°, and 90° (Fig. 1a-e) [2]. Devices were fabricated by digital light processing (DLP, Fig. 1b) and subsequently sealed by UV-assisted bonding. To produce W/O emulsions, Tween®20 and Brilliant Black were dissolved in de-ionized water to act as surfactant and pigment, respectively, with the dye enhancing visualization of droplet formation and packing. Flow rates of the dispersed and continuous phases were precisely regulated using a twin syringe pump, while droplet dynamics were recorded through a stereo microscope equipped with a 3000-fps high-speed camera. Droplet characterization was carried out using a machine-learning workflow, which was developed by our collaborators at the Istituto per le Applicazioni del Calcolo (CNR-IAC, Rome) and Istituto Italiano di Tecnologia [Eur Phys J E Soft Matter. 46, 32 (2023)]. The custom DropTrack software integrates YOLO and DeepSORT algorithms to automatically detect and track droplets across frames, providing bounding-box dimensions (Fig. 1f). This enabled quantitative evaluation of droplet deformation, size, and structural rearrangement within the expanding microchannel (Fig. 1f). Droplet deformation was quantified through the aspect ratio (width/height) extracted from DropTrack detections. Analysis across a range of water and oil flow rates revealed that increasing α generally leads to reduced droplet deformability (Fig. 1g). As droplets move through the main channel, they undergo shape deformation due to hydrodynamic interactions and spatial confinement. The maximum deformation typically occurs near the entrance of the expansion region, where crowding effects are strongest, and progressively decreases downstream as droplets attain a more relaxed configuration. Data of Fig. 1g reflects the weaker confinement in wider expansions. Further analysis revealed the spatial arrangement of droplets [2] and enabled precise shape characterization [3].

Overall, this study highlights how channel geometry and injection conditions modulate droplet behaviour and demonstrates the utility of machine learning for rapid, cost-effective, and high-throughput quantification of droplet size distribution, deformation, and packing dynamics.

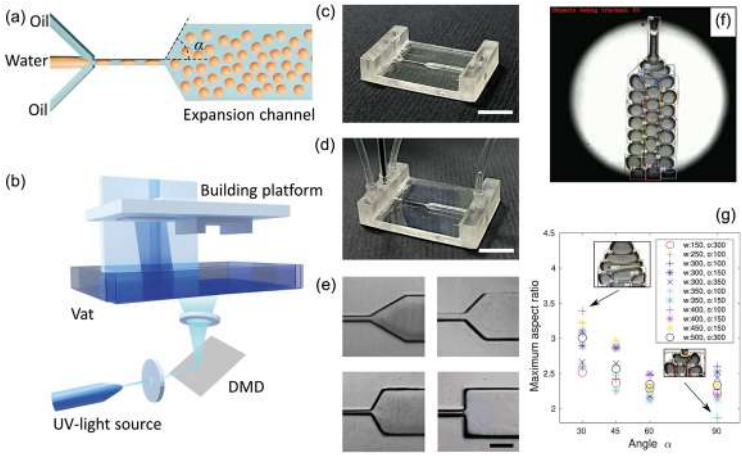

Fig. 1
(a) Schematic illustration of the flow-focusing junction and the expansion channel. (b) Representation of DLP 3D printing system. (c, d) Photographs of the printed device. Scale bars: 9 mm. (e) Optical micrographs of the inlet of the expansion chamber with α: 30°, 45°, 60°, and 90°. Scale bar: 1 mm. (f) Example of the DropTrack output. Each droplet is marked by a labelled box. (g) Aspect ratio of droplets for different microchannel geometries. The aspect ratio is defined as the ratio of the droplet's width to its height. The inset labels display the injection rates of water (w) and oil (o) in µl/min. The images show droplets at maximum (top) and minimum (bottom) deformation for two distinct values of α. Reproduced under the terms of the Creative Commons Attribution License from [2]. © 2024 The Authors. Published by The American Institute of Physics.

Contact persons
Sibilla Orsini (sibilla.orsini@nano.cnr.it)
Andrea Camposeo (andrea.camposeo@cnr.it)

References
[1] 3D printing and artificial intelligence tools for droplet microfluidics: Advances in the generation and analysis of emulsions. S. Orsini, M. Lauricella, A. Montessori, A. Tiribocchi, M. Durve, S. Succi, L. Persano, A. Camposeo, and D. Pisignano. Appl. Phys. Rev. 12, 011306 (2025).
[2] Measuring arrangement and size distributions of flowing droplets in microchannels through deep learning using DropTrack. M. Durve, S. Orsini, A. Tiribocchi, A. Montessori, J. M. Tucny, M. Lauricella, A. Camposeo, D. Pisignano, and S. Succi. Physics Fluids 36, 022105 (2024). [OA]
[3] Minimal droplet shape representation in experimental microfluidics using Fourier series and autoencoders. M. Durve, J. M. Tucny, S. Orsini, A. Tiribocchi, A. Montessori, M. Lauricella, A. Camposeo, D. Pisignano, and S. Succi. Physics Fluids 36, 112005 (2024).

Projects
Next Generation EU PNRR, THE, project nr. ECS_00000017.

Increasing the resolution of transmission electron microscopy by computational ghost imaging

By means of numerical simulations, we have demonstrated the innovative use of computational ghost imaging in transmission electron microscopy to retrieve images with a resolution that overcomes the limitations imposed by coherent aberrations. By using a simple 8-electrode device as a specific example, a twofold increase in resolution beyond the aberration limit is expected to be possible under realistic experimental conditions. Early experimental data are also shown.

The primary limitation to achieving high lateral resolution in Transmission Electron Microscopy (TEM) is not the probe wavelength but aberration. Rotationally symmetric lens systems possess an unavoidable positive spherical aberration. Costly aberration correctors can then be eliminated through computational means. If the imaging system is coherent, the high-resolution information is retained despite aberrations, making retrieval possible using techniques like holography or ptychography.

In our activity on Computational Ghost Imaging (CGI), the innovative approach demonstrated by numerical simulations is to overcome aberration-imposed limits: spatial information is inferred through the structuring of the probing beam and the massive use of computation, without a camera. The method requires measuring the intensity using a single-pixel detector (such as an annular dark-field detector or X-ray signals) in response to a series of known, different structured illuminations. Aberrations are incorporated into the reconstruction scheme.

A challenge of structuring the probe is afforded by microelectromechanical systems (MEMS)-based electron modulator in which our group is world leader. The modulator generates these necessary high-frequency intensity oscillations in the probe. Simulations using a twisted bilayer confirmed the efficacy. For a STEM with resolution 1.5, the CGI reconstruction, computed using a larger convergence semiangle, achieved a resolution of 0.8 Å or less: a twofold increase in resolution beyond the aberration limit.

The current experimental results in figure are, for the moment, limited to a resolution of 0.5 nm. This limitation is mainly due to the limited precision we have in describing the probe because of the limitation of the post specimen imaging system. For this reason, we are planning to use the structured ptychography to reconstruct the probe, with a reciprocal advantage of the two techniques.

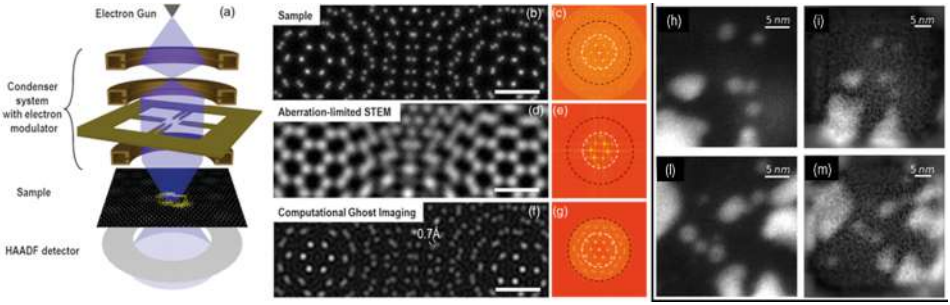

Fig. 1
Left: Scheme of the modulation and detection with different structured probes where (a) MEMS modulator in the condenser is modifying the beam shape on the sample while overall intensity is collected on a HAADF detector. The sample of twisted bilayer with a projected potential as in (b). It is compared with aberration limited STEM imaging (d) and with the theoretical CGI reconstruction (f) that is clearly better approximating the ideal potential in (b). Right: Examples of experimental ghost imaging and medium resolution of gold particles (bright objects) on carbon (h, l) along with the standard STEM image of the same area (i, m).

Contact persons
Vincenzo Grillo (vincenzo.grillo@nano.cnr.it)
Enzo Rotunno (enzo.rotunno@nano.cnr.it)

References
[1] Increasing the Resolution of Transmission Electron Microscopy by Computational Ghost Imaging. P. Rosi, L. Viani, E. Rotunno, S. Frabboni, A. H. Tavabi, R. E. Dunin-Borkowski, A. Roncaglia, and V. Grillo. Phys. Rev. Lett. 133, 123801 (2024). [OA]

Projects
MUR PRIN 2022, AI-TEM, project nr. 2022249HSF.

Ultrafast dynamics of photoinduced polaron formation in cerium oxide

The dynamic evolution of the electronic and atomic structure in photoexcited cerium oxide films is investigated using pump–probe X-ray absorption spectroscopy at the Ce L_3 edge, covering both the near-edge and extended energy regions, at the European X-ray free-electron laser. The results show an ultrafast relaxation within the first few hundred femtoseconds, followed by the formation of a long-lived excited state accompanied by a structural distortion, consistent with the generation of photoinduced small polarons. Constrained density functional theory simulations provide detailed insight into the electronic rearrangements and lattice distortions in the photoexcited material.

Pump-probe X-ray absorption spectroscopy (XAS) using X-ray free-electron lasers (XFELs) offers element-specific insights into the ultrafast processes occurring in photocatalysts following photoexcitation, which are essential for the rational optimization of the efficiency of these materials. Cerium oxide is widely used as a catalyst or photocatalyst, due to its ability to undergo reversible Ce^{3+}/Ce^{4+} redox transitions, enabling oxygen vacancy formation and annihilation.

The dynamics of photoexcitation in cerium oxide are investigated using ultrafast pump-probe X-ray near-edge spectroscopy (XANES) and extended energy range X-ray absorption fine structure (EXAFS) at the Ce L_3 edge at the FXE instrument of the European XFEL facility, simultaneously probing the ultrafast electronic and local atomic structure modifications (Fig. 1). The analysis of transient XANES (Fig. 1b) shows that in the first few tens of femtoseconds, the electronic structure undergoes modifications that are compatible with a transient occupation of Ce 4f states. Within approximately 500 femtoseconds, the electronic structure partially relaxes to a metastable photoexcited state with a lifetime of the order of hundreds of picoseconds. The analysis of transient EXAFS (Fig. 1d) identifies a structural distortion of about 0.14 Å in the first O coordination shell around the excited Ce atom, occurring on the same timescale as the partial relaxation of the electronic structure, consistent with the formation of a photoinduced small polaron state.

Constrained DFT simulations of cerium oxide – in which an excited electron occupies the Ce 4f band, while the hole resides within the O 2p valence band - offer insights into the electronic modifications and the structural distortions in the photoexcited material. The formation of a polaronic state via lattice distortion induced by the localization of the excited electron on a Ce atom – which acquires Ce^{3+} spin-polarized character – is observed (Fig. 2). The calculated Ce—O bond elongation is 0.08 Å, in fair agreement with the experimental value.

Fig. 1
Ce L_3-edge XAS: (a) steady-state XANES; (b) transient XANES; (c) steady-state EXAFS; (d) transient EXAFS. The transient XANES and EXAFS spectra, shown for the same delay times, were acquired using a pump of 267 nm wavelength, that excites cerium oxide above the band gap.

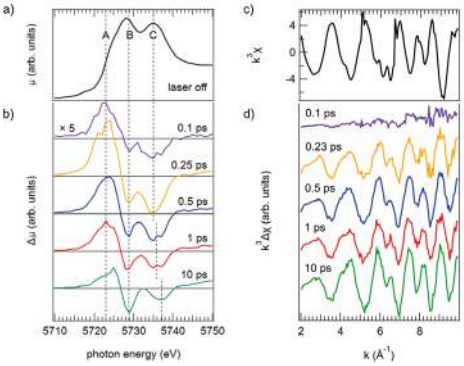

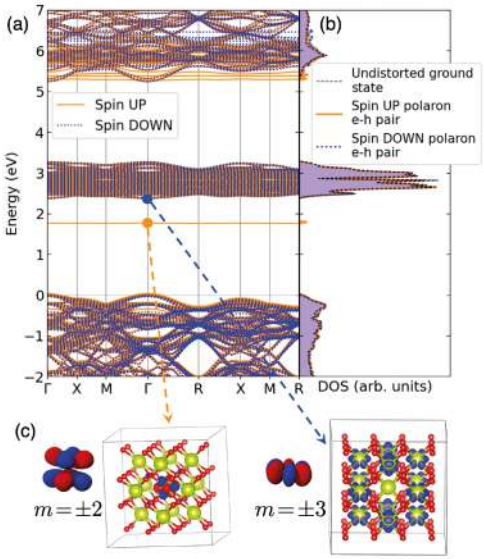

Fig. 2
(a) Calculated constrained DFT+U band structure of CeO_2 hosting an electron-hole pair. The polaronic Ce^{3+} level is 0.57 eV below the unoccupied f-band. (b) Calculated spin-polarized density of states of the distorted CeO_2 structure. (c) Left: real-space representation of the electronic wave function for the Ce^{3+} polaronic level, showing strong electronic localization (corresponding to a f atomic orbital with m=±2). Right: Real-space representation of the electronic density at the bottom of the unoccupied f band, delocalized on the remaining Ce^{4+} atoms (corresponding to f atomic orbitals with m=±3). Ce atoms are displayed in yellow and O atoms in red.

Contact persons
Paola Luches (paola.luches@nano.cnr.it)
Fulvio Paleari (fulvio.paleari@nano.cnr.it)

References

[1] Ultrafast Dynamics of Electronic and Structural Modifications Induced by Photoexcitation in Cerium Oxide. S. Pelatti, E. Spurio, D. Catone, P. O'Keeffe, S. Turchini, G. Ammirati, F. Paleari, D. Varsano, S. Benedetti, A. di Bona, S. D'Addato, Y. Jiang, P. Zalden, Y. Uemura, H. Wang, D. Vinci, X. Huang, F. Lima, M. Biednov, D. Khakhulin, C. J. Milne, F. Boscherini, and P. Luches. Adv. Electron. Mater. 11, e00429 (2025). [OA]

Projects

MUR PRIN 2022 PNRR, e-DYNAFOX, project nr. 2022YXJ55F.
MAECI Italy-Germany joint project, U-DYNAMEC.
MUR PRIN 2022 PNRR, ResET, project nr. P2022ZHCT3.

Carbon-based nanostructure engineering for robust and humidity-resistant ultralow friction in DLC coatings

Diamond-like carbon (DLC) coatings exhibit very low-friction performance in dry or inert environments after functionalization with graphene and carbon nanoparticles. This is partly due to the in-operando formation of nanoscroll-like carbon structures—diamond cores wrapped by graphitic layers—as shown in a first study performed on industrial, rough DLC substrates. Here we show that graphitic nanodiamonds (Gr-NDs), i.e., nanoparticles which intrinsically possess a similar core-shell arrangement, enable humidity-resistant ultralow friction. Their integration promotes a stable graphitic tribolayer, offering a scalable solution for ambient-condition lubrication.

Diamond-like carbon (DLC) coatings are widely used in mechanical components thanks to their hardness, chemical stability, and excellent low-friction behavior under dry or inert conditions. A key factor behind this performance is the formation of ordered carbon arrangements generated during sliding. In a first study on industrial DLC with intrinsic multiscale roughness, we showed that carbon nanostructures can trigger the development of nanoscroll-like architectures—diamond-like nuclei wrapped by graphitic sheets—leading to ultralow friction even on non-polished, industrially relevant substrates [1]. This was a significant step forward, since earlier demonstrations of nanoscroll-mediated lubrication relied on ideal, atomically smooth samples.

Building on this insight, we investigated nanoparticles that intrinsically replicate such core-shell features. Graphitic nanodiamonds (Gr-NDs), composed of a rigid sp^3 core and few-layer graphitic shells, were selected as candidates capable of reproducing nanoscroll-like behaviour in a controlled manner. Their structural affinity with DLC tribolayers made them suitable for addressing a long-standing limitation: the degradation of frictional performance in humid environments.

When applied to industrial DLC, Gr-NDs enable humidity-resistant ultralow friction [2]. During sliding, they integrate into the contact and promote the formation of a robust graphitic tribolayer. TEM and Raman analyses show that Gr-NDs act as nucleation sites for ordered carbon restructuring. Moreover, tribochemical oxidation on the graphitic shell further stabilizes the tribolayer under ambient humidity, while the diamond core remains intact.

This results in a reproducible coefficient of friction below 0.1 even in moist atmospheres—an uncommon achievement for carbon-based lubricants, which typically lose efficiency in the presence of water. The use of scalable nanostructures and real industrial substrates strengthens the technological relevance of this strategy. Overall, these results outline a coherent research pathway: elucidating nanoscale mechanisms governing dry ultralow friction and translating them into a humidity-tolerant lubrication concept based on intrinsically core-shell carbon nanoparticles.

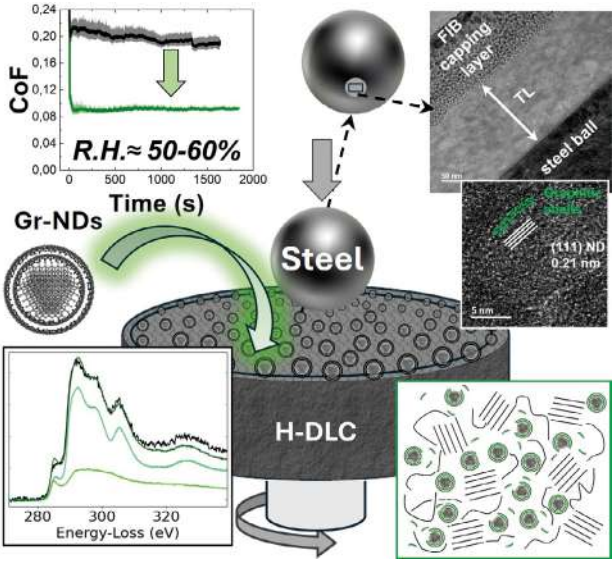

Fig. 1
Schematic overview of the mechanisms enabling humidity-resistant ultralow friction on DLC coatings functionalized with graphitic nanodiamonds (Gr-NDs). The friction-reduction plot under 50–60% relative humidity highlights their tribological effect. The core–shell structure of Gr-NDs is shown, with a diamond core wrapped by graphitic layers. During sliding, the nanoparticles integrate into the contact region and promote the formation of a stable tribolayer, as confirmed by cross-sectional TEM and high-resolution imaging. EELS analysis supports the presence of Gr-NDs within the tribolayer, with fitted spectra revealing contributions from the nanoparticles and a minor amount of amorphous carbon. The schematic illustrates the resulting carbonaceous tribolayer, where intact Gr-NDs and oxidized graphitic fragments stabilize the interface under ambient humidity.

Contact persons
Andrea Mescola (andrea.mescola@nano.cnr.it)
Guido Paolicelli (guido.paolicelli@nano.cnr.it)

References
[1] Synergistic effect of graphene and nanodiamonds to achieve ultra-low friction on rough DLC coatings. A. Mescola, A. Lodi, F. Zanni, A. Rota, A. Gerbi, C. Bernini, M. Schott, L. Repetto, A. Camisasca, S. Giordani, R. Buzio, and G. Paolicelli. Diamond and Related Materials 145, 111149 (2024). [OA]
[2] Humidity-resistant ultralow friction in diamond-like carbon coatings enabled by graphitic nanodiamonds. A. Mescola, G. Bertoni, G. C. Gazzadi, M. Bartkowski, A. Camisasca, S. Giordani, R. Buzio, and G. Paolicelli. Small Structures 6, 2500236 (2025). [OA]

Projects
Next Generation EU PNRR, ECOSISTER, Spoke 3 ECS_00000033.

Energy harvesting by nanostructuring piezoelectric nanocomposites

Enhancing the piezoelectric performance of natural, biocompatible polymers and integrating them into complex electronic systems hold great potential for (self-)powered devices, with applications spanning healthcare monitoring, sensing, and soft robotics. Techniques such as micro/nano-structuring, organic filler composites, and electrospun nanofiber networks are used. We present scalable assemblies of cellulose nanocrystals within multilayered piezoelectric polymer systems exhibiting excellent responsiveness. Sub-micrometer patterning of the nanocomposite yields record output power and pressure sensitivity to gentle touch, paving the way for flexible, biodegradable, and implantable devices.

With the increasing global emphasis on sustainability, developing biodegradable and biocompatible materials for electronics and medical devices is now crucial for technological advances. We address such challenge by showing piezoelectric devices from natural, biodegradable materials yielding record-setting power and pressure sensitivity.

Many natural materials originating from biological systems show piezoelectric properties and offer biocompatibility and biodegradability, as well as mechanical flexibility. These properties make them well-suited for electromechanical interfacing with biological and soft systems in sensing, tissue engineering, stimulation, and energy harvesting.

We used rod-like nanocrystalline cellulose (CNCs) from natural cellulose as key piezoelectric component. CNCs are promising as for their intrinsic piezoelectric properties and can potentially enable the fabrication of biocompatible and biodegradable devices. Still, their application in devices is challenging due to difficulties in aligning and organizing them across large surfaces to enhance piezoelectric performance. Indeed, they tend to lie flat in thin films, generating in-plane polarization and weak out-of-plane response. Hierarchical fabrication schemes can be used by a combination of chemical and physical strategies, to enhance their out-of-plane piezo-response [1].

CNCs were incorporated into a polyvinyl alcohol (PVA) matrix and structured into sub-micrometric architectures using soft-imprint lithography. This approach helped vertical alignment and out-of-plane deformation under applied pressure, improving electromechanical coupling and enhancing piezoelectric response, when embedded in multi-stacked metal-polymer-metal structures. Such flexible, fully biodegradable devices attained record output power density of up to 0.6 $\mu W/cm^2$ and a pressure sensitivity of 4.2 V/kPa within the gentle touch range. Biocompatibility with cell lines from different tissues have been proved and packaged bioresorbable devices deliver consistent outputs when implanted on the epicardium of swine hearts [2].

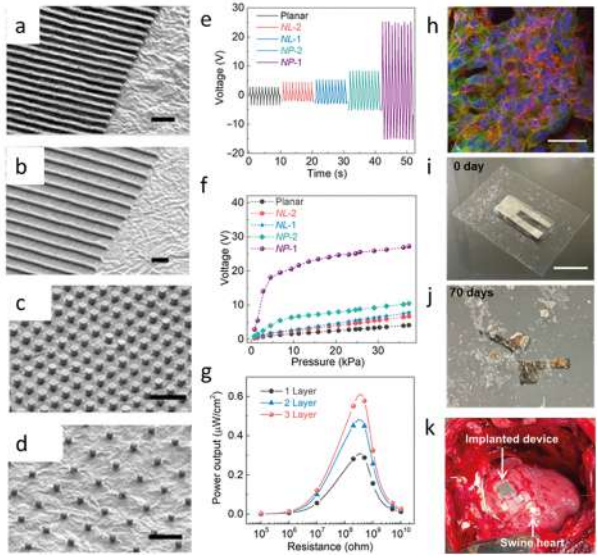

Fig. 1
(a, d) SEM micrographs of sub-micrometer CNCsPVA patterns (lines and pillars). Scale bars 2μm. (e, f) Voltage and corresponding pressure response curves of device with nanopatterned CNCsPVA. (g) Power output, measured by different resistance loads. (h) Confocal micrograph of HL-1 cells cultured for 3 days on the CNCsPVA device and immunostained for nuclei (blue), tubulin (green), and actin fibers (red). Scale bar 25 μm. Photographs showing the biodegradable device in the buffered solution at 37°C taken at (i) day 0 and (j) day 70. Scale bar 2 cm. (k) Photograph of a biodegradable device on the right ventricle of an adult swine heart. Reproduced under the terms of the Creative Commons Attribution License 4.0 (CC BY) © 2025 The Authors. Published by AAAS.

Contact persons
Francesca Matino (francesca.matino@nano.cnr.it)
Luana Persano (luana.persano@nano.cnr.it)

References
[1] Advanced Materials for Energy Harvesting and Soft Robotics: Emerging Frontiers to Enhance Piezoelectric Performance and Functionality. L. Persano, A. Camposeo, F. Matino, R. Wang, T. Natarajan, Q. Li, M. Pan, Y. Su, S. Kar-Narayan, F. Auricchio, G. Scalet, C. Bowen, X. Wang, and D. Pisignano. Adv. Mater. 36, 2405363 (2024). [OA]
[2] Fully biodegradable hierarchically designed high-performance nanocellulose piezo-arrays. S. K. Ghosh, F. Matino, F. L. Favrin, I. Tonazzini, R. D'Orsi, J. G. de la Ossa, A. Camposeo, J. Li, W. Liu, T. A. Hacker, D. Pisignano, A. Operamolla, X. Wang, and L. Persano. Sci. Adv. 11, eads0778 (2025). [OA]

Projects
H2020-MSCA-IF-2019, BIOIMD, project nr. 896811.
Next Generation EU PNRR, PE 2 NEST, project nr. PE00000021.

Artificial Intelligence-assisted workflow for transmission electron microscopy: from data analysis automation to materials knowledge unveiling

We present an automated workflow for holistic (S)TEM data analysis, modelling, and simulation of device heterostructures. The system extracts crystallography, 3D orientation, composition, and strain maps in minutes instead of days, using a physics-guided Artificial Intelligence (AI) to generate representative material descriptions. It produces digital twins of non-periodic systems enabling predictive simulations of device behaviour. Demonstrated on SiGe heterostructures for spin qubits, the workflow connects atomic structure to phononic, electronic, and spin–orbit properties, and its versatility extends across diverse materials, device architectures, and morphologies.

Modern nano- and quantum-devices operate in regimes where small variations in atomic structure lead to large changes in performance. Transmission electron microscopy (TEM) allows resolving these structures with sub-Ångström precision, but interpreting TEM data remains slow, operator-dependent, and difficult to scale. A single cross-section may require days of manual analysis, limiting statistical reliability and slowing the feedback loop between fabrication and device optimisation.

This work introduces an AI-assisted orchestration workflow that coordinates image processing, crystallographic analysis, and physics-based modelling into a coherent, automated pipeline. AI is not used as a black box: it organises and accelerates established microscopy and simulation tools, ensuring traceable, reproducible outputs, while keeping the scientist in the loop.

The workflow (Fig. 1) begins by segmenting the TEM images to identify layers, interfaces, and geometrical motifs. It then extracts the Fourier patterns (FFT) from each region to identify diffraction peaks, which are indexed to determine crystal phase, orientation and local lattice parameters. Low- and high-magnification views are correlated to capture both device-scale geometry and atomic-scale detail. From these inputs, the pipeline performs strain mapping, constructs finite-element mechanical models, and generates atomistic 3D structures with millions of atoms using symmetry-guided reconstruction. These digital twins are finally linked to multiphysics simulations to assess how the measured microstructure impacts transport and qubit-relevant properties.

Applied to Si/Ge heterostructures for quantum-information devices, the workflow condenses multi-day manual analysis into an automated procedure requiring minutes, while broadening the range of extractable physical insights. More broadly, it demonstrates how AI-orchestrated TEM can transform microscopy into a high-throughput, quantitatively reproducible tool, enabling statistically significant studies across materials science, nanotechnology, and quantum engineering.

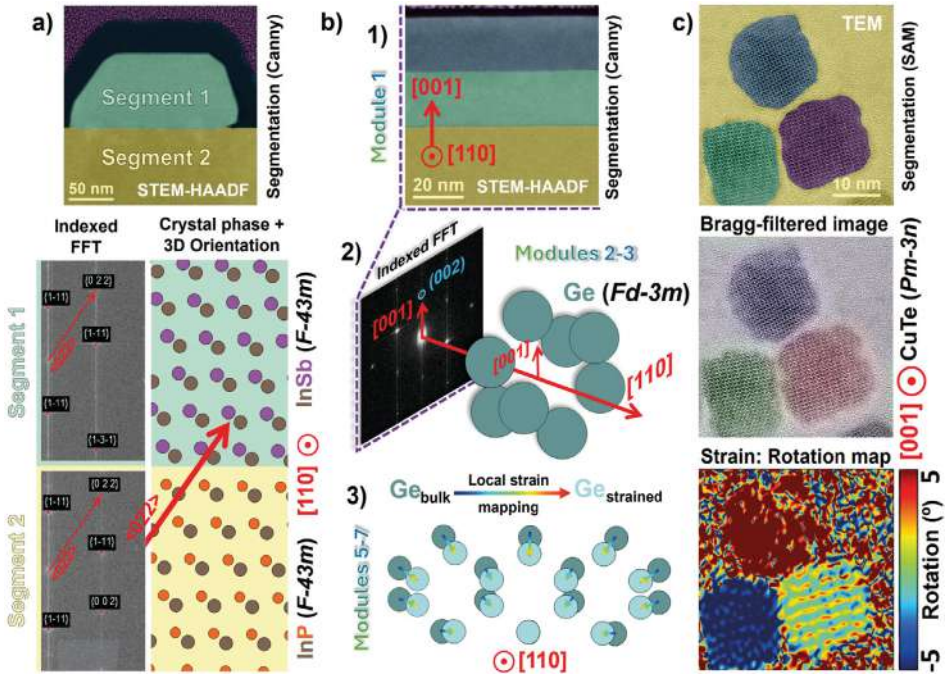

Fig. 1
Automated crystallographic-analysis pipeline applied to heterogeneous TEM datasets. Starting from raw micrographs, the workflow identifies distinct layers and regions (1a, b), extracts their local diffraction patterns (2b), and automatically indexes the corresponding crystal phases and orientations through model–experiment comparison (2a, 3a). The approach is robust across different materials systems: it resolves multiple Si/Ge phases in complex heterostructures (1b) and correctly identifies the Pm-3n symmetry in low-contrast CuTe nanoparticles (1c) among numerous candidate structures. The same information is used to drive automated Bragg filtering and to reveal the spatial distribution of crystal planes and planar defects (2c). The resulting maps provide a consistent, quantitative basis for subsequent strain analysis (3c) and structural modelling (3b).

Contact persons
Enzo Rotunno (enzo.rotunno@nano.cnr.it)
Vincenzo Grillo (vincenzo.grillo@nano.cnr.it)

References
[1] Artificial Intelligence-Assisted Workflow for Transmission Electron Microscopy: From Data Analysis Automation to Materials Knowledge Unveiling. M. Botifoll et al. Adv. Mater. e06785 (2025). [OA]

Projects
HORIZON-INFRA-2022-TECH-01, IMPRESS, project nr. 101094299.

Surface reconstruction and novel 2D materials obtained by metal intercalation in epitaxial graphene

Atom intercalation is a widely utilized technique to develop novel materials for energy applications, catalysis, and sensors. The availability of high-quality 2D materials has advanced this technique, enabling applications and novel 2D materials (gold, lead, tin, etc.). We report on the intercalation of several metals (rubidium, platinum, and gallium) and our results demonstrate great potential to obtain novel structures and 2D materials, also in the perspective of hydrogen storage applications. Gallium intercalation shows the elusive Ga III phase, theoretically expected to be a 2D superconductor, now under investigation.

The availability of wafer-scale epitaxial graphene opens the perspective of large-scale applications and boosts the research of novel materials based on graphene. The metal intercalation in graphene is a fascinating field which spans from electronic devices to energy related materials, to the development of new 2D structures. Indeed, the intercalation in graphene offers many possibilities, which reflects on the surface morphology that we observe by scanning tunneling microscopy (STM). The intercalation of monolayer rubidium reveals the emergence of two different surface reconstructions and a strong n-type doping of the graphene [1]. As an example, the (2x2) reconstruction is shown in Fig. 1a. It is caused by Rb intercalation in between the buffer and monolayer. The separation between graphene and buffer layer increases from 3.5 to 5.8 Å.

Platinum is a relevant material due to its catalytic properties toward hydrogen storage through the spillover mechanism. We have achieved single layer Platinum intercalation at the SiC-buffer layer interface and between mono- and buffer-layer [2], and investigated the hydrogen storage efficiency [3]. Fig. 1b shows the intercalation of Pt monolayer (L1) and bilayer (L2). A zoom in on the moiré pattern with atomic resolution is shown in Fig. 1c.

Confinement heteroepitaxy, obtained by intercalation of atoms, allows for the fabrication of large-area, high quality, two-dimensional sheets of non-exfoliable materials. Moreover, it has the benefit of protecting the materials from oxidation. Investigations on Gallium intercalation have shown different surface reconstructions, with the emergence of the Ga(III) phase [4]. Fig. 2 shows the striped reconstruction generated by Ga(III). Fig. 2b displays an atomically-resolved image of the striped area, showing the rectangular lattice of Ga(III) and the overlying graphene lattice, demonstrating the gallium intercalation. Ga(III) is theoretically expected to be a 2D superconductor. Work is in progress to investigate this feature.

Fig. 1

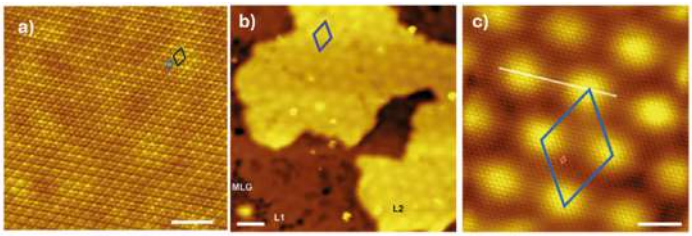

STM topographic images of Rb- and Pt-intercalated regions in monolayer graphene. (a) Atomically resolved STM image showing the Rb (2×2) arrangement together with the graphene lattice, highlighted by black and blue rhombi, respectively. (b) Pt-intercalated graphene with levels L1, L2, and a clean monolayer graphene (MLG) area. The contrast-saturated, approximately rounded, features correspond to Pt-adsorbed clusters. The blue rhombus highlights a unit cell of the Pt-induced moiré in L2. (c) Close-up view of level L2 showing the honeycomb lattice of graphene together with the (12×12) moiré pattern. The two-unit cells are highlighted in blue and red, respectively. Scale bar: (a) 2 nm, (b) 5 nm, and (c) 2nm.

Fig. 2

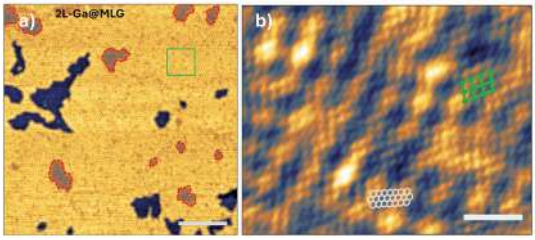

a) STM image (3.0 V, 0.8 nA) of 2L-Ga@MLG in which the striped pattern is imaged. b) Atomically resolved STM image (0.24 V,0.6 nA) in which the stripes, the graphene lattice, and the centered rectangular lattice of Ga(III) are visible. Sketches of graphene and Ga lattices are superimposed to the image. Scale bars in (a) and (b) are 20 and 2 nm, respectively.

Contact persons
Stefano Veronesi (stefano.veronesi@nano.cnr.it)
Stefan Heun (stefan.heun@nano.cnr.it)

References

[1] Rubidium intercalation in epitaxial monolayer graphene. L. Ferbel, S. Veronesi, T. O. Mentes, L. Bußß, A. Rossi, N. Mishra, C. Coletti, J. I. Flege, A. Locatelli, and S. Heun. Nanoscale 17, 12465 (2025). [OA]
[2] Intercalated structures formed by platinum on epitaxial graphene on SiC(0001). L. Ferbel, S. Veronesi, A. Rossi, S. Forti, Y. Vlamidis, C. Coletti, and S. Heun. Carbon 234, 119989 (2025). [OA]
[3] Platinum-decorated graphene: Experimental insight into growth mechanisms and hydrogen adsorption properties. L. Ferbel, S. Veronesi, Y. Vlamidis, A. Rossi, L. Sabattini, C. Coletti, and S. Heun. FlatChem 45, 100661 (2024). [OA]
[4] Novel Structures of Gallenene Intercalated in Epitaxial Graphene. E. Pompei, K. Skibinska, G. Senesi, Y. Vlamidis, A. Rossi, S. Forti, C. Coletti, F. Beltram, S. Rubini, L. Sorba, S. Heun, and S. Veronesi. Small 21, e05640 (2025). [OA]

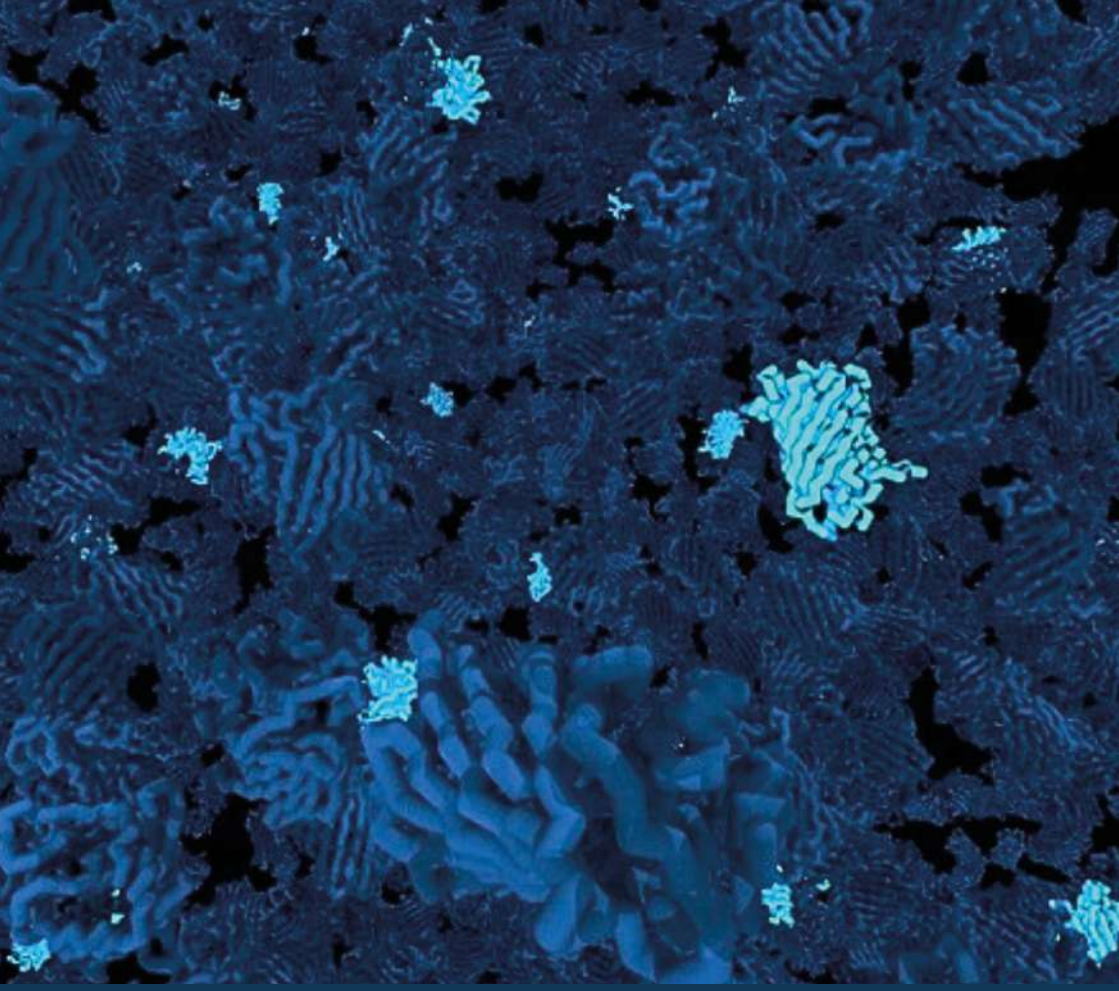

Highlights
-
Nanoscale theory modelling and computation

Theory and modelling lie at the heart of our mission to drive scientific progress, from fundamental principles to transformative applications. Through pioneering approaches, we simulate and understand novel materials and systems before they can be realized in the laboratory. By harnessing quantum mechanics and bridging it with continuum theories, we reveal mechanisms across scales to enable breakthroughs. At the cutting edge of computational science, we create synergy with experiments to accelerate discovery and innovation. Our insights and predictions extend beyond the limits of current technologies, opening new frontiers of knowledge.

Over the past two years, we have achieved remarkable progress across multiple frontiers. Pushing the boundaries of computational science, we have extended the reach and power of our methods through innovations. We accelerated **many-body perturbation theory** for 2D semiconductors and metals, preserving spectroscopic-level accuracy at significantly improved efficiency. We pioneered **dynamical-Hubbard-based functionals** to compute energies and forces, revealing hidden broken-symmetry phases in correlated solids. We advanced **density functional theory beyond its traditional limits** to capture excited states and magnetic phenomena, unveiling elusive double excitations and critical spin-orbit effects. These advances expand the boundaries of computational capabilities and open transformative pathways for discovery.

Tackling some of the most pressing real-world challenges, we have developed advanced descriptors and algorithms to explore vast configurational spaces, integrate complementary computational strategies, and address systems under extreme conditions. These innovations empower us to predict, design, and optimize

complex materials and processes, leading to impactful insights.

We uncovered **resourceful multipartite entanglement** even in common electronic states. We modelled graphene-based systems for hydrogen and carbon dioxide storage to support **sustainable energy solutions**. We discovered magnetic transparent conductors for **emerging spintronic devices**. We elucidated ultrafast vibronic processes in molecules and hybrid interfaces for **next-generation photovoltaics**. We designed aptamer-functionalized gold nanoparticles for innovative **virus detection** enhancing surveillance and pandemic preparedness. We combined advanced spectroscopy with simulations to decode local chemistry in **battery electrodes** for guiding strategies to mitigate capacity fade. Furthermore, we developed a modelling framework that enables the discovery of high-performance **ceramic materials** with potential relevance to aerospace and energy technologies.

The significance, impact, and key publications of our latest achievements are presented in the following highlights. Collectively, these accomplishments underscore our commitment to high-performance computing, quantum technologies, and the discovery of innovative materials. This progress has been powered by strong national and international collaborations and supported by major national and European funding programs (EuroHPC Centre of excellence MaX, PNRR National Centre ICSC, national funded PRIN and PNRR projects).

[OA] *in the References indicates an Open Access publication.*

Graphene-based materials for energy and gas storage

Multiscale computational modelling is used to design and simulate graphene-based materials, including three-dimensional and functionalized architectures, for hydrogen and carbon dioxide storage. By combining atomistic simulations at different levels of theory, this approach clarifies how structural and chemical features govern hydrogen adsorption, chemisorption, and desorption, as well as carbon dioxide adsorption, supporting the design of efficient carbon materials for sustainable energy applications.

Starting from reduced graphene oxide (rGO) and its hydrogenated derivative (H-rGO), we investigated the reversible chemical adsorption of hydrogen, a key process for energy storage and release. Large-scale ReaxFF simulations (over 120 rGO and 480 H-rGO models) revealed that oxygen atoms play a crucial role in tuning the C–H bond stability and desorption barriers, enabling material-controlled reversibility of hydrogen loading [1] (Fig. 1a). Complementary studies on hydrogenated graphene identified distinct desorption pathways, assigning thermal desorption peaks to isolated hydrogen atoms, pairs of neighbouring H in different conformations, and edge sites [2] (Fig 1b). Together, these works provide a quantitative picture of H_2 chemisorption and release mechanisms, offering insights for the design of chemisorption-based hydrogen storage systems and for coupling hydrogen storage with electrochemical energy conversion.

Another research line developed a hybrid top-down/bottom-up workflow to generate realistic three-dimensional graphene-based porous frameworks with controlled density, porosity, and specific surface area [Nanotechnology 32, 045704 (2021)]. This expanding set of models, with varying density and morphology, enables systematic exploration of structure—property relationships. The structures have also been used to train machine-learning potentials for new graphene-based models and to study CO_2 adsorption. The workflow has generated a database of over 5,000 graphene-based porous models spanning a broad range of densities and morphologies (Fig. 1c), and its expansion is ongoing. This dataset is now available as a reference platform to support research on carbon materials for sustainable energy storage.

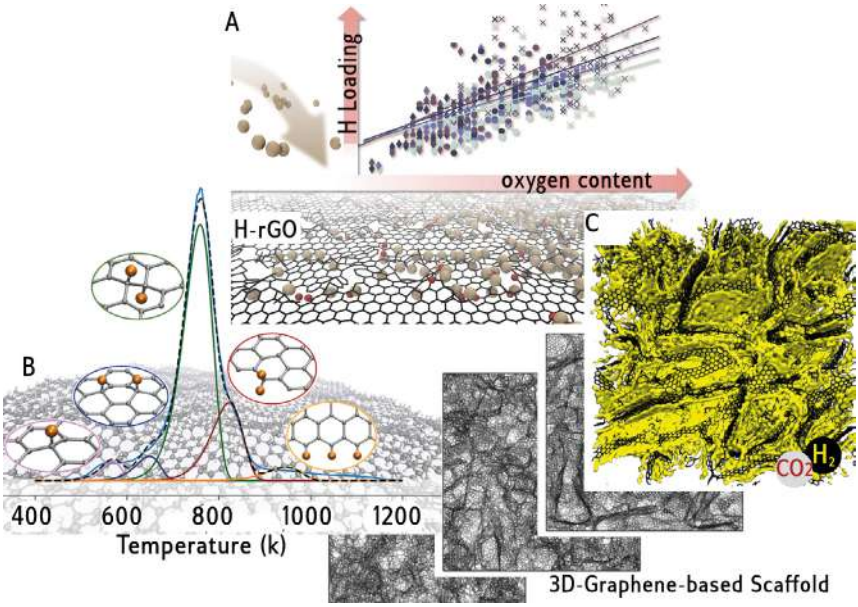

Fig. 1
Multiscale computational models.
(a) Relationship between oxygen/defect content in reduced graphene oxide (rGO) and hydrogen chemisorption, illustrated through large-scale atomistic models and statistically sampled loading trends. (b) Rationalization of Temperature-Programmed Desorption (TPD) features in hydrogenated graphene, with representative local H-binding configurations linked to the corresponding desorption peaks. (c) Three-dimensional graphene-based porous scaffold dataset used to investigate hydrogen and CO_2 adsorption.

Contact persons
Luca Bellucci (luca.bellucci@nano.cnr.it)
Valentina Tozzini (valentina.tozzini@nano.cnr.it)

References
[1] Hydrogen chemisorption capability of reduced graphene oxide membranes. Z. G. Fthenakis, F. Delfino, M. F. Sgroi, V. Tozzini, and L. Bellucci. International Journal of Hydrogen Energy 153, 149925 (2025). [OA]
[2] Multi-methodological analysis of hydrogen desorption from graphene. F. Delfino, C. Ros, S. M. Palardonio, N. M. Carretero, S. Murcia-López, J. R. Morante, J. Martorell, Z. G. Fthenakis, M. F. Sgroi, V. Tozzini, and L. Bellucci. Carbon 227, 119211 (2024). [OA]

Projects
MUR PRIN 2022, CHERISH-C, project nr. 202278NHAM.
Next Generation EU PNRR, CN1 HPC IG-ENI, National Centre for HPC, Big Data and Quantum Computing.

A multiscale framework for DNA-aptamer-functionalized plasmonic nanoparticles

We introduce a computational framework for engineering next-generation viral biosensors. The multiscale pipeline integrates aptamer folding, structural docking, and enhanced molecular dynamics to elucidate how aptamer-functionalized gold nanoparticles recognize viral proteins. Direct comparison of Au_{144} and Au_{314} cores reveals how size, surface chemistry, and ionic environment govern binding stability, providing a basis for the rational design of robust aptamer–nanoparticle constructs.

In the face of growing global threats from flaviviruses, there is an urgent need for diagnostic platforms that are both highly sensitive and specific. We address this challenge by combining aptamer folding predictions, structural docking, and atomistic molecular dynamics in a unified multiscale framework to elucidate aptamer–target recognition at the nanoparticle interface. Focusing on two well-characterized gold nanoclusters (Au_{144} and Au_{314}) functionalized with single-stranded DNA aptamers targeting West Nile virus (WNV), we investigate how nanoparticle size, surface chemistry, and ionic conditions modulate protein binding. To support future work, we developed ad hoc force-field parameters specifically optimized for aptamer-functionalized gold nanoclusters.

We identify a reproducible interaction between residue ADE38 of the single-stranded DNA aptamer and ARG388 within domain III of the WNV E (envelope) protein (in light blue, Fig. 1), supported by additional stabilizing contacts in domain II that together establish a robust multi-point binding mechanism. Ion distribution analyses reveal local electrostatic reorganization upon binding, while diffusion simulations show that aptamer loading strongly impacts nanoparticle mobility, with implications for biosensor sensitivity.

This work represents a step toward developing an aptamer-based diagnostic platform for WNV detection, to be validated through Surface Plasmon Resonance (SPR) measurements in collaboration with F. Petronella and A. Masi at CNR-IC, Rome. The molecular-level insights obtained here will be directly compared with forthcoming SPR data, ensuring a strong correspondence between theoretical predictions and experimental results.

Our computational approach demonstrates that nanocluster size, aptamer flexibility, and surface coverage play key roles in modulating interaction dynamics, providing a generalizable framework for the rational design of plasmonic AuNP–aptamer conjugates, supporting One Health strategies for flavivirus surveillance and pandemic preparedness.

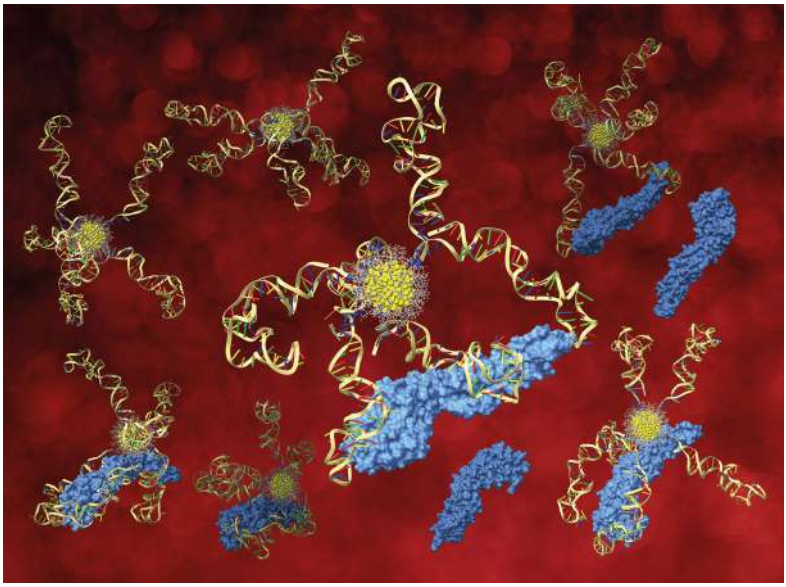

Fig. 1
Atomistic simulations show how the size of gold nanoparticles, the number of DNA single-stranded aptamers attached to their surface, and the surrounding salt conditions affect the way the nanoparticles move, change shape, and recognize viruses. The image illustrates a gold nanoparticle functionalized with DNA aptamers designed to bind the West Nile virus. The viral WNV E protein is shown in light blue, and the DNA aptamer (Tr-WNV-37) is shown in yellow on the nanoparticle surface. The red background represents a blood sample, highlighting the use of this system for virus detection and diagnostics. Image selected as front cover picture in Nanoscale 2025.

Contact persons
Giorgia Brancolini (giorgia.brancolini@nano.cnr.it)

References
[1] Rational design of gold nanoparticles functionalized with aptamers for improved West Nile virus detection. A. Mossa and G. Brancolini. Nanoscale (2025). DOI: 10.1039/D5NR03228H. [OA]

Projects
Next Generation EU PNRR, PE13 INF-ACT, project nr. PE00000007.
CINECA award, MMDTS, project nr. HP10B9RKDH-2023.
CINECA award, RDNPA, project nr. HP10BGP2IY-2025.

Plasmonic high-entropy carbides in extreme conditions

High-entropy ceramics is an emerging class of materials with an ever-growing set of applications, including aerospace and nuclear energy. They stand out for their mechanical properties and thermal stability. Yet, their discovery is hampered by trial-and-error experiments. To accelerate this process, we introduced DEED, a descriptor conceived to capture the balance between entropy gains and enthalpy costs. DEED provides the correct classification of functional synthesizability of multicomponent ceramics. Finally, we demonstrated that many high-entropy carbides have robust plasmonic resonance at room and high (T > 1000°C) temperatures, paving the way for plasmonics in extreme conditions.

High-entropy (HE) ceramics can be transformative for several applications, including aerospace, novel energy, and nuclear fusion reactors. They stand out for their mechanical properties, thermal, and chemical stability, but their development is limited by costly and time-consuming experimental processes. On the theoretical side, the problem of predicting the synthesizability of single-phase HE materials translates in the estimate of the balance between the entropic gain—favored by the chemical disorder—and the enthalpic cost—associated with structural incompatibility. Traditional descriptors, such as entropy-forming ability or valence electron concentration, fail for systems with complex, non-flat enthalpy landscapes, like borides and carbonitrides.

In a joint work [1] with Duke University, we introduced DEED (Disordered Enthalpy–Entropy Descriptor), a thermodynamic metric quantifying the ratio between entropy gain and enthalpy cost, directly linked to the critical temperature of order–disorder transitions (Fig. 1a). Large DEED values indicate materials likely to form single-phase solid solutions under hot-pressed sintering. To overcome the computational burden of evaluating vast configuration spaces, we developed cPOCC (Fig. 1b): a convolutional algorithm that drastically reduces the number of required ab initio calculations, for determining the relevant partial occupations (POCC), while preserving descriptor accuracy [2].

Based on DEED results and through a synergic theoretical-experimental work in collaboration with Penn State University, we demonstrated that many high-entropy carbides have a robust plasmonic resonance at room, high (T > 1000°C), and variable temperatures [3], with a remarkable plasmonic stability upon thermal cycling (Fig. 2). The unique optical properties, coupled with the well-known mechanical stability, make HE carbides promising prototypes for manufacturing thermal plasmonic technologies at variable temperatures for applications in extreme conditions.

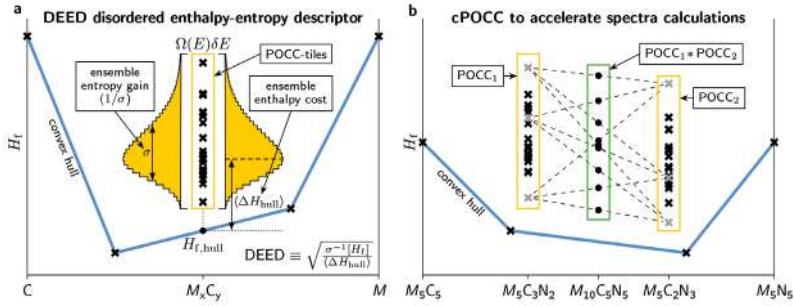

Fig. 1

(a) DEED workflow. Calculations of the phase diagram convex hull (blue line) and POCC-tiles (black crosses) give enthalpy spectral momenta. During synthesis, the enthalpy ensemble average is associated to the enthalpy loss of order, while the variance gives the entropic disorder gain. DEED is the balance of the two. (b) cPOCC workflow. The POCC expansion of a $M_{10}C_5N_5$ (M = metal species) high-entropy ceramic (green box) with five unique metal species would require 17.5 million 20-atom tiles. This is overcome by a partition into $M_5C_2N_3$ and $M_5C_3N_2$ subsystems (yellow boxes), each giving 490 ten-atom tiles (black crosses) and the subsequent energy convolutions (black circles). Adapted from [1].

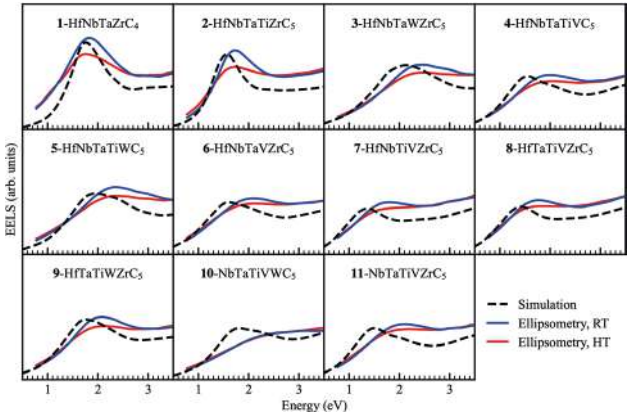

Fig. 2

Room temperature (RT) and high temperature (HT) EELS spectra taken by ellipsometry, along with simulation results, for eleven HEC compositions (HT=1000°C).

Contact persons

Arrigo Calzolari (arrigo.calzolari@nano.cnr.it)

References

[1] Disordered enthalpy–entropy descriptor for high-entropy ceramics discovery. S. Divilov et al. Nature 625, 66 (2024). [OA]

[2] AFLOW4: heading toward disorder. S. Divilov et al. High Entropy Alloys & Materials 3, 178 (2025).

[3] Variable-Temperature Plasmonic High-Entropy Carbides. S. Divilov et al. High Entropy Alloys & Materials 3, 273 (2025).

Efficient *Ab Initio* representation of the dynamical screening in metals and 2D materials

Many-Body Perturbation Theory is the state-of-the-art for computing quasiparticle and optical properties of materials. In particular, the GW approximation yields highly accurate electronic band gaps and band structures. It is however computationally very expensive, especially for two-dimensional systems and metals. We present recent algorithmic advances that drastically reduce Brillouin-zone and frequency sampling of the screened interaction, accelerating GW simulations by orders of magnitude, while preserving predictive accuracy.

We introduce a unified *ab initio* GW framework [1] for bulk and two-dimensional materials, building upon our previously developed W-av [npj Comput. Mater. 9, 44, (2023)] and multipole approximation (MPA) [Phys. Rev. B 104, 115157 (2021)] methods. The W-av technique enables fast convergence with respect to Brillouin-zone sampling, by combining an interpolation and a Monte Carlo integration. Complementarily, MPA provides an efficient and compact representation of the frequency dependence of the screened Coulomb interaction. The combined W-av/MPA approach has been extended to metals, by including the correct long-wavelength limit of screening and an efficient extrapolation scheme, that properly treats intra-band transitions—a main bottleneck in GW calculations for metals.

We validated W-av/MPA across a broad set of systems, showing that it provides an accurate evaluation of quasiparticles (QP), spectral functions, and renormalisation factors beyond the linearised quasiparticle approximation, while greatly reducing the computational cost with respect to standard implementations. The quasiparticle band structures of graphene [1] and doped monolayer Mo_S - [arXiv:2508.06930 (2025)], show excellent agreement with Angle Resolved Photoemisson (ARPES) experiments. We also demonstrate the crucial role of dynamical screening in the logarithmic velocity renormalisation near the graphene Dirac point, resolving subtle many-body effects. We have also studied metallic MXenes [2] with the same class of methods.

Finally, we extend the MPA scheme—originally proposed for the screened interaction—to the self-energy (MPA-S) and Green's function (MPA-G) in the full-frequency domain [3], enabling a fully consistent and scalable treatment of dynamical correlations in materials of different dimensionalities and electronic character.

Overall, the combined W-av/MPA framework significantly advances GW methodology by expanding its applicability to complex 2D semiconductors, layered systems, and metals, while preserving high quantitative accuracy with dramatically reduced computational demands.

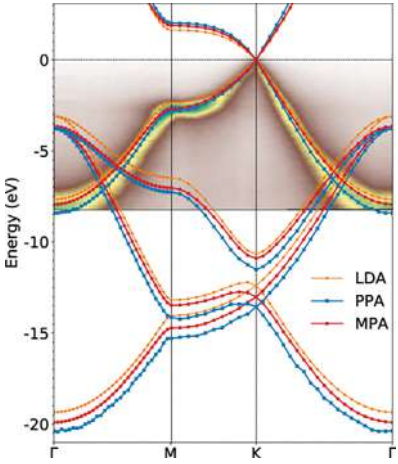

Fig. 1
Graphene QP band structure computed within DFT, *GW* with the Plasmon Pole approximation (PPA) and *GW* with MPA, compared with ARPES results [Phys. Rev. B 84, 115401 (2011)].

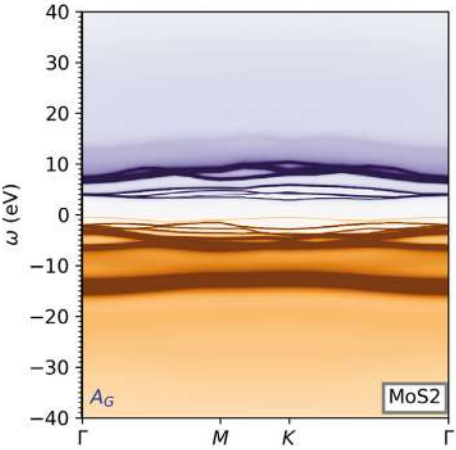

Fig. 2
Spectral band structures of the Green's function, $A_G(k, \omega)$ calculated for MoS_2 with MPA-G.

Contact persons
Claudia Maria Pereira Cardoso (claudiamaria.cardosopereira@nano.cnr.it)

References
[1] Efficient GW calculations via interpolation of the screened interaction in momentum and frequency space: The case of graphene. A. Guandalini, D. A. Leon, P. D'Amico, C. Cardoso, A. Ferretti, M. Rontani, and D. Varsano. Phys. Rev. B 109, 075120 (2024).
[2] Optical properties of metallic MXene multilayers through advanced first-principles calculations. Z. Kandemir, P. D'Amico, G. Sesti, C. Cardoso, M. V. Milošević, and C. Sevik. Phys. Rev. Mat. 8, 075201 (2024).
[3] Spectral properties from an efficient analytical representation of the GW self-energy within a multipole approximation. D. A. Leon, K. Berland, and C. Cardoso. Phys. Rev. B 111, 195147 (2025).

Projects
HORIZON-EUROHPC-JU-2021-COE-01, MAX, project nr. 101093374.
Next Generation EU PNRR, PE13 INF-ACT, project nr. PE00000007.
CINECA award, MMDTS, project nr. HP10B9RKDH-2023.
CINECA award, RDNPA, project nr. HP10BGP2IY-2025.

Magnetic transparent conductors for spintronics

Transparent Conductors (TCs) exhibit optical transparency and electron conductivity, the most common being electron-doped oxides. By searching for non-oxides TCs, able to accept transition metals as doping elements without losing their key characteristics, we extend this class of systems to the magnetic realm. Besides, we introduce new functional materials that combine transparency and conductivity with magnetic spin polarization opening the way to spintronic applications, such as spin filters.

The most common TCs are heavily doped wide-bandgap metal oxides (TCOs), such as indium tin oxide, aluminum zinc oxide, and fluorine tin oxide. The extension of transparent conductivities to magnetic materials would open the integration into transparent spintronic applications and spin-manipulation through electronic and/or optical interactions, such as field effect, spin filtering, and photo carrier injection. Doping metal-oxides with magnetic transition metal (TM) elements would seem the easiest way to impart a magnetic character to TCs. However, the high chemical affinity between the d-orbitals of TMs and oxygen states often results in localized chemical bonds and the emergence of mid-gap states (i.e., no free-charge donation), which are detrimental for both the conductivity (carrier traps) and the transparency (optical interband transitions) of the system. To overcome the limitations in TCOs, we exploit high-throughput ab-initio methodologies in order to identify a set of non-oxides TCs that show additionally spin-filtering properties once doped with TMs [1].

Starting from the identification of physical descriptors, able to capture the essential features of the band structure of a typical TC (such as band gap, effective mass, and energy differences among the conduction bands), we first identify a large set of potential hosts, containing several non-oxides. We then select five of them, focusing our attention on binary compounds and restricting our search on TM-halides (AgF, AgCl, CuCl, $CdCl_2$) and on an alkali-chalcogenide (Na_2S), that are representatives of different gap type, anion/cation valence, and stoichiometry. By systematically doping the selected materials with the TMs, we identify a set of host-dopant systems that exhibit, in addition to the basic properties of the TC, also a spin-polarization of the conductivity $P=(\sigma^{\uparrow}-\sigma^{\downarrow})/(\sigma^{\uparrow}+\sigma^{\downarrow})$, where $\sigma^{\uparrow(\downarrow)}$ are the spin-dependent conductivities. In Fig. 1 we show the polarization for the identified systems: as it can be seen, values up to 90% can be reached [2].

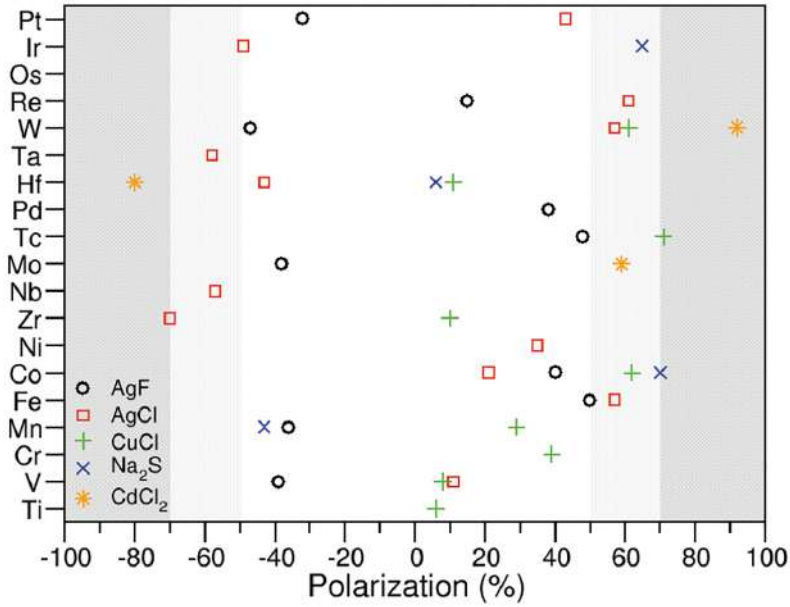

Fig. 1
Maximum value of the spin-polarization P for all the dopant-host systems, where the hosts are the five selected ones from the full list. Different colors (shapes) correspond to different hosts; on the x-axis we indicate the value of P obtained for the different dopants, reported on the y-axis. The light-grey and the dark-grey areas indicates the ranges 50% < |P| < 70% and 70% < |P| < 100%, respectively.

Contact persons
Pino D'Amico (pino.damico@nano.cnr.it)

References
[1] Magnetic transparent conductors for spintronic applications. P. D'Amico, A. Catellani, A. Ruini, M. Fornari, S. Curtarolo, and A. Calzolari. Acta Materialia 289, 120850 (2025). [OA]
[2] Spin-filters magnetic transparent conductors. P. D'Amico. Migliori Comunicazioni SIF: Il Nuovo Cimento C. 48, 205 (2025). [OA]

Exploiting dynamical potentials in electronic structure methods

We present a practical framework for computing both total energies and single-particle spectra of correlated solids by using a dynamical Hubbard functional. In this approach the propagators are represented using sum-over-poles and the Dyson equation leads to a rational nonlinear eigenvalue problem that can be linearized and solved using the algorithmic inversion method (AIM). We demonstrate the method accuracy for $SrVO_3$, obtaining spectra, thermodynamic, and vibrational properties in close agreement with experiment. Moreover, the AIM has been successfully applied to self-consistent Green's function methods in lattice models, revealing broken-symmetry (magnetic or charge-density-wave) phases.

In the following, we present an overview of the main methodological and conceptual advances introduced in Ref. [1, 2, 3]. The central contribution is the formulation of a dynamical Hubbard functional that embeds local many-body interactions within a frequency-dependent and variationally-consistent framework [1]. By employing a compact sum-over-poles (SOP) representation of propagators, frequency integrals are turned into algebraic manipulations of pole structures. Moreover, the nonlinear eigenvalue problem associated to the Dyson equation can be linearized by the algorithmic inversion method, by defining an effective one-body Hamiltonian augmented by auxiliary degrees of freedom. As a result, total energies and spectral properties are obtained within a single formalism, enabling controlled studies of correlated materials.

The approach is applied to representative transition-metal oxides such as $SrVO_3$, showing that key spectral features—quasiparticle weights, band narrowing, and satellite structures—are reproduced with accuracy comparable to state-of-the-art many-body methods while retaining a modest computational cost. Moreover, because the method operates at the level of energy functionals rather than self-energies alone, it naturally provides access to forces, free energies, and vibrational properties, paving the way for structural and thermodynamic investigations of correlated solids.
We establish the theoretical foundation for these applications by deriving closed analytic expressions for Klein-type functionals, embedding potentials, and response quantities within the SOP formalism [2].

We then extend and validate the approach in one-dimensional lattice models, examining competing broken-symmetry phases through fully self-consistent Dyson solutions [3]. There, we explore antiferromagnetic and charge-ordered states, the reconstruction of the Kohn–Sham potential via the Sham–Schlüter equation, and the emergence of the derivative discontinuity, providing insight into how dynamical correlations shape spectral gaps and order parameters in low-dimensional systems.

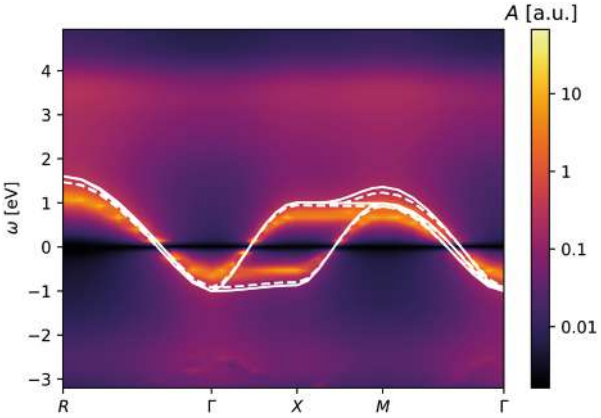

Fig. 1
Spectral function of $SrVO_3$ from this work (color plot) compared to PBEsol (solid-white line) and PBEsol+U (dashed-white line). Only the t2*g* bands are displayed. The chemical potential is shifted to 0 in all three cases.

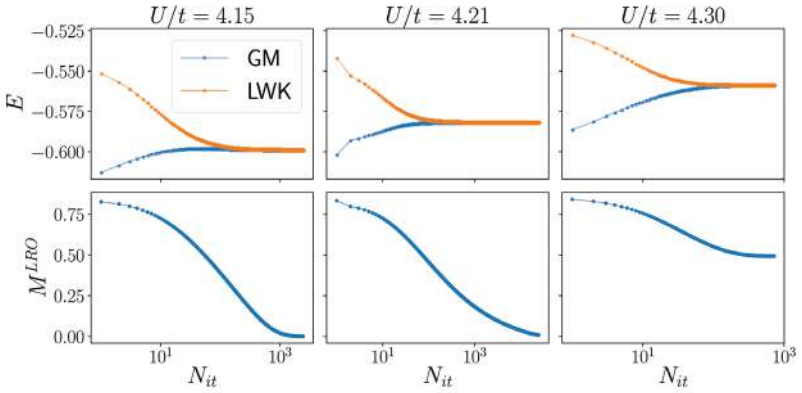

Fig. 2
Total energies (first row) and values of the order parameter M^{LRO} (second row) during self-consistency convergence, for the half- filled Hubbard dimer studied with *GW*. N_{it} is the index of the iteration step. The total energy is calculated both with the Galitskii-Migdal (GM) formula and the Klein (LWK) functional.

Contact persons
Andrea Ferretti (andrea.ferretti@nano.cnr.it)
Marco Gibertini (marco.gibertini@unimore.it)

References
[1] Energies and spectra of solids from the algorithmic inversion of localized *GW*. T. Chiarotti, A. Ferretti, and N. Marzari. Phys. Rev. Res. 6, L032023 (2024). [OA]
[2] Green's function embedding from sum-over-poles representations. A. Ferretti, T. Chiarotti, and N. Marzari. Phys. Rev. B. 110, 045149 (2024). [OA]
[3] Broken symmetry solutions in one-dimensional lattice models via many-body perturbation theory. M. Quinzi, T. Chiarotti, M. Gibertini, and A. Ferretti. Phys. Rev. B 111, 125148 (2025).

Unlocking density functional solutions for excited states and magnetic materials

Density Functional Theory (DFT) is a computational method widely used across thousands of studies annually. Based on the principle that electron distribution governs material properties, DFT maps a complex quantum many-body problem onto a simpler auxiliary problem solvable with practical approximations. This enables predictive simulations for material discovery and characterization. However, its original formulation is mainly suited for non-magnetic ground states. Our research expands the scope of DFT to accurately model excited states and magnetic materials—critical for next-generation materials and quantum technologies.

DFT in its original formulation determines the energy of non-excited states, i.e., states of lowest energy. The time-dependent formulation of DFT (TDDFT) can tackle states of higher energy: in practice, it is most useful for excitations obtained via single-particle excitations. This restriction is due to the (omnipresent) adiabatic approximation by which methods for ground states are reused directly. For non-dynamical excitations, one can circumvent any reference to time by representing the targeted excitations via auxiliary mixed states: i.e., (statistical) ensembles. For ensembles, one can solve a problem that resembles the one for ground states via ensemble-DFT (eDFT).

We introduced a local-density approximation for eDFT (eLDA) and demonstrated that it can capture challenging excitations, including double excitations [1]. However, achieving higher accuracy requires approximations beyond eLDA. We showed that advanced DFT approximations can be extended to eDFT by incorporating components specific to eDFT [2]. Examples are reported in Fig. 1.

The magnetized state of matter plays a pivotal role in technologies like memory of computers. Relativistic magnetic interactions such as spin-orbit coupling enable the transition from conventional electronics to spintronics by reducing energy consumption while introducing novel ways to store and process information.

Applying DFT to magnetic systems, however, poses challenges. Primarily because standard approximations typically violate U(1)×SU(2) invariance. We demonstrated that enforcing this invariance enables accurate modeling of spin-current effects, which is essential for describing important quantum materials [3]. Building on this, we introduced a U(1)×SU(2)-invariant extension of the electron-localization function (ELF) to achieve a consistent description of atomic shells and bonds in magnetized materials (see Fig. 2) [4]. Finally, we addressed the persistent over-magnetization issues in a widely used DFT approximation, paving the way for more accurate material simulations [5].

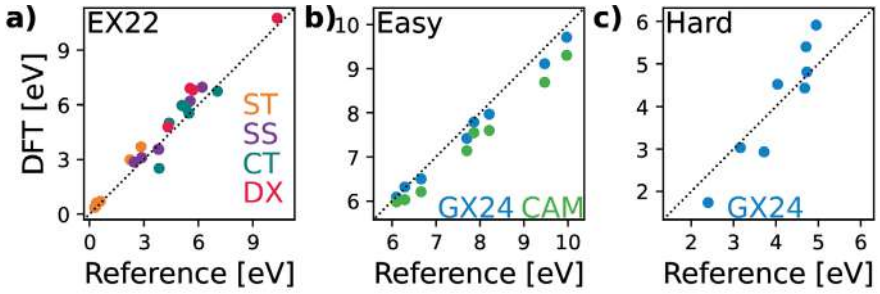

Fig. 1

Excitation energies (y axis) as a function of reference values (x axis). a) Results for the benchmark EX22 using the eDFT functional GX24. Colors indicate type of excitation (Singlet-Triplet, Singlet-Singlet, Charge Transfer, and Double eXcitation). b) GX24 results (blue) and TDDFT results using the CAM-B3LYP functional (green) for 'easy' excitation energies. c) As in b) but for 'hard' double excitations that TDDFT cannot tackle. See [1] for details.

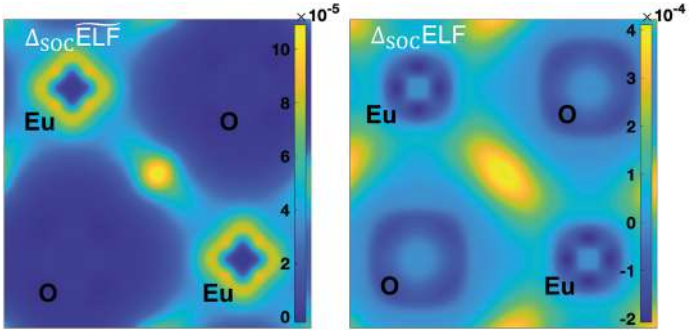

Fig. 2

Localization of the effects of spin-orbit coupling in EuO. While the U(1)xSU(2) gauge invariant ELF can localize the effects where expected (left), a naïve extension of the ELF misses the invariance and misplaces the localization. See [2] for details.

Contact persons

Stefano Pittalis (stefano.pittalis@nano.cnr.it)

References

[1] Local density approximation for excited states. T. Gould and S. Pittalis. Phys. Rev. X 14, 041045 (2024). [OA]

[2] State-specific density functionals for excited states from ensembles. T. Gould, S. G. Dale, L. Kronik, and S. Pittalis. Phys. Rev. Lett. 134, 228001 (2025).

[3] Spin currents via the gauge-principle for meta-generalized-gradient exchange-correlation functionals. J. K. Desmarais, J. Maul, B. Civalleri, A. Erba, G. Vignale, and S. Pittalis. Phys. Rev. Lett. 132, 256401 (2024).

[4] Electron localization function for non-collinear spins. J. K. Desmarais, G. Vignale, K. Bencheikh, A. Erba, and S. Pittalis. Phys. Rev. Lett. 133, 136401 (2024).

[5] Meta-Generalized-Gradient Approximation made Magnetic. J. K. Desmarais, A. Erba, G. Vignale, and S. Pittalis. Phys. Rev. Lett. 134, 106402 (2025).

Local chemistry uncovered in battery materials

Spectroscopic characterization of battery materials provides essential insight into bonding environments, charge transfer, and redox mechanisms, which are critical in energy storage performance and degradation. Yet, the complex nature of the measured spectra often hampers a direct, quantitative interpretation. By combining advanced x-ray and vibrational spectroscopies with density-functional-theory (DFT) based simulations, we establish quantitative structure–spectra correlations in prototypical battery materials, ranging from Li- and Na-based cathodes to Si- and C-based anodes, ultimately revealing how the local chemistry evolves during operation.

Next-generation batteries rely on complex electrode materials, where performance and degradation are governed by the evolution of local chemical environments during cycling. Spectroscopic techniques such as x-ray and vibrational spectroscopies offer powerful probes, but the resulting spectra encode many intertwined effects and are hard to interpret for tracking the origin of the observed variation upon cycling.

We address this challenge by combining advanced experimental techniques with DFT based simulations of prototypical battery materials. By combining spatially resolved micro-Raman mapping and DFT simulations, we investigate potassium intercalation in few-layer graphene [1]. The simulations reveal how charge redistribution, layer-dependent strain and staging of K atoms correlate with the measured spectroscopic fingerprints, demonstrating that both electronic doping and geometric strain contribute to Raman shifts. For Si-based anodes (Fig. 1), the DFT calculated spectra support the identification of unknown local motifs and the quantitative deconvolution of experimental multi-edge x-ray scattering data from cycled electrodes, enabling the disentanglement of reversible and irreversible lithiation processes and tracking the phases mostly responsible for the permanent loss of active Li and capacity fade [2]. In layered nickel oxide cathodes ($LiNiO_2$ and $NaNiO_2$), our calculations reproduce the evolution of x-ray spectra as a function of state of charge, resolving how changes in Ni oxidation, metal–oxygen covalency and local coordination govern the redox activity upon cycling [3].

Across these case studies, ab initio spectroscopy emerges as a versatile framework to link atomic-scale structure, electronic states and spectroscopic observables, enabling a deeper understanding of local chemistry in present and future battery materials.

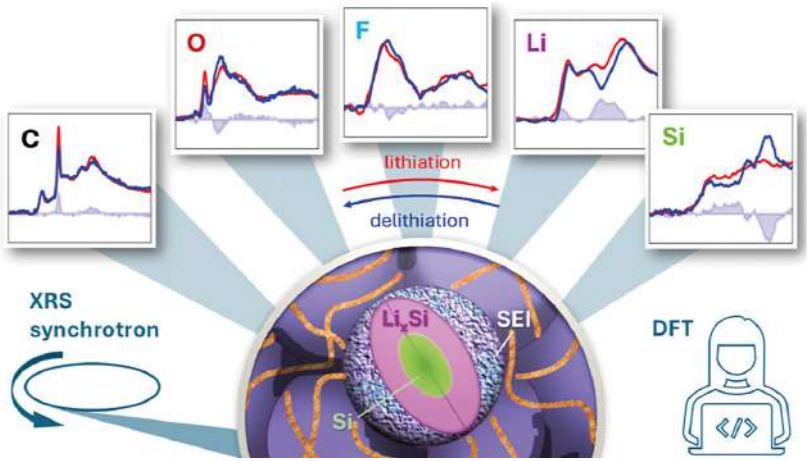

Fig. 1
Multi-edge non resonant inelastic X-ray scattering of Si-based electrodes is coupled to ab initio simulations for an in-depth understanding of electrode evolution and irreversible Li loss upon cycling (see [2]).

Contact persons
Deborah Prezzi (deborah.prezzi@nano.cnr.it)

References

[1] Spatial mapping of potassium diffusion and intercalation in few-layer graphene studied by ultra-high vacuum micro-Raman spectroscopy. D. Marchiani, N. Jimenez-Arevalo, M. Sbroscia, C. Cardoso, D. Prezzi, C. Mariani, M. G. Betti, and R. Frisenda. Nano Energy 142, 111274 (2025). [OA]
[2] Understanding the Irreversible Lithium Loss in Silicon Anodes Using Multi-edge X-ray Scattering Analysis. M. A. Hernandez Bertran, D. Zapata Dominguez, C. L. Berhaut, S. Tardif, A. Longo, C. J. Sahle, C. Cavallari, E. de Clermont Gallerande, I. Marri, N. Herlin-Boime, E. Molinari, S. Pouget, D. Prezzi, and S. Lyonnard. Chemistry of Materials 37, 3648-3660 (2025).
[3] A Fundamental Correlative Spectroscopic Study on $Li_{1-x}NiO_2$ and $NaNiO_2$. Q. Jacquet, N. Mozhzhukhina, P. N. O. Gillespie, G. Wittmann, L. P. Ramirez, F. G. Capone, J. P. Rueff, S. Belin, R. Dedryvère, L. Stievano, A. Matic, E. Suard, N. B. Brookes, A. Longo, D. Prezzi, S. Lyonnard, and A. Iadecola. Advanced Energy Materials 14, 2401413 (2024).

Projects

H2020-LC-BAT-2020-3, BIG-MAP, project nr. 957189.
MUR PRIN 2022, 2D-FRONTIERS, project nr. 20228879FT.

Effects of coherent vibrations on ultrafast photoinduced dynamics

Electronic relaxation and charge transfer in hybrid interfaces are critically shaped by vibronic interactions. Combining *ab initio* simulations with time-resolved spectroscopy, we elucidated how selected molecular vibrations steer photoinduced dynamics on the femtosecond timescale in functionalized organic molecules —both in solution and deposited on graphene—with the broader aim to design efficient optoelectronic and energy-conversion materials.

The adiabatic and non-adiabatic perspectives provide complementary points of view on the coupled dynamics of electrons and nuclei. While the former allows us to shape the energy landscape of nuclear configurations through the concept of Potential Energy Surface (PES), in ultrafast dynamics, the coupling between electronic excited states can be quite strong and the idea of slowly moving classical nuclei at the base of the Born-Oppenheimer scheme is disrupted. At critical points, known as conical intersections, the coherent motion of the quantum wave packet cannot be neglected and phenomena such as non-radiative recombination may occur at an extremely fast rate.

Whether this is detrimental or beneficial for a given optoelectronic or energy-harvesting device depends on many factors. In any case, the ability of controlling the rate of desired and undesired events and to correlate it with the chemical design of specific materials depends on the understanding of the intricate relations existing between the PES, the coupling between the electronic states, and the probability of crossing conical intersections, i.e., the system dynamics.

We developed a theoretical protocol based on TDDFT that integrates the adiabatic analysis based on vibronic modeling and non-adiabatic molecular dynamics based on fewest switches surface hopping. The former is a simple linear model of independent nuclear vibrations in electronically excited states, while the latter is a quantum-classical scheme for non-adiabatic dynamics. Applying this protocol, we discovered a crossing between the PES of the Q_x and Q_y sub-bands in a modified porphyrin, which leads to unusually fast internal conversion. Applying the method to a graphene–phthalocyanine interface, we linked experimentally observed oscillations of the photocurrent in the substrate to specific molecular vibrations in the chromophore promoting interfacial charge transfer. These findings explain the link between the chemical structure of the chromophore and its effect on charge dynamics in a working photovoltaic hybrid interface.

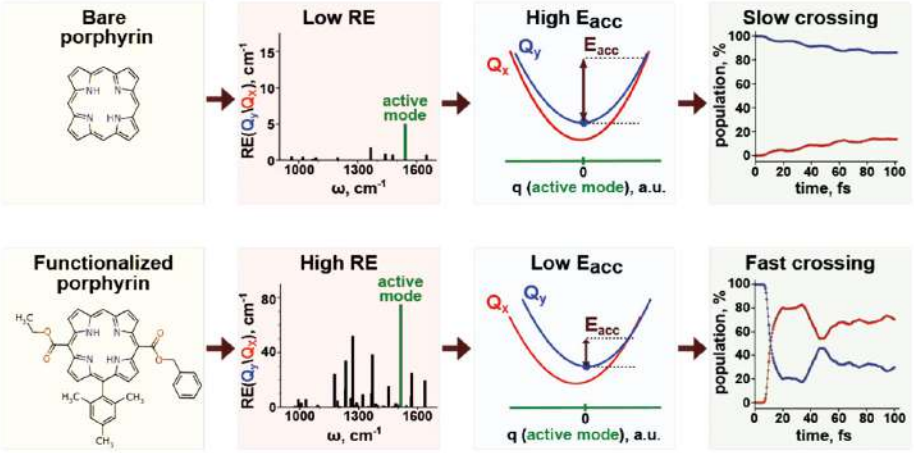

Fig. 1
Sketch of the combined adiabatic/non-adiabatic workflow applied to a bare porphyrin and a modified one. The addition of side groups to the bare porphyrin ring enhances the activity of specific modes and causes the crossing between Q sub-bands which leads to an ultrafast population switch.

Contact persons
Carlo Andrea Rozzi (carloandrea.rozzi@nano.cnr.it)
Deborah Prezzi (deborah.prezzi@nano.cnr.it)

References
[1] Vibronic Coupling Drives the Ultrafast Internal Conversion in a Functionalized Free-Base Porphyrin. V. Petropoulos, P. S. Rukin, F. Quintela, M. Russo, L. Moretti, A. Moore, T. Moore, D. Gust, D. Prezzi, G. D. Scholes, E. Molinari, G. Cerullo, F. Troiani, C. A. Rozzi, and M. Maiuri. Journal of Physical Chemistry Letters 15, 4461-4467 (2024).
[2] Coherent Vibrations Promote Charge-Transfer across a Graphene-Based Interface. A. Casotto, P. S. Rukin, E. Fresch, D. Prezzi, S. Freddi, L. Sangaletti, C. A. Rozzi, E. Collini, and S. Pagliara. Journal of the American Chemical Society 146, 14989-14999 (2024).
[3] Complementing Adiabatic and Nonadiabatic Methods To Understand Internal Conversion Dynamics in Porphyrin Derivatives. P. S. Rukin, M. Fortino, D. Prezzi, and C. A. Rozzi. Journal of Chemical Theory and Computation 20, 10759-10769 (2024). [OA]

Projects
MUR PRIN 2019, HARVEST, project nr. 201795SBA3_005.
MUR PRIN 2022, VIBETWO, project nr. 202284JP34.

Genuine multipartite entanglement from many-electron systems

We demonstrate that, contrary to common wisdom, genuine multipartite entanglement (GME) can be abundantly generated from simple non-correlated many-electron states. We show that the extracted GME can be maximized via spin-independent transformations derived from the quantum Fourier transform. We further demonstrate the possibility of maximizing the GME through localized orbitals in a variety of realistic systems and correlated states. Towards the exploitation of potentially useful entanglement, we rationalize system-specific and universal features of the extracted GME.

This work overturns the long-standing assumption that genuine multipartite entanglement (GME) cannot arise from simple, uncorrelated many-electron states. In fact, we show that abundant —and even maximal— GME can be extracted from closed-shell, single-determinant electronic states by assuming suitable relations between natural and detection orbitals. Spin-independent orbital transformations derived from the quantum Fourier transform generate highly-entangled multi-spin states from otherwise non-correlated electronic wave functions.

The study bridges electronic states of increasing complexity, from non-interacting closed-shell configurations to the ground state of the Hubbard model and of atomistic molecule Hamiltonians. Remarkably, correlated ground and excited states of realistic molecule models yield near-maximal GME when electrons are extracted via physically meaningful, spatially localized orbitals. Cyclic systems, such as benzene, mirror the behaviour of Heisenberg and Hubbard rings, revealing universal entanglement structures tied to symmetry. Conversely, linear conjugated molecules display reduced GME due to the alternation —within the chains— of single and double bonds, resulting in a partial dimerization of the extracted multispin states.

Beyond its conceptual impact, this work identifies genuine multipartite entanglement as a potentially accessible resource in electronic systems where superselection rules are respected. The results open promising avenues for exploiting many-electron states —from model Hamiltonians to real molecules— as platforms for quantum technologies.

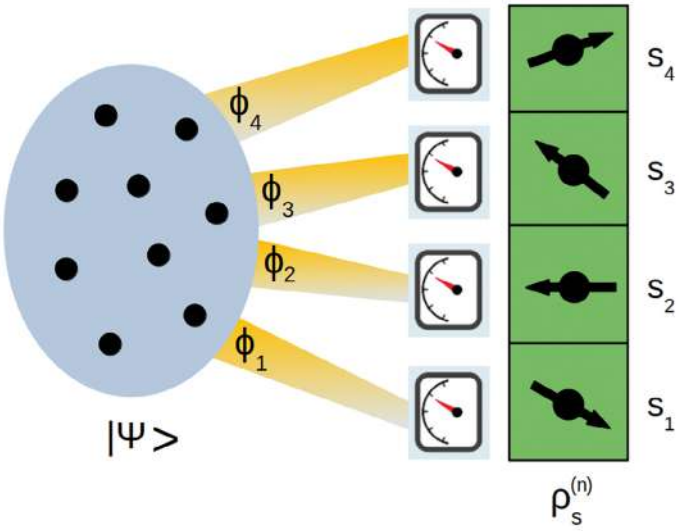

Fig. 1
Schematic representation of the considered procedure: from an N-electron system in a state $|\Psi>$, one extracts an n-spin state $\rho_s^{(n)}$ ($n \leq N$ in general, N=9 and n=4 in the figure). Each of the n spins s_i is labelled by the respective orbital Φ_i.

Contact persons
Filippo Troiani (filippo.troiani@nano.cnr.it)

References

[1] Genuine multipartite entanglement from many-electron systems. F. Troiani, C. Angeli, A. Secchi, and S. Pittalis. Phys. Rev. B 111, L161110 (2025).
[2] Spins extracted from fermionic states and their entanglement properties. F. Troiani, A. Secchi, and S. Pittalis. Phys. Rev. A 112, 012808 (2025).

Projects

MUR PRIN 2022, QCC, project nr. 2022W9W423.
Next Generation EU PNRR, PE4 NQSTI, project nr. PE0000023.

Projects and grants

Cnr Nano research activity is mainly supported by funding obtained through competitive calls at different levels, from international to local. Projects running in 2024-2025 are listed below with the following details: acronym, project name, call details, project ID, coordinator, Cnr Nano principal investigator (if different from coordinator), dates, website (if available). A short abstract is given for European-funded projects. For further information, please contact the project's Cnr Nano principal investigator.

European projects

BIG-MAP. Battery interface Genome – Materials Acceleration Platform. H2020-LC-BAT-2020-3; GA 957189. Technical University of Denmark – DTU, DK (T. Vegge); Cnr Nano (E. Molinari and D. Prezzi). 2020-2024.
www.big-map.eu

The BIG-MAP project aims to accelerate the development of innovative, sustainable battery technologies. To address the lack of efficient energy-storage solutions, it proposes a modular, closed-loop platform that integrates machine learning, computer simulations, and AI-driven experiments. This approach will speed up the discovery and optimization of new battery materials and interfaces, contributing to the creation of a versatile, chemistry-neutral European Materials Acceleration Platform.

EXTREME-IR. Extreme Optical Nonlinearities in 2D materials for Far-Infrared Photonics. H2020-FETOPEN-2018-2020; GA 964735. CNRS, FR (S. Dhillon); Cnr Nano (M. S. Vitiello). 2021-2026.
www.extreme-ir.eu

The EXTREME-IR project seeks to overcome the current limitations of quantum cascade lasers, which cannot cover the far-infrared range between 5 and 12 THz. By using nonlinear optics in 2D materials, the project aims to develop compact, coherent light sources in this frequency region, enabling new sensing applications and advancing the study of light-matter interactions.

HANAMI. Hpc AlliaNce for Applications and supercoMputing Innovation: the Europe - Japan collaboration. HORIZON-EUROHPC-JU-2022-INCO-04; GA 101136269. CEA, FR (F. Boillod-Cerneux); Cnr Nano (D. Varsano). 2024-2027.
www.hanami-project.com

HANAMI promotes scientific projects involving both Europe and Japanese institutes and assists the researchers to access supercomputers in Japan and Europe. HANAMI embeds leading research institutes and supercomputing centres to tackle exascale areas and beyond.

H-CUBE - Attract Phase II. Micromechanical Bolometers arrays for Terahertz hyperspectral imaging. H2020-INFRAIN-NOV-2019-2020; GA 10100442. Cnr Nano (A. Pitanti). 2021-2025.
www.phase2.attract-eu.com/projects/h-cube/

The H-Cube project develops a low-cost, portable terahertz (THz) hyperspectral imaging sensor. Building on three earlier ATTRACT projects, it aims to deliver high sensitivity, broad THz coverage, and scalable production. This technology will make THz imaging accessible beyond specialized, expensive systems—enabling everyday uses such as crop monitoring, building inspection, and security screening in crowded environments.

IMPRESS. Interoperable electron Microscopy Platform for advanced Research and Services. HORIZON-INFRA-2022-TECH-01; GA 101094299. Cnr IOM, IT (R. Ciancio); Cnr Nano (V. Grillo). 2023-2027.
www.e-impress.eu

The IMPRESS project aims to transform transmission electron microscopy (TEM) by developing a standardised, cartridge-based platform with common interfaces and data formats. This flexible system will enable advanced correlative experiments across different instruments and support the co-development of new TEM methods not yet available commercially. The project will also establish an open hub for knowledge and innovation in TEM.

IQubits. Integrated Qubits Towards Future High-Temperature Silicon Quantum Computing Hardware Technologies. H2020-FETOPEN-2018-2019-2020-01; GA 829005. Akademia Gorniczo-Hutnicza Im. Stanislawa Staszica W Krakowie, PL (D. Zito); Cnr Nano (E. Molinari and F. Troiani). 2019-2024.
www.iqubits.eu

The IQubits project aims to develop and experimentally demonstrate high-temperature Si and SiGe spin qubits and integrated qubit circuits using commercial 22 nm FDSOI CMOS technology. It assesses scalability down to 10 nm through fabrication tests and uses atomistic simulations to show that 2 nm devices could operate at 300 K. The project also explores more aggressively scaled Si- and nitride-channel qubit structures, with the goal of ultimately integrating III-nitride qubits on SOI wafers for CMOS compatibility.

LESGO. Light to Store chemical Energy in reduced Graphene Oxide for electricity generation. FETPROACT-EIC-05-2019; GA 952068. ICFO, ES (J. Martorell); Cnr Nano (V. Tozzini). 2020-2024.
www.lesgo-project.eu

The LESGO project proposes storing renewable energy in the carbon–hydrogen bonds of reduced graphene oxide (rGO-H) as a clean alternative to conventional hydrogen production from hydrocarbons. rGO-H offers safe handling, easy transport, over 100 times the energy density of gaseous hydrogen, and zero CO_2 emissions during electricity generation. The project aims to provide an affordable, environmentally friendly solution for on-demand power supply.

MaX. Materials design at the eXascale. European Centre of Excellence in materials modelling, simulations, and design. HORIZON-EUROHPC-JU-2021-COE-01; GA 101093374. Cnr Nano (E. Molinari and A. Ferretti). 2023-2026.
www.max-centre.eu

MaX aims to prepare major quantum-mechanical materials-modelling codes for Europe's pre-exascale and exascale computers. It pursues this through a new software-development model that adapts community codes to heterogeneous hardware without altering their core structure; an integrated HPC/HTPC ecosystem to manage large-scale, reproducible simulations and curated data; a co-design strategy aligning hardware and software development; and measures that simplify access, engage users, and broaden the community of trained developers.

MUQUABIS. Multiscale quantum bio-imaging and spectroscopy. HORIZON-CL4-2021-DIGITAL-EMERGING-01; GA 101070546. Cnr Ino, IT (N. Fabbri), Cnr Nano (M. S. Vitiello). 2022-2026.
www.muquabis.eu

MUQUABIS aims to develop advanced quantum-based tools for biosensing and bioimaging, offering highly sensitive, non-invasive, high-resolution methods that surpass classical technologies. Focusing on the structure and function of cardiac cell layers, the project studies healthy and diseased tissues to better understand arrhythmias. It explores new concepts—such as quantum frequency combs, infrared lasers, and low-light spectro-imaging—and integrates diamond-based quantum magnetometry with optical imaging to map local electric and magnetic fields in cardiac activity. The project lays the groundwork for next-generation quantum technologies for medical diagnostics and treatment.

OpenModel. Integrated Open Access Materials Modelling Innovation Platform for Europe. H2020-NMBP-TO-IND-2018-2020; GA 953167. Fraunhofer IFAM, DE (W. Leite Cavalcanti); Cnr Nano (A. Calzolari). 2021-2025.
www.open-model.eu

OpenModel aims to create and sustain an integrated open platform that provides reliable, validated, and traceable simulation workflows, seamlessly combining third-party

physics-based models, solvers, post-processors, and databases. It bridges industrial challenges to actionable insights that support informed business decisions. Six use cases demonstrate its broad applicability across different materials and processing technologies, showing how OpenModel streamlines experiments, reduces errors, and improves development efficiency.

PERSEUS. 2D Material-Based Multiple Oncotherapy Against Metastatic Disease Using a Radically New Computed Tomography Approach. HORIZON-EIC-2022-PATHFINDEROPEN-01; GA 101099423. Cnr Imem, IT (G. Salviati); Cnr Nano (I. Tonazzini). 2023-2027.
www.perseusproject.eu

The PERSEUS project aims to expand the use of computed tomography (CT) from imaging to treating hard-to-reach tumours, such as metastatic triple-negative breast cancer and pancreatic cancer. It aims at developing a nanotechnology-based therapy in which a nanosystem activated by the CT beam kills cancer cells through heat and reactive oxygen species, while the resulting release of tumour antigens may stimulate anti-cancer immune responses.

QATACOMB. Quantum correlations in Terahertz qcl COMBs. H2020-ERA-NET-QuantERA II Call 2021. Cnr Ino, IT (L. Consolino); Cnr Nano (M. S. Vitiello and L. Sorba). 2022-2025.
www.qatacomb.ino.cnr.it

QATACOMB aims to develop a miniaturized solid-state platform for generating, detecting, and fully characterizing non-classical squeezed terahertz (THz) light. By leveraging THz quantum cascade laser frequency combs, graphene-based quantum sensors, and ultrafast cavity-coupled detectors, the project seeks to enable continuous-variable entangled THz states. These advances could support future quantum computing, teleportation, and secure free-space communication, while exploiting the unique properties of THz radiation for use in challenging or opaque environments.

QCEED. Quantum Dot coupling engineering: 2-dimensional cluster state generation for quantum information processing. HORIZON-EIC-2024-PATHFINDEROPEN-01; GA 101185617. University College Cork, IE (G. Juska); Cnr Nano (L. Sorba). 2025-2029.
www.qceed.eu

QCEED addresses the main obstacle in photonic quantum computing: the lack of reliable, large-scale, on-demand 2D photonic cluster states. The project develops engineered paired semiconductor quantum dots with enhanced coherence, using techniques such as deep nuclei cooling and spin decoupling. Through two complementary quantum-dot platforms and optimized photon-funnelling structures,

QCEED aims to generate multidimensional cluster states efficiently. By delivering a scalable semiconductor source of 2D cluster states, the project brings practical, large-scale quantum photonic computation significantly closer.

QC4QT. Advancing Quantum Computers for (and with) Quantum Thermodynamics. HORIZON-MSCA-2021-PF-01; GA 101063316. Cnr Nano (M. Campisi). 2022-2025.

The project develops quantum-computing algorithms to simulate thermal behavior in quantum systems and to test key fluctuation relations from quantum thermodynamics. It also applies thermodynamic principles to create an algorithmic cooling method aimed at improving qubit performance. The project combines expertise in quantum computing, quantum thermodynamics, and computational science, enabling a strong exchange of knowledge and supporting the success of both research goals.

SMART-*electron*. Ultrafast all-optical spatio-temporal electron modulators: opening frontiers in electron microscopy. H2020 FETOPEN 2018-2020; GA 964591. Università di Milano Bicocca, IT (G. Vanacore); Cnr Nano (V. Grillo). 2021-2025.
www.smartelectron.eu

SMART-electron develops an all-optical, rapidly programmable platform for shaping electron wave functions using ultrafast electromagnetic fields. This approach enables unprecedented control over the space, time, energy, and momentum of electron matter waves, surpassing traditional passive methods and transforming how materials are probed in electron microscopy.

SPECTRUM
THE QUANTUM SWITCH

SPECTRUM. Superconducting Radio-frequency switch for quantum technologies. HORIZON-EIC-2021-TRANSITIONOPEN-01; GA 101057977. Cnr Nano (F. Giazotto). 2022-2025.
www.spectrum-project.eu

Spectrum presents QueSt, a quantum-computer–oriented RF switch that enables ultrafast, near-zero-downtime switching with minimal heat generation. By reducing the number and thermal load of signal lines, QueSt improves scalability and stability in quantum processors. Its superconducting design offers low power dissipation, fast switching, voltage control, CMOS compatibility, and support for multiple qubit configurations, helping accelerate the development of scalable quantum computers.

SPIN-FERT

SPIN-FERT. Innovative practices, tools and products to boost soil fertility and peat substitution in horticultural crops. HORIZON-MISS-2023-SOIL-01; GA 101157265. INHORT, PL (E. Malusa); Cnr Nano (M. Cecchini). 2024-2027.
www.spinfert.eu

SPIN-FERT integrates and validates improved soil-management practices and peat-free substrates to enhance soil health in vegetable, fruit, and ornamental crops. It optimizes fertiliser production, upgrades formulations with innovative protocols, and converts agro-food by-products into high-quality peat-free substrates enriched with selected microbes, especially for nurseries. All products will be tested in field trials across four European regions. The project will also deliver tools, including a Soil Holistic Quality Index, and conduct economic, social, and environmental assessments to support sustainable policy development. Close involvement of SMEs, authorities, and citizens ensures practical relevance, while creative communication raises awareness of the importance of soil health.

STAR. HyperSpectral Terahertz near-field nanoscope exploiting miniaturized frequency-combs. ERC-2022-POC2; GA 101081567. Cnr Nano (M. S. Vitiello). 2022-2024.

STAR develops a graphene-integrated terahertz quantum cascade laser to enable compact, low-cost nanoscale imaging without external detectors. The resulting system will produce amplitude- and phase-resolved images of objects as small as 40–100 nm, with potential applications in biology, medicine, and materials science. It will be demonstrated through a working prototype shown to commercial end users.

SUPERGATE. Gate Tunable Superconducting Quantum Electronics. H2020-FETOPEN-2018-2020; GA 964398. University of Kostanz, DE (E. Scheer); Cnr Nano (F. Giazotto). 2021-2024.
www.supergate.uni-konstanz.de

SuperGate develops a new superconducting logic-gate approach that delivers equal or better performance than current supercomputing technologies while significantly reducing energy consumption. By overcoming key limitations in today's superconducting quantum systems, it aims to enable the next major leap in supercomputer efficiency and capability.

TeraScan. Terahertz HyperSpectral low-Cost fAst GrapheNe Camera. ERC-2023-POC; GA 101157731. Cnr Nano (M. S. Vitiello). 2024-2026.

TeraScan advances ultrafast single-layer graphene terahertz detectors by developing a hyperspectral graphene-based camera that outperforms current commercial systems. The project will build a portable imaging device using multiwavelength high-power quantum cascade lasers, offering compact, low-cost, energy-efficient, room-temperature operation for applications ranging from engineering to medicine. The technology will be validated with end users.

National projects

2D-FRONTIERS. 2D van der Waals heterostructures for novel concepts in energy storage. MUR Prin 2022; project nr. 20228879FT. Cnr Nano (D. Prezzi). 2023-2026.

AI-TEM. Artificial intelligence enhanced transmission electron microscopy for advanced imaging. MUR Prin 2022; project nr. 2022249HSF. Cnr Nano (V. Grillo). 2023-2026.

AMONIX. Amorphous conductors as a new route for plasmonics. MUR Prin 2022; project nr. 2022BTMXZT. Cnr Nano (S. Benedetti). 2023-2026.

ASTROSECRET. Molecular mechanisms of astrocyte maturation and secretome in neurodevelopmental disorders associated with prenatal inflammation. MUR Prin 2022; project nr. 2022Y544HH. Cnr IN (E. Menna); Cnr Nano (G. Losi). 2023-2026.

CHERISH-C. Chemical and electrochemical energy storage materials from organic wastes: the treasure hidden in C based materials. MUR Prin 2022; project nr. 202278NHAM. Università di Pavia (C. Milanese); Cnr Nano (L. Bellucci). 2023-2026.

e-DyNaFOx. Electron Dynamics in Nanostructured Functional Oxides. MUR Prin 2022; project nr. 2022YXJ55F. Cnr Nano (P. Luches). 2025-2027.

ENGInerve. Development of nano/micro-engineered devices for applications in peripheral nervous system pathological models. MUR Prin 2022; project nr. 2022ZH5M72. Cnr Nano (I. Tonazzini). 2023-2026.

EnvELOP. Environmental tuning of microbial rhodopsins Electronic Landscape for new Optogenetic Potentialities. MUR Prin 2022; project nr. 2022WS44W4. Università di Siena (C. A. Guido); Cnr Nano (L. Zanetti Polzi). 2023-2026.

EQUATE. Defect engineered for electro-thermal quantum technology. MUR Prin 2022; project nr. 2022Z7RHRS. Scuola Normale Superiore (F. Paolucci); Cnr Nano (F. Bianco). 2023-2026.

ERACLITO. Earth abundant and non-toxic doped metal oxide-based electro optic photonic structures for smart windows and radiative cooling. MUR Prin 2022; project nr. 2022ZMA4X3. Cnr Spin (F. Scotognella); Cnr Nano (A. di Bona). 2023-2026.

GAMESQUAD. Gate-induced microscopic effects on superconducting quantum devices. MUR Prin 2022; project nr. 2022A8CJP3. Università di Genova (A. Amoretti); Cnr Nano (A. Crippa). 2023-2026.

GeFinder. Novel protein-based Genetically-Encoded Fluorescent Indicators (GEFI) for Functional Super-Resolution Imaging of Biomolecular Activities in Living Cells. MUR prin 2022; project nr. 2022RRFJC4. Università di Parma (C. Viappiani); Cnr Nano (B. Storti). 2023-2026.

GROUNDS. Growth and optical studies of tunable quantum dots and superlattices in semiconductor nanowires. MUR Prin 2022; project nr. 20223WZ245. Sapienza Università di Roma (M. De Luca); Cnr Nano (V. Zannier). 2023-2026.

LOVE. Lab-on-chip for sustainable olive value chain: development of a lab-on-chip for detecting polyphenolic compounds in olives and its derivates. MUR Prin 2022; project nr. 2022M4WB3M. Università di Pisa (C. Sanmartin); Cnr Nano (A. Battisti). 2023-2026.

MAGNETISE. Rare-earth single atom magnets anchored at oxide surfaces as a platform for new low-consumption magnetic devices. MUR Prin 2022; project nr. 2022KXN79M. Cnr Ism (A. Barla); Cnr Nano (V. Bellini). 2023-2026.

MaX. Materials design at the eXascale. Bando MIMIT - transnazionale congiunto EuroHPC 2022 "Centres of Excellence for HPC Applications" (Horizon-EuroHPC-JU-2021-COE-01) di cui al D.M. 16 dicembre 2022 e D.D. 25 gennaio 2023. Cnr Nano (A. Ferretti). 2023-2026.

NAVIGANS. Novel Architecture of ultralow-Volume Integrated Gyroscopes for Advanced. MIMIT – Fondo per la crescita sostenibile, Accordo per l'innovazione. Cnr Nano (M. S. Vitiello). 2024-2026.

NEThEQS. Non-equilibrium coherent thermal effects in quantum systems. MUR Prin 2022; project nr. 2022B9P8LN. Politecnico di Torino (F. Dolcini); Cnr Nano (F. Taddei). 2023-2026.

PACECOR. Early phase preclinical development of PACECOR, a mutation-independent Anti-SARS-Co2 therapeutic strategy. MIUR Prin 2021; project nr. 2020LW7XWH. Cnr Nano (A. Sgarbossa and G. Brancolini). 2022-2025.

PLINIOS. A molecular platform for intracellular nitric oxide sensing. MUR Prin 2022 PNRR (Mission 4, Component 2, Investment 1.1); project nr. P2022F4WR8. Cnr Nano (R. Nifosì). 2023-2026.

QCC. Quantum computing for computational chemistry and materials science. MUR Prin 2022; project nr. 2022W9W423. Università dell'Aquila (L. Guidoni); Cnr Nano (R. Di Felice and S. Corni). 2023-2026.

q-LIMA. Light-matter interactions and the collective behavior of quantum 2D materials. MIUR Prin 2020; project nr. 2020JLZ52N. Cnr Nano (F. Bianco). 2022-2025.

REMEDY. Stabilized Reversed Micelles for Brain Delivery of Hydrophilic Drugs. FISA 2022 – MUR; project id. FISA2022-00627. Cnr Nano (M. Cecchini). 2024-2026.

ResET. Resonant energy transfer from plasmonic nanoparticles to semiconductors: a route to improve solar photocatalytic efficiency. MUR Prin 2022 PNRR (Mission 4, Component 2, Investment 1.1); project nr. P2022ZHCT3. Cnr Nano (P. Luches). 2023-2026.

THERmIR. Continuous thermal monitoring with wearable mid-infrared sensors. MUR Prin 2022 PNRR (Mission 4, Component 2, Investment 1.1); project nr. P2022AHXE5. Cnr Nano (L. Viti). 2023-2026.

TOAC. Touch on a chip. MUR Prin 2020; project nr. 20208TPFLN. Cnr Nano (I. Tonazzini). 2022-2025.

TopoFlag. Non-reciprocal supercurrent and topological transitions in hybrid Nb-InSb nanoflags. MUR Prin 2022; project nr. 2022PH852L. Università di Genova (M. Sassetti); Cnr Nano (S. Heun). 2023-2026.

Tripartite-AD. Interaction between cholinergic and glumatergic synaptic trasmission at tripartite synapse in the pathophysiology of Alzehimer's disease. MIUR Prin 2020; project nr. 2020AMLXHH. Cnr Nano (G. Losi). 2022-2025.

TRUST. Trampolines as ultra-sensitive thermomechanical bolometers. MUR Prin 2022; project nr. 2022M5RSK5. Università di Pisa (S. Roddaro); Cnr Nano (A. Pitanti and S. Zanotto). 2023-2026.

TUNES. Tuning the electronic structure of graphene from low to high electron doping. MUR Prin 2022; project nr. 2022NXLTYN. Sapienza Università di Roma (M. G. Betti); Cnr Nano (A. Ferretti). 2023-2026.

UDynamec. Ultrafast DYNAmics in Materials for Energy Conversion. MAECI 2023 Italy-Germany Science and Technology Cooperation. CUP B53C23006060001. Cnr Nano (P. Luches); European XFEL (M. Izquierdo). 2023-2025.

VIBETWO. Understanding and optimizing coherent vibronic coupling in 2D hybrid light-harvesting heterostructures for photovoltaic performance. MUR Prin 2022; project nr. 202284JP34. Cnr Nano (C. A. Rozzi). 2023-2026.

Next Generation EU - PNRR (2022-2025) projects

Cnr Nano participation to Next Generation EU - PNRR (2022-2025) projects is listed below. In the description, M stands for Mission, C for Component, and I for Investment. For each Spoke the relevant Cnr Nano scientist is indicated.

Ecosister. Ecosystem for Sustainable Transition in Emilia-Romagna. M 4, C 2, I 1.5; project nr. ECS_00000033.
www.ecosister.it

- Spoke 1 "Materials for sustainability and ecological transition". S. Benedetti.
- Spoke 1 "HYTS". A. di Bona.
- Spoke 3 "Green manufacturing for a sustainable economy". G. Paolicelli.

THE. Tuscany Health Ecosystem. M 4, C 2, I 1.5; project nr. ECS_00000017.
www.tuscanyhealthecosystem.it

- Spoke 1 "Advanced radiotherapies and diagnostics in oncology". V. Tozzini and M. Santi.
- Spoke 4 "Nanotechnologies for diagnosis and therapy". A. Camposeo and M. Cecchini.

CN1 HPC. National Centre for HPC, Big Data and Quantum Computing. M 4, C 2, I 1.4; project nr. CN0000013.
www.supercomputing-icsc.it/en/icsc-home

- Spoke 7 "Materials and Molecular Sciences". A. Ferretti.
- Spoke 7 "Innovation Grant Granarolo". G. Brancolini.
- Spoke 7 "Innovation Grant Lavazza". G. Brancolini.
- Spoke 7 "Innovation Grant Leonardo". D. Prezzi.
- Spoke 7 "Innovation Grant ENI". V. Tozzini and L. Bellucci.
- Spoke 10 "Quantum Computing". R. Di Felice.

CN3 RNA Drug development. National Centre for Gene Therapy and Drugs based on RNA Technology. M 4, C 2, I 1.4; project nr. CN00000041.
www.rna-genetherapy.eu/

- Spoke 6 "RNA Drug Development". B. Storti.

CN4 MOST. National Centre on Sustainable mobility. M 4, C2, I 1.5; project nr. CN00000023.
www.centronazionalemost.it

- Spoke 11 "Innovative Materials and Lightweighting Description of the Spoke Activities". P. Luches.

PE2 NEST. Enlarged partnership "Network 4 Energy Sustainable Transition". M 4, C2, I 1.3; project nr. PE00000021.
www.fondazionenest.it

- Spoke 2 "Energy harvesting and off-shore renewables". L. Persano.

PE4 NQSTI. Enlarged partnership "National Quantum Science and Technology Institute". M 4, C 2, I 1.3; project nr. PE0000023.
www.nqsti.it

- Spoke 2 "Simulation, sensing and metrology". F. Troiani.
- Spoke 4 "Photonic platform for quantum technologies". M. S. Vitiello.
- Spoke 5 "Electron-based platform for quantum technologies". L. Sorba and V. Grillo.

PE11 MICS. Enlarged partnership "Circular and Sustainable Made in Italy". M 4, C 2, I 1.3; project nr. PE0000004.
www.mics.tech/en/home

- Spoke 6 "Additive manufacturing as disruptive enabler of the twin transition". A. Camposeo.

PE13 INF-ACT. Enlarged partnership "One Health Basic and Translational Research Actions addressing Unmet Needs on Emerging Infectious Diseases". M 4, C 2, I 1.3; project nr. PE00000007.
www.inf-act.it/

- Spoke 5 "New therapeutic strategies". A. Sgarbossa and G. Brancolini.

PE14 RESTART. Enlarged partnership "Research and innovation on future Telecommunication systems and networks, to make Italy more smart". M 4, C 2, I 1.3; project nr. PE00000001.
www.fondazione-restart.it

- Spoke 3 "Wireless Networks and Technologies". M. S. Vitiello.

iENTRANCE@ENL. Infrastructure for Energy Transition and Circular Economy @ EuroNanoLab. M 4, C 2, I 1.3; project nr. IR0000027. V. Grillo.
www.ientrance.eu

Regional projects

ADAPTA. Sinonasal cancer: In depth genetic analysis of patients for personalized treatment and disease monitoring. Regione Toscana; Bando Ricerca Salute 2018 - DD15397/2018. Università di Pisa (A. Franchi); Cnr Nano (L. Persano). 2020-2024.

DECODE-EE. Developmental and epileptic encephalopathies: epidemiology, comorbidities, molecular diagnosis, personalized management, and costs analysis. Regione Toscana; Bando Ricerca Salute 2018 - DD15397/2018. Scuola Superiore S. Anna (P. Castoldi); Cnr Nano (G. M. Ratto and M. Santi). 2020-2024.

DEM-AGING. Neurodegenerative disorders throughout the lifespan. Autophagy-dependent biomarkers for trial readiness from infantile neuronal ceroid-lipofuscinoses to senile dementias. Regione Toscana; Bando Ricerca Salute 2018 - DD15397/2018. IRCCS Stella Maris (F. Santorelli); Cnr Nano (G. M. Ratto and M. Santi). 2020-2024.

END. Isolation and molecular characterization of neuronal exosomes in models of neurodevelopmental disorders. Regione Toscana Fondo per lo Sviluppo e la Coesione – Bando per progetti di alta formazione attraverso l'attivazione di assegni di ricerca (Bando Assegni 2021); project nr. DSB.AD008.729. Cnr Nano (I. Tonazzini). 2022-2024.

Hollow Fiber 2.0. Metodi innovativi per la modifica delle proprietà idrofobiche di Hollow Fibers in polipropilene: dai nano-additivi ai nano-coatings. POR FESR Regione Emilia-Romagna 2021-2027 - Progetti di ricerca industriale rivolti agli ambiti prioritari della Strategia di Specializzazione Intelligente 2023-2024; project nr. 38657 PG/2023/312455 HF2.0. Tecnopolo Mario Veronesi Mirandola (L. Rovati); Cnr Nano (V. De Renzi). 2024-2026.

MACE4IAM. "Modelli fondazionali per la progettazione e lo sviluppo di materiali avanzati". Bando RER/DGR 565/2025 "Invito a presentare manifestazioni di interesse per l'integrazione dei progetti di ricerca dell'ecosistema regionale dell'innovazione con i programmi a gestione diretta della Commissione Europea". Cnr Nano (D. Prezzi). 2025.

MaX. "MaX materials at the exascale". Bando RER/DGR 565/2025 "Invito a presentare manifestazioni di interesse per l'integrazione dei progetti di ricerca dell'ecosistema regionale dell'innovazione con i programmi a gestione diretta della Commissione Europea". Cnr Nano (L. Neri). 2025.

MELA. MEtasurface based Lidar system for Agrifood. Regione Toscana - FSE+ 2021-2027 - Bando RT 2023 - Progetti Alta Formazione. Cnr Nano (S. Zanotto). 2024-2026.

MERIDIAN. MatERIali polimerici bioDegradabili a basso Impatto AmbieNtale. Regione Toscana - FSE+ 2021-2027 - Bando RT 2023 - Progetti Alta Formazione. CUP B53C23003160009. Cnr Nano (A. Battisti). 2023-2026.

SAPORE. Sistema Avanzato Per l'Ottimizzazione e la Rivoluzione del processo Enologico, Advanced System for Optimizing and Revolutionizing the Winemaking Process. Programma Regionale Toscana FESR 2021-2027. Cnr Nano (M. Cecchini). 2024-2026.

SENSIDROGEN. Sviluppo di Sensori innovativi per il monitoraggio di perdite di Idrogeno in siti di produzione, stoccaggio e utilizzo. POR FESR Regione Emilia-Romagna 2021-2027 - Progetti di ricerca industriale rivolti agli ambiti prioritari della Strategia di Specializzazione Intelligente 2023-2024; project nr. E67G22000590007. Romagna Tech S.C.P.A. (M. Campana); Cnr Nano (A. di Bona). 2024-2026.

TOSCANO. The Omics sciences against osteosarcoma. Regione Toscana - Bando Ricerca Salute 2018; DD15397/2018. Cnr Nano (M. Cecchini). 2020-2024.

Other funding agencies

gpr65. Study of GPR65 as a new Krabbe disease drug target. European Leukodystrophy Association (ELA) International. Cnr Nano (S. Carpi and M. Cecchini). 2025-2027.

InnovAS. Innovative brain-targeting nano-tools and imaging methods for therapeutic development in Angelman Syndrome. Angelman Syndrome Alliance. Cnr Nano (I. Tonazzini). 2022-2027.

Optoelectronics and nano-photonics in two-dimensional nanomaterial heterostructures. Fondazione Internazionale Premio Balzan. Cnr Nano (M. S. Vitiello). 2017-2028.

TOTheM. Topological Thermal Machines. Royal Society through the International Exchanges between the United Kingdom and Italy. Grant No. IEC\R2\212041. Cnr Nano (F. Taddei and A. Braggio). 2021-2024.

2024-2025 external funding (in €)

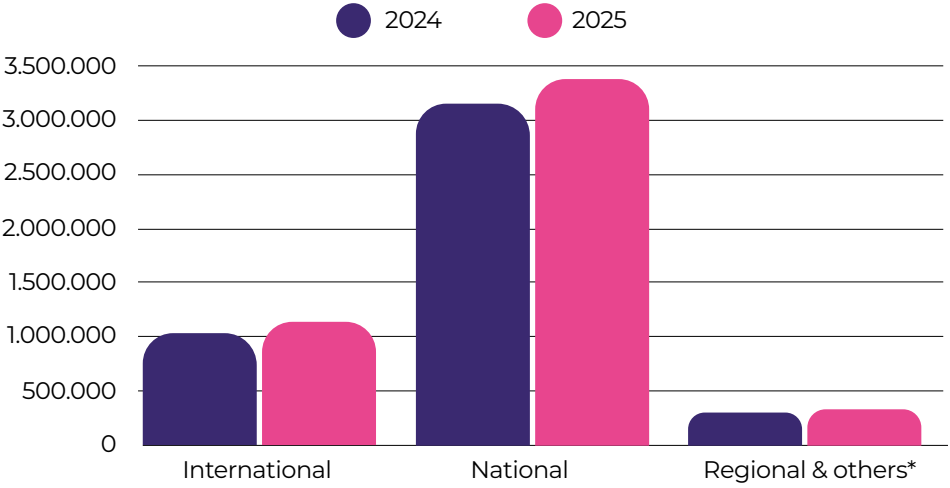

*include regional projects, other financing institutions, and commercial projects.

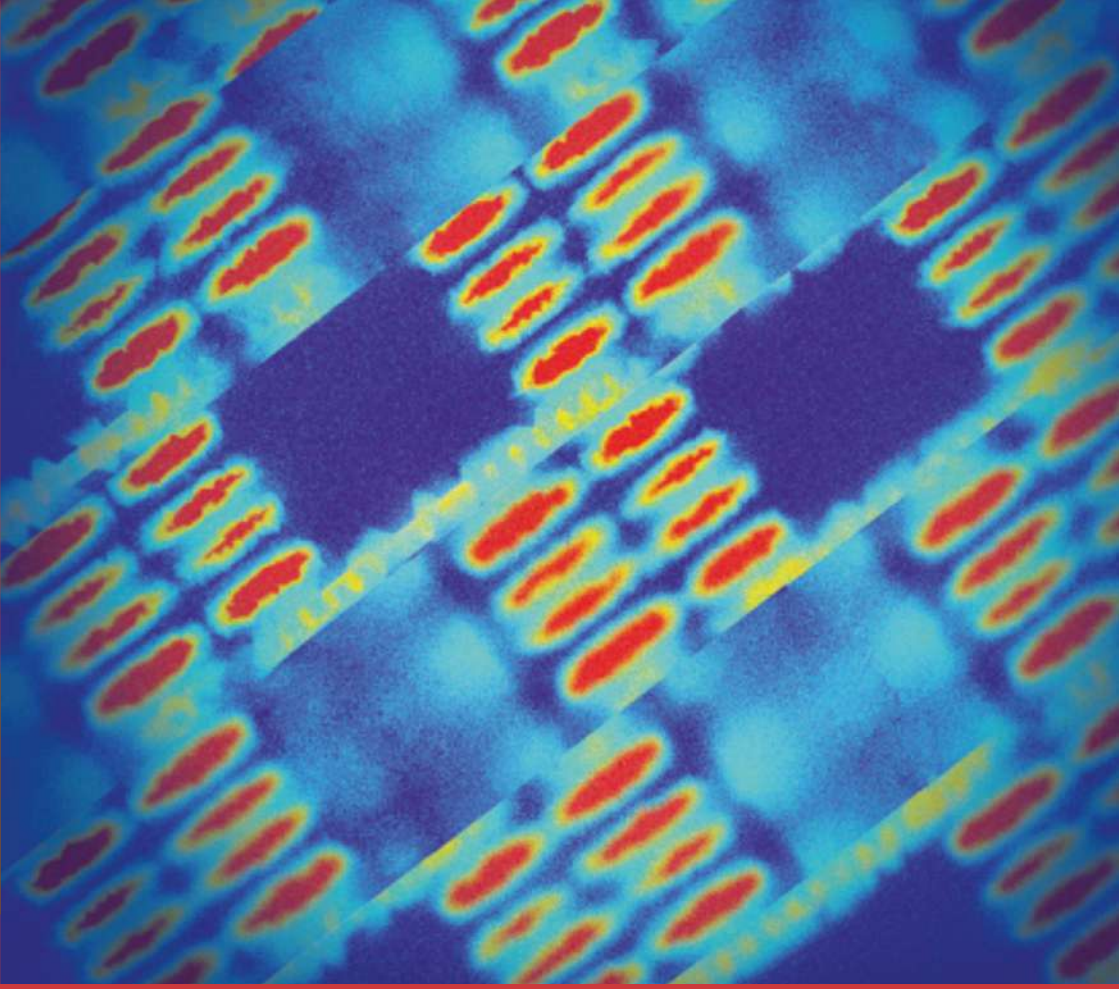

Dissemination

This section presents an overview of key indicators reflecting the scope and impact of the Institute's scientific dissemination activities, drawing on both research output and broader engagement within the scientific community.

The publication indicators highlight overall research productivity, the proportion of Open Access papers, and the distribution of authorship roles–such as first, last, or corresponding authorships–as well as collaborative activities. Journal covers featuring publications by Cnr Nano researchers are also included.

Additional indicators reflect the relevance of Cnr Nano researchers within the scientific community and its ability to attract and collaborate with international scientists. These metrics include invited talks, oral presentations, participation in organizing committees that featured Cnr Nano researchers, and Cnr Nano-hosted colloquia and seminars.

A comprehensive list of all publications is available on the Institute's official website. Use the QR code to access the complete list.

Publication output

436

2024-2025 Journal articles
(Indexed)

Q1 quartile *

51%
(105 of 207*)

* Q1 data refer to 2024 only, as 2025 data are not yet available in InCites.

Key authorship **

60%
(262)

** Authorship take into account first OR last OR corresponding author (each paper counted once).

Open Access

77%
(337)

International collaborations

60%
(259)

Source: InCites dataset updated 2026-02-27.

Journal covers

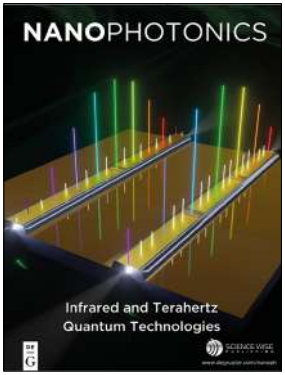

L. Sorba and M. S. Vitiello, Nanophotonics 13 (10), 2024

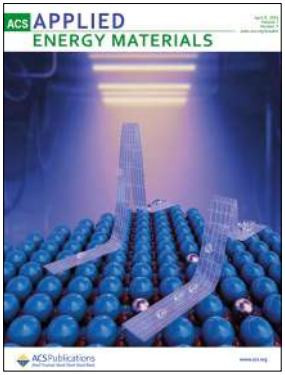

S. D'Addato, P. Luches, S. Benedetti, et al., Applied Energy Materials 7 (7), 2024

L. Viti, M. S. Vitiello, et al., Nano Letters 25 (6), 2025

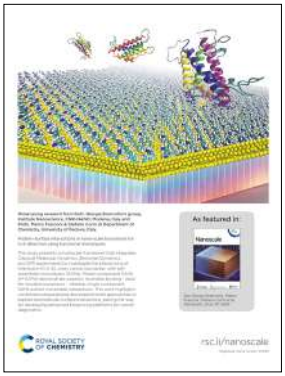

G. Brancolini, S. Corni, et al., Nanoscale 17, 2025

G. Scamarcio et al., Advanced Material Interfaces 12 (6), 2025

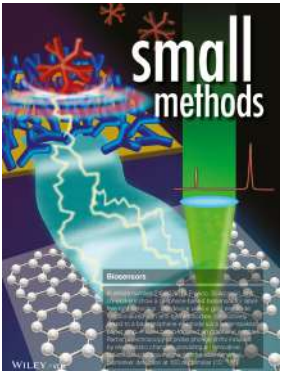

G. Scamarcio et al., Small Methods 9 (8), 2025

L. Viti, C. Schiattarella, M. S. Vitiello, et al., Light Science & Applications 14, 2025

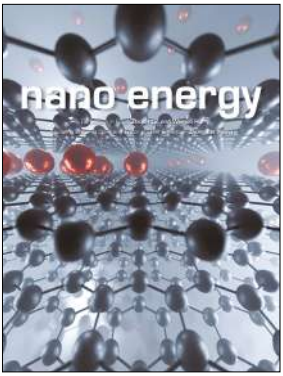

C. Cardoso, D. Prezzi, et al., Nano Energy 142, 2025

S. Heun, L. Sorba, F. Giazotto, F. Beltram, V. Zannier, et al., Nano Letters 25 (39), 2025

B. Storti, R. Bizzarri, et al., The FEBS Journal 292 (22), 2025

L. Viti, G. Scamarcio, M. S. Vitiello, et al., Small Methods 9 (11), 2025

A. Paghi, G. De Simoni, L. Sorba, F. Giazotto, et al., Advanced Functional Materials 35, 2025

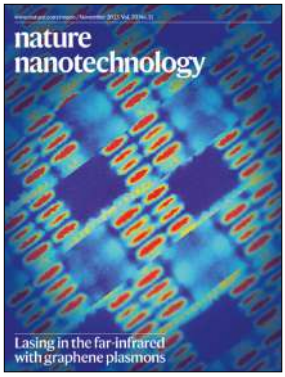

A. Di Gaspare, M. S. Vitiello, et al., Nature Nanotechnology 20 (11), 2025

Scientific collaborations

Main international institutions

- Swiss Federal Institutes of Technology Domain
- Centre National de la Recherche Scientifique (CNRS)
- Helmholtz Association
- Consejo Superior de Investigaciones Cientificas (CSIC)
- Barcelona Institute of Science & Technology
- Ecole Polytechnique Federale de Lausanne
- Universitat Politecnica de Catalunya
- Institut de Ciencies Fotoniques (ICFO)
- Paul Scherrer Institute
- University of Leeds
- Harvard University
- National Institute for Materials Science

Main Italian institutions

- Scuola Normale Superiore
- Università di Modena e Reggio Emilia
- Università di Pisa
- Istituto Italiano di Tecnologia (IIT)
- Istituto Nazionale di Fisica Nucleare (INFN)
- Università di Padova
- Istituto Superconduttori, Materiali Innovativi e Dispositivi (SPIN-CNR)
- Università di Milano
- Università di Salerno
- Università di Torino
- Università di Firenze
- Istituto di Fotonica e Nanotecnologie (IFN-CNR)

Co-author nationality distribution

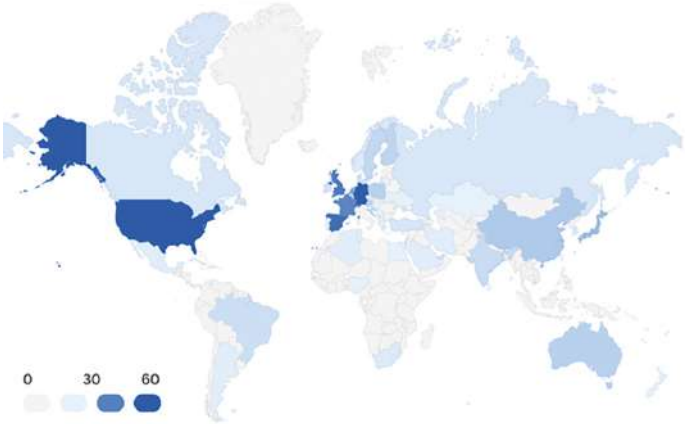

Source: InCites dataset updated 2026-02-27.

Engagement Activities

Given by Cnr Nano

182
Invited talks

147
Oral contributions

96
Organizing Committees

Hosted by Cnr Nano

46
Cnr Nano Seminars
manly featuring external speakers

38
Cnr Nano Colloquia
featuring Cnr Nano researchers and affiliated scientists

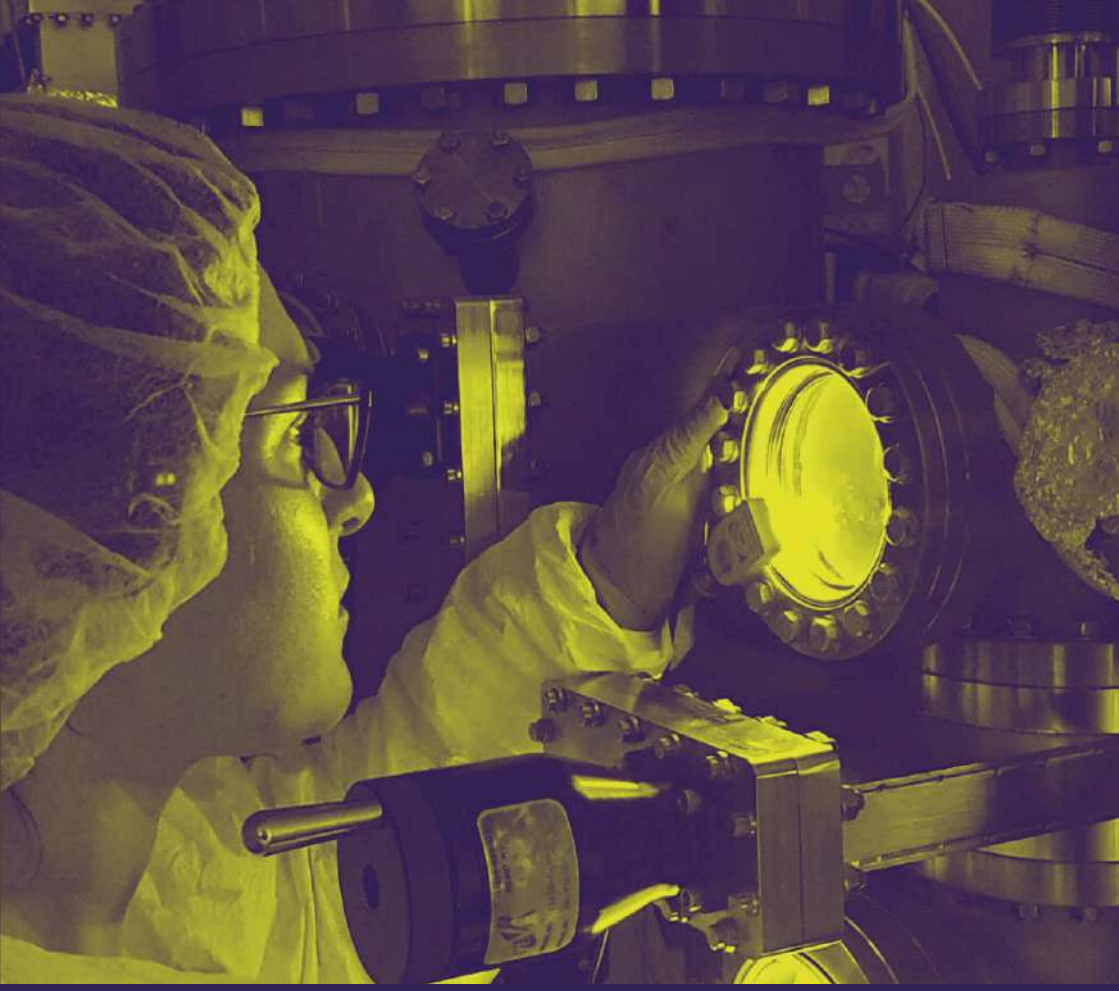

Facilities

Research activities at Cnr Nano are supported by a wide range of advanced facilities and specialized equipment, providing access to state-of-the-art technologies across diverse research areas. The Institute operates at two sites, Modena and Pisa, both embedded in highly collaborative research environments that include universities and other research institutions.

Cnr Nano researchers benefit from shared laboratories, jointly managed infrastructures, and cross-access to instrumentation, facilitated through formal agreements. Cnr Nano Modena shares facilities with the Università di Modena e Reggio Emilia, including access to the Centro Interdipartimentale Grandi Strumenti (CIGS–Unimore). Cnr Nano Pisa has access to the extensive laboratory infrastructures of the Scuola Normale Superiore (SNS) and the Istituto Italiano di Tecnologia (IIT). The combination of the Institute's own laboratories and jointly operated facilities expands the availability and diversity of experimental capabilities, enabling cutting-edge research across multiple disciplines.

This section provides a detailed overview of the Institute's facilities and the techniques available to researchers, organized by laboratory and research area.

Advanced Materials and Nanostructures Realization

THIN FILM GROWTH SYSTEMS

Advanced deposition facilities dedicated to the growth of metals, oxides, semiconductors, and carbon-based materials with thicknesses ranging from nanometers to micron.

- Reactive Molecular Beam Epitaxy (MBE) growth
- Reactive e-beam growth
- 3" multi-target sputter deposition system (DC, RF, reactive)
- 4" multi-target sputter deposition system (DC, RF, reactive)
- Thermal evaporation system

NANOCLUSTER GROWTH

Inert-gas-aggregation nanoparticle source for producing controlled metallic and oxide clusters in the 10 nm diameter range.

- Reactive MBE growth system
- Magnetron-sputtering-based inert-gas-aggregation nanocluster source with mass filter and nano-shell coater
- Thermal evaporation system

OPTICAL LITHOGRAPHY

- 4" Mask Aligner and Exposure System
- 4" Spin coater
- 6" Hot plate
- HDMS vapor priming system
- Wet bench

CLEAN ROOM (ISO 6 and 7)

[Shared facility owned by SNS (Pisa)]

It is mainly devoted to nanofabrication and device development.

- Bonder
- Spin coater
- Hot plate
- Optical and Electron Beam Lithography (EBL)
- Reactive Ion Etching (ICP/RIE)

EPITAXIAL GROWTH SYSTEM

The epitaxy laboratory growth facilities allow epitaxial growth of III-V semiconductors with a precision at the atomic scale.
The Molecular Beam Epitaxy activity is focused on the growth of quantum cascade lasers emitting in the THz range (PASQUA infrastructure, Pisa) and on high Indium-based heterostructures.
The Chemical Beam Epitaxy activity is focused on the growth of gold catalyzed semiconductor nanowires and nanoflags.

- Molecular Beam Epitaxy growth
- Knudsen cells for Ga, Al, In, Si, and As deposition
- Chemical Beam Epitaxy growth [Shared facility owned by SNS]
- Low and high temperature injectors for TMIn, TEGa, TDMASb, TBP, TBA
- Triple-axis X ray diffraction QC3 for heterostructures and superlattices characterization

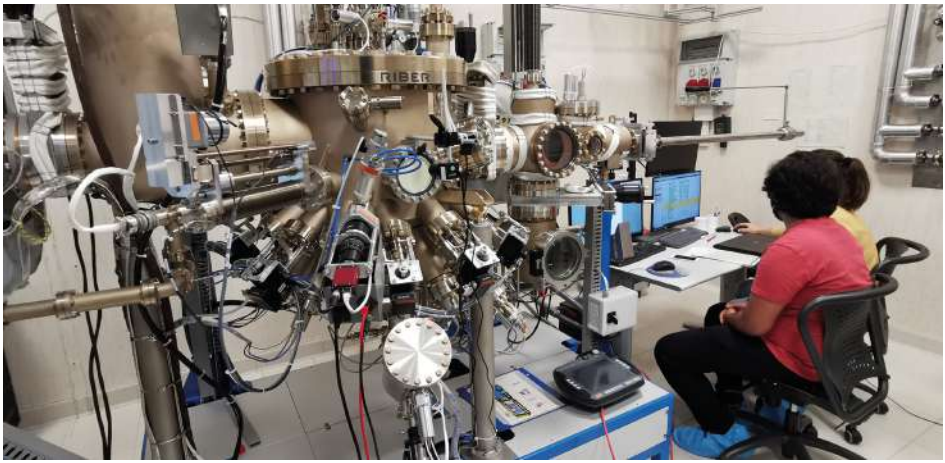

NANOLITHOGRAPHY

Advanced equipment dedicated to realization of nanostructures, analysis of thin film depth profiles, preparation of lamellae and nanodevices for TEM microscopy.

- Dual Beam System: Focused Ion Beam and Scanning Electron Microscope (FIB-SEM)
- Electron Beam Lithography (EBL)
- Reactive Ion Etching (RIE) 6" system for Ar, O_2, CF_4, CHF_3, N_2 processes

Advanced Materials and Nanostructures Characterization

SURFACE ANALYSIS SYSTEMS

Surface sensitive chemical analysis based on electron spectroscopy. Surface morphology characterization by scanning probe microscopy.

- X-ray photoelectron spectroscopy (XPS)
- UV photoelectron spectroscopy (UPS)
- Low energy electron diffraction (LEED)
- High Resolution Electron Energy Loss Spectroscopy (HREELS)
- Scanning Tunnelling Microscopy (STM – variable temperature)
- Atomic Force Microscopy (AFM)

ELECTRICAL AND OPTICAL CHARACTERIZATION

Characterization of thin films and prototype devices via Probe Stations and optical set-up for UV-VIS-NIR spectrophotometry.

- 4" precision probe station
- Hall/Van der Pauw stage -190 °C to 600 °C
- 4-point probe sensor
- DC, high resistivity switch/measure system for precision Hall and Van der Pauw measurements
- 40 Hz – 110 MHz Precision impedance analyzer
- UV-VIS-NIR spectrophotometer (transmittance and reflectance) (200 nm 2700 nm range)

Low Temperature and High Magnetic Field

QUANTUM MAGNETISM

Magnetic resonance spectroscopy, pulsed time-domain manipulation, magneto-transport. Focus on quantum sensing, hybrid spin-photon systems, (molecular) spin centres, cavity magnonics.

- Closed cycle He3-He4 dilution fridge (20 mK, 20 GHz) with magnetic field (8 T)
- Variable temperature system (350-2 K, 7 T) and He3 fridge (250 mK, with vector magnet 9, 1, 1 T). He4 recovery system
- Variable temperature probe station
- Helmholtz coil electromagnet (1 T)

SUPERCONDUCTIVE QUANTUM ELECTRONICS

Quantum transport setup for superconductive device measurements up to 40 GHz. Devices are fabricated in a cleanroom using available facilities that allow sputtering and evaporation of metals, superconductors, insulators, and ferromagnets in single- or multilayer configurations.

- 4 fridge systems He3-He4 closed Cycle (20 mK, 40 GHz) with vector magnet (3T)
- 2 fridge systems He4 (3 K, 10 GHz)

Advanced Microscopy

TRANSMISSION ELECTRON MICROSCOPY (TEM)

High resolution electron microscope spectra 300 with high brightness field emission gun and “ultimono” monochromator operable at 60 and 300KeV. The microscope can work in TEM and in STEM scanning mode and with QUANTUM GIF spectrometer. It can acquire both EELS spectral imaging and Energy Filtered TEM imaging. It is also equipped with special attachments for beam shaping and electron-light interaction studies.

- TEM, information resolution <1 Å
- STEM, resolution 1.5 Å
- Energy resolution 30meV

SCANNING TUNNELING MICROSCOPY (STM)

[Shared facility owned by IIT (Pisa)]

The main activities are related to the development of graphene-based materials for hydrogen storage and the study of metal functionalization/intercalation of epitaxial graphene with atomic scale precision.

- STM (variable temperature)

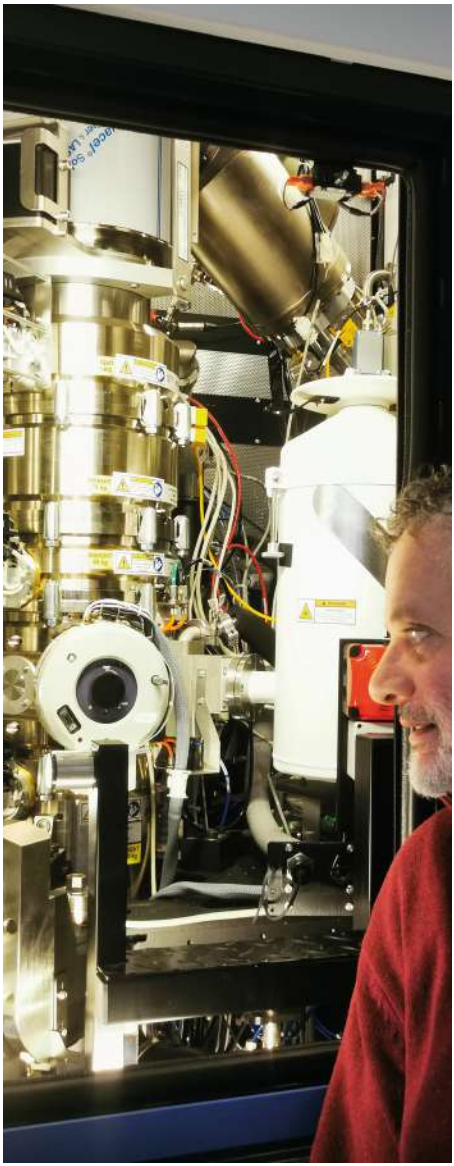

Nanobio Activities

MECHANOBIOLOGY

Atomic force microscopy and home developed devices to study mechanical properties of systems of biological interest and to study the effect of physical stimuli on living cells.

- Atomic Force Microscopy (AFM)
- Micropipette Aspiration Technique (MAT)
- Cell Stretchers and Live-Cell Imaging Incubators
- Epifluorescence Microscope

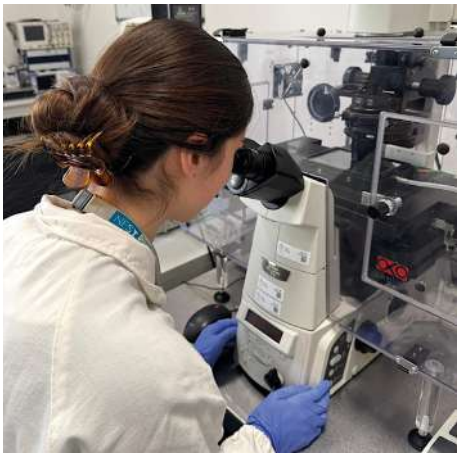

BIOSENSOR AND NANOMEDICINE

Facilities related to the development of nanomaterials for brain pathologies and nerve regeneration, and the development of electroacoustic devices for microfluidics and sensing applications.

- High-frequency Quartz Crystal Microbalance with dissipation (QCM-D) monitoring
- 2 portable quartz crystal microbalance with dissipation (QCM-D) systems
- Vector Network Analyzer (4 ports, up to 8.5 GHz)
- Signal generator (up to 3.5GHz)
- RF Switch Matrix (2 in × 24 out, up to 9 GHz)
- Contact Angle Meter

CELLS CULTURE

[Shared lab owned by SNS (Pisa)]

Activities involve maintaining and experimenting with cells in vitro, with a focus on developing novel scaffolds for cell cultures for regenerative medicine applications.

- Biohazard hoods (2x)
- CO_2 cell incubators (4x)
- Aspiration system
- Inverted optical microscope; epifluorescent inverted microscope with PC
- Centrifuges and water-bath (37°C)
- Nitrogen dewar for cell storage
- Countess Automated Cell Counter
- Cell microporator
- Cold Room
- Facilities for biomolecular assays (plate reader, gel imager, protein electrophoresis system, PCR system)

Advanced Photonics and Photonic Materials

THz PHOTONICS

Activities focused on experimental light–matter interaction phenomena, two-dimensional nanomaterials (graphene, phosphorene, van der Waals heterostructures, topological insulators), micro- and nanosystems, nanophotonics, quantum optics, far-infrared photonics, and optoelectronic devices.

- THz Quantum Cascade Laser characterization setup
- Two mid-far IR Fast Fourier transformer spectrometer (FTIR)
- Under vacuum, ultrahigh resolution (0.075 cm^{-1}) FTIR (from mid-IR to THz) (step and rapid scan mode)
- Helium flow cryostat with gas exchange and with optical access
- Micro-cryostat and Stirling cryocoolers
- He-flux Cryostat (4 K) with optical access
- Liquid He & N_2 cooled bolometers
- Hot electron bolometer
- THz source
- 500 GHz-800 GHz tunable source
- Nano-detectors and quantum dot devices characterization setup
- THz Pump and probe reflectivity set-up
- Micro-Raman (from RT to low T)
- Micro-photoluminescence set-up (from RT to low T)
- Scattering near field optical microscope (s-SNOM) in the mid-IR
- Detectorless s-SNOM in the Terahertz
- Terahertz Time domain spectroscopy (TDS)

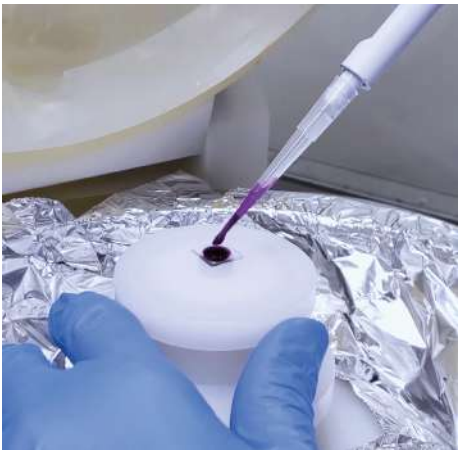

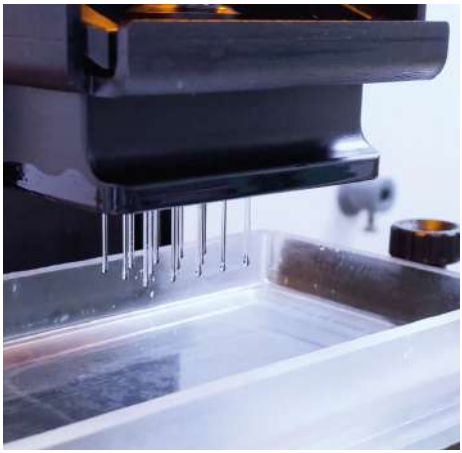

SOFT MATTER

Focus on the development of optically and electrically active micro- and nanostructures, 3D printing and additive manufacturing of materials with control on their optical and piezoelectric properties for applications in photonics, energy harvesting, and biotechnology.

ADDITIVE MANUFACTORING

- UV Digital Light Processing
- UV Stereolithography
- Fused deposition modelling
- Direct Ink Writing
- Electrospinning set-up
- Spin coater
- Doctor Blade

SPECTROSCOPY

- Femtosecond excitation laser sources (400 nm, 800 nm)
- Streak camera
- CW multi-wavelength excitation and angle-resolved emission spectroscopy
- UV-Vis spectrophotometer
- FTIR Spectrometer
- Piezoelectric coefficients, capacitance, and dielectric loss measurement system

Computational Facilities

Theoretical and computational research at Cnr Nano is supported by dedicated Nanobio Activities performance computing (HPC) facilities, providing access to local HPC clusters equipped with high-end CPUs, GPUs, and large storage capacities to handle computationally intensive tasks. These resources enable multi-scale modeling, simulations, and data analysis across diverse research areas.

HPC FOR NANOSCALE THEORY AND SIMULATION

Usage: Electronic structure simulations of ground state and excitations using Density Functional Theory (DFT), time-dependent DFT, and Green's function methods; applications to bulk and two-dimensional materials, organic systems, and interfaces. Multi-scale modelling approaches combining DFT, reactive classical Molecular Dynamics, and coarse-grained models. Applications to materials and biomolecular systems. Machine learning applications: development of neural-network empirical potentials and ML based analyses.

LYRA Cluster: 24 nodes, 40 cores per node (Intel Xeon Gold 6320), 392 GB RAM per node; Infiniband interconnects.

ARIES Cluster: 58 nodes, 54 cores per node, 512–1024 GB RAM per node; 1 node equipped with NVIDIA A100 GPU.

Fat nodes (interconnected, 2 units): 2 × NVIDIA GPUs (Quadro RTX 6000), 2 × Intel Xeon Gold 6258R CPU @ 2.70 GHz (28 cores each), 60 TB storage (RAID6), 754 GB RAM.

Single workstations (4 units): 1 × NVIDIA GPU (RTX 4000), 2 × Intel Xeon Silver 4214R CPU @ 2.40 GHz (14 cores each), 10 TB storage, 256 GB RAM.

Cnr Nano Life

JANUARY

Publication in Nature – Breakthrough in high-entropy ceramics

A study co-authored by Arrigo Calzolari describing a computational method to rapidly identify high-entropy ceramics with exceptional thermal and mechanical resilience was published in Nature 625, 66 (2024). Developed within an international collaboration led by Stefano Curtarolo (Duke University, USA), the DEED algorithm predicts the synthesizability of hundreds of extreme-performance materials, accelerating their use in energy, electronics, and aerospace applications.

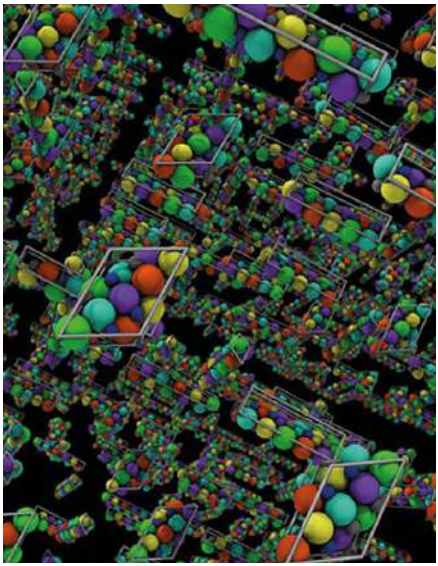

JANUARY

Nano Colloquia Series kicks off at Cnr Nano

The long-running Nano Colloquia series continued throughout 2024 and 2025, with 38 colloquia delivered over the two-year period. Starting afresh every year, Colloquia offer the stage to researchers from Cnr Nano or collaborating institutions to present the latest results, spark discussion, and foster connections across the nanoscience community. Sessions are hosted in Modena and Pisa and are held both in person and online.

JANUARY

ERC Proof of Concept for Far-Infrared Imaging

Miriam Serena Vitiello was awarded a European Research Council Proof of Concept grant for TeraScan, a project advancing compact terahertz imaging systems in the far-infrared range. Building on previous ERC-funded research, TeraScan aims to bring ultra-fast graphene-based detectors closer to real-world applications in industry, healthcare, and security. The award is Vitiello's third ERC grant. With this project, Vitiello reaches the outstanding number of three ERC grants awarded.

FEBRUARY

11 February – #womenatCNR for Women and Girls in Science

On the International Day of Women and Girls in Science, Cnr Nano gave voice to its female researchers through the #womenatCNR social media campaign, contributing to a collective celebration of women in science. Twenty-seven scientists from the Institute shared words of inspiration — on openness, curiosity, and perseverance — composing a mosaic of voices as a legacy for the next generation of women scientists.

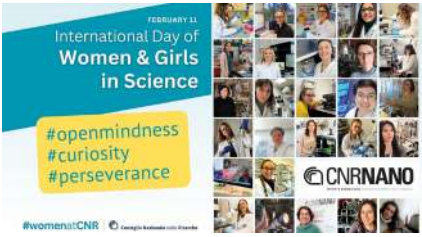

MARCH

DSQM wins Premio America Innovazione

Digital Superconducting Quantum Machines (DSQM), a Cnr Nano spin-off, received the America Innovazione Award from the Italia-USA Foundation which recognizes outstanding Italian startups. The prize highlights DSQM's superconducting technology, rooted in research at Cnr Nano, and underscores the Institute's ability to translate frontier physics into high-impact innovation.

APRIL

Flowering European-Japanese collaborations

HANAMI Project officially launched under EuroHPC Joint Undertaking and Horizon Europe. It gathers 15 European and 11 Japanese institutions to advance cooperation in High-Performance Computing. As a project partner, Cnr Nano applies its expertise in advanced materials design, supporting future exascale HPC applications and reinforcing Europe–Japan collaboration - a key step in connecting with leading Japanese research teams.

JUNE

Innovative nanomedicine research in REMEDY project

Cnr Nano launched the REMEDY project, developing stabilized reversed micelles - an innovative nanostructure - to transport therapeutic agents across biological barriers, including the brain. Coordinated by Marco Cecchini, the initiative aims to advance treatments for central nervous system diseases, combining nanotechnology and medicine in a forward-looking approach.

JULY

Exploring quantum materials and light at Erice

On July 6-12, Miriam Vitiello with Federico Capasso (Harvard University, USA) and Oleg Mitrofanov (UCL, UK) organized the International Workshop "Quantum Materials and Structured Light" (QMSL 2024) at the Ettore Majorana Foundation in Erice, Sicily. The week-long event brought together scientists and engineers to explore frontier topics in quantum science, including light–matter interactions at the nanoscale, nano-structured quantum materials, plasmonics, and topological photonics. The event fostered interdisciplinary exchange and highlighted the Institute's role in advancing quantum materials and photonic research on the international stage.

AUGUST

Superconducting quantum technologies on stage

On August 30, Elia Strambini delivered a talk at TEDx Forte Dei Marmi, exploring the frontiers of superconducting quantum technologies, drawing on his extensive research experience. He shared insights on how these breakthroughs could transform computing and telecommunications, offering the audience a glimpse into the future of quantum science and its potential real-world applications.

AUGUST

Celebrating 30 years of the Quantum Cascade Laser

To mark 30 years since the first Quantum Cascade Laser, Cnr Nano coorganized the International Quantum Cascade Laser School & Workshop in Ischia (August 25-30). The conference gathered 210 participants worldwide, including leading experts and emerging talents, the enduring impact of QCL technology and the Institute's significant contributions including pioneering terahertz QCL development, and advanced infrastructure.

SEPTEMBER

Gaetano Scamarcio is the new Cnr Nano Director

On September 1, Gaetano Scamarcio took office as Director of Cnr Nano. A full professor of experimental physics with an international research profile in optoelectronics and photonics, known for his pioneering work in quantum devices, Scamarcio succeeds founding director Lucia Sorba, who left after 14 years.

NOVEMBER

Italian Chemical Society awards a Cnr Nano researcher

Matteo Capone, postdoctoral researcher in Modena, was awarded the Premio Primo Levi 2024 by the Italian Chemical Society. The prize recognizes outstanding research by early-career chemists and was attributes for his 2023 Nature study uncovering the molecular mechanisms of photosynthetic water oxidation — a key step in understanding how nature converts light into energy.

DECEMBER

Cnr Nano lands on LinkedIn

Cnr Nano launched its official LinkedIn page, extending its digital presence within the international research community. Through this new channel, the Institute aims to share research and perspectives, support open and accessible science, and connect with researchers, industry, and early-career talents.

JANUARY

Electron microscopy milestone

On January 24, SPEQTEM, an advanced Spectroscopic Quantum Transmission Electron Microscope developed with Thermo Fisher Scientific and supported by Unimore, was inaugurated in Modena. Based on the Thermo Scientific Spectra 300 platform, the instrument delivers atomic-resolution imaging and advanced spectroscopic analysis. As a long-term strategic resource for Cnr Nano, it will open new frontiers in quantum electron optics and materials research, supporting innovation for the energy transition and circular economy.

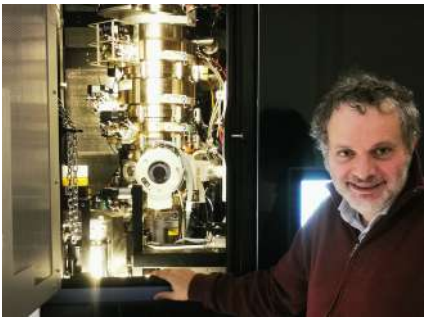

JANUARY

ERC and SPIE honours for Miriam Vitiello

Miriam Serena Vitiello gained international recognition with two major honors. She received an ERC Proof of Concept grant for her project CLEAR – *Chip scaLE terAheRtz dualcomb system*, aimed at developing compact terahertz frequency comb devices with potential applications in spectroscopy, diagnostics, and communications. Besides, she was selected for the SPIE Achievement Award granted by the namesake international society for optics and photonics, for her scientific contributions and service to the community.

APRIL

DSQM wins again

For the second year, Cnr Nano spin-off DSQM received the Premio America Innovazione from the Italia-USA Foundation. The award recognizes DSQM's advances in superconducting technologies, including field-effect devices with potential for highspeed telecommunications and next-generation computing. This repeated recognition highlights the spinoff's innovation and its success in translating nanoscience into technology.

MAY

OPERA European epitaxy conference in Pisa

From May 19 to 23, Lucia Sorba co-organized the European Conference on Innovative and Advanced Epitaxy at the Scuola Normale Superiore in Pisa. The event brought together about 100 researchers from across Europe, including keynote speakers on quantum dots, 2D materials, and advanced optoelectronic devices. The conference highlighted the extensive expertise at Cnr Nano in cutting-edge epitaxial growth and fostered academia-industry collaboration.

MAY

Empowering the next generation of materials scientists

On May 19-23, Cnr Nano hosted the YAMBO School 2025 in Modena, training around 50 early-career scientists from 15 countries in advanced excited-state simulations and many-body theory using the open source YAMBO code. The five-day program combined lectures and hands-on sessions on advanced computational methods for light–matter interactions, key to designing future technologies, such as solar cells, optoelectronics, and quantum technologies. A distinctive aspect of this edition was its commitment to gender balance: women were one third of the participants, meeting the organizers' goals.

JUNE

Miriam Vitiello wins fifth ERC Grant

Miriam Serena Vitiello was awarded a prestigious ERC Advanced Grant for her project NODE, which aims to pioneer a new class of integrated photonic devices across the far-infrared spectrum by combining semiconductor and 2D quantum materials. NODE will enable breakthroughs in quantum sensing, telecommunications, and biomedical diagnostics. Vitiello has secured her fifth ERC grant, a remarkable achievement that highlights both her outstanding scientific leadership and Cnr Nano's influential role in advancing quantum photonics nanotechnologies.

JUNE

Building community and vision at Cnr Nano

Over 170 researchers, technologists, and staff gathered under the theme "Reconnecting, inspiring interactions" on June 5-6 in Modena, for Cnr Nano's fourth Scientific Meeting. The two-day program included plenary talks, thematic sessions, dynamic poster discussions across quantum materials, advanced electron microscopy, photonics, and computational science, and awards for outstanding early-career contributions. The meeting strengthened dialogue across laboratories and career stages, reinforcing a shared scientific vision, while a free evening concert, open to the public, highlighted the connection between science, creativity, and community.

JUNE

Plasmonica 2025 Workshop

From June 25 to 27, Modena hosted the 11th annual Plasmonics and Nano-Optics Workshop, organized by Cnr Nano and chaired by Stefania Benedetti, the first woman to lead a Plasmonica workshop. About ninety participants from Italy and abroad met to explore the latest advances in plasmonics, nano-optics, and nanophotonics. Early-stage researchers were a central focus of the workshop, making up 54 of the 90 participants.

SEPTEMBER

Hunting for 2D Excitonic Insulators

For the Two-Dimensional Excitonic Insulators Workshop forty researchers from around the world gathered in the historic centre of Modena from September 1 to 3. Co-organized by Cnr Nano and the University of Modena and Reggio Emilia, the meeting featured presentations, poster sessions, and panel discussions designed to spark dialogue on the field's most challenging questions, from macroscopic quantum coherence to the interplay with unconventional phases.

SEPTEMBER

Cnr Nano at the European Researchers' Night

Cnr Nano's community loves engaging with the public and inspiring curiosity. In 2024 and 2025, researchers brought nanoscience to life in Modena and Pisa. Visitors explored quantum mechanics, advanced materials, and virtual reality through interactive labs, playful games, and one-on-one "quantum speed dates." Science-bites talks and hands-on demos offered engaging insights into how light and matter interact at the nanoscale, and how nanotechnologies impact health, the environment, and computing.

OCTOBER

New leadership at Cnr Nano Modena

On October 16, Arrigo Calzolari succeeded Massimo Rontani as Head of Cnr Nano's Modena unit. On the occasion, colleagues gathered to celebrate Rontani 's tenure and welcome Arrigo as new head of the branch.

OCTOBER

Back to schools

Throughout 2024 and 2025, Cnr Nano strengthened its commitment to science outreach in schools, inspiring students and supporting their orientation toward scientific careers. As part of an agreement with the Regional School Office for Tuscany, our researchers delivered several seminars in middle and high schools, reaching approximately 500 students. They talked about nanoscience applications in medicine and the role of natural and artificial biomaterials in biomedical and environmental fields, offering students direct insight into the societal impact of research and conveying the enthusiasm and passion that drive our scientific work.

DECEMBER

25 Years of the Cnr Pisa Research Area

Marking a quarter century of activity, the Cnr Pisa Research Area celebrated its anniversary on December 10, with an event bringing together its 14 institutes to reflect on past achievements and future challenges. Cnr Nano contributes to this multidisciplinary ecosystem by advancing science as a driver of innovation and regional development. The celebration also featured the presentation of a commemorative volume retracing the Area's history and highlighting the scientific excellence of its institutes.

People

The following list includes all researchers and staff active at Cnr Nano in 2024-2025. A total of 251 people have been working in our institute (38% female, 62% male), coming from 22 different countries besides Italy (Albania, Brazil, China, Cuba, France, Germany, Greece, India, Iran, North Macedonia, Mexico, Morocco, Nigeria, Pakistan, Poland, Portugal, Romania, Russia, Spain, the United Kingdom, Ukraine, and the United States).

** indicates people who are no longer at Cnr Nano.*

CNR NANO STAFF

Researchers

Laura Andolfi
Antonella Battisti
Valerio Bellini
Luca Bellucci
Stefania Benedetti
Andrea Bertoni
Giovanni Bertoni
Federica Bianco
Alessandro Braggio
Giorgia Brancolini
Arrigo Calzolari
Michele Campisi
Andrea Camposeo
Sara Carpi
Alessandra Catellani *
Chiara Cavallini
Marco Cecchini
Valdis Corradini
Alessandro Crippa
Pino D'Amico
Giorgio De Simoni
Ambra Del Grosso
Alessandro di Bona
Rosa Di Felice
Alessandra Di Gaspare
Filippo Fabbri †
Riccardo Farchioni
Andrea Ferretti
Mariacristina Gagliardi
Gian Carlo Gazzadi
Alberto Ghirri
Francesco Giazotto
Angelo Greco
Vincenzo Grillo
Stefan Heun
Gabriele Losi
Paola Luches
Francesca Matino
Andrea Mescola
Riccardo Nifosì
Sibilla Orsini
Fulvio Paleari
Guido Paolicelli
Claudia Maria Pereira Cardoso
Luana Persano
Sergio Pezzini
Stefano Pittalis
Deborah Prezzi
Vladimir Pushkarev
Elisa Riccardi
Massimo Rontani
Francesco Rossella *
Enzo Rotunno
Carlo Andrea Rozzi
Melissa Santi
Gaetano Scamarcio
Chiara Schiattarella
Antonella Sgarbossa
Lucia Sorba
Nicola Spallanzani
Eleonora Spurio
Barbara Storti
Elia Strambini
Fabio Taddei
Ilaria Tonazzini
Valentina Tozzini
Filippo Troiani
Daniele Varsano
Stefano Veronesi
Leonardo Viti
Miriam Serena Vitiello
Laura Zanetti Polzi
Valentina Zannier
Simone Zanotto

† Passed away in January 2026

Postdoctoral fellows and scholarship

Bamidele Ibrahim Adetunji *
Francesca Alimonti *
Greta Amendola
Omer Arif *
Xavier Ballu *
Shadi Bashiri *
Sara Ben Abid *
Costanza Borghesi
Marco Brondi *
Matteo Capone
Sara Chiarugi
Luca Chirolli *
Chiara De Cesari *
Stefano Antonio De Santis
Miriam De Sarlo *
Armida Di Fenza *
Nicoletta Di Leo
Zacharias Fthenakis *
Sara Ghayeb Zamharir *
Shuvaraj Ghosh
Roberto Giacomantonio *
Madiha Khan *
Naveen Kumar *
Kristi Kume *
Lorenzo Lavista
Giuseppe Emanuele Lio *
Peter Nicholas Oliver Gillespie *
Manuel Alejandro Justo Guerrero
Francesco Lamberti
Savio Laricchia *
Alice Lunghi
Neetu Malik *
Manuel Martin Bravo *
Vladyslav Matkivskyi *
Debayan Mondal *
Alessandro Mossa *
Lindsay Elizabeth Bassman Oftelie *
Said Oukahou *
Alessandro Paghi *
Riccardo Panico
Samuele Pelatti
Andrea Pintus *
Lucrezia Pucci
Sreyan Raha *
Saravanan Rajamani *
Subhankar Roy *
Paolo Rosi
Pavel Rukin *
Luca Scaccini *
Andrea Secchi *
Giulio Senesi *
Giacomo Sesti
Lili Shi
Gaurav Shukla *
Pintu Singha *
Faezeh Soofivand *
Katarzyna Stanislawa Skibinska *
Robert Andrei Sorodoc *
Andrea Tonelli
Nicole Tonesi *
Manuela Tore *
Ylea Vladimis *
Chunxu Zhang *

Administrative, technical, and support staff

Maria Grazia Angelini
Francesco Baesso
Maria Bartolacelli
Antonio Betzu *
Elisa Bolognesi
Davide Calanca
Susanna Cavicchioli
Paola Corezzola
Daniele Desiati
Giovanna Diprima
Giuseppe Genovese
Sandro Guerrazzi
Lucia Martorana

Luisa Neri
Francesco Nicolussi Golo
Patrizia Pucci
Maddalena Scandola
Federica Sighinolfi
Simone Spinozzi
Anna Grazia Stefani *

Support staff located in Genova

Alberto Arnone
Matilde Bolla
Barbara Cagnana
Enrico Camauli
Marco Campani
Paolo Ciocia
Monica Dalla Libera
Fabio Distefano
Francesca Fortunati
Danilo Imperatore Antonucci *
José Carlos Manganaro
Diletta Miceli
Elisabetta Narducci
Marco Punginelli *
Milena Toselli
Claudia Valentini

AFFILIATED PERSONNEL FROM OTHER INSTITUTIONS

Researchers

Marco Affronte
Andrea Alessandrini
Maria Allegrini
Fabio Beltram
Giuliano Benenti *
Roberto Biagi
Raffaello Bianco *
Ranieri Bizzarri
Igor Bodrenko
Pietro Bonfà
Claudio Bonizzoni
Paolo Bordone
Marilia Junqueira Caldas
Giuseppe Cantarella
Francesco Cardarelli
Franco Carillo *
Ciro Cecconi
Stefano Corni
Sergio D'Addato
Valentina De Renzi
Elena Degoli *
Angelo Di Bernardo *
Mariagrazia Di Luca *
Daniele Ercolani *
Stefano Frabboni
Denis Garoli *
Simone Gasparinetti *
Marco Gibertini
Giacomo Giorgi
Vittorio Giovannetti
Guido Goldoni *
Marco Govoni *
Federico Grasselli
Stefano Luin
Rita Magri *
Franca Manghi
Ivan Marri
Claudia Menozzi
Elisa Molinari
Stefano Ossicini
Gioacchino Massimo Palma *
Maurizia Palummo
Pasqualantonio Pingue
Dario Pisignano
Alessandro Pitanti
Stefano Roddaro
Alberto Rota
Alice Ruini

Mauro Francesco Sgroi *
Alessandra Toncelli
Alessandro Tredicucci
Giovanni Maria Vanacore *
Giampaolo Zuccheri *

Postdoctoral fellows

Lyudmyla Adamska *
Michael Alejandro Hernandez Bertan
Jannis Christian Krumland
Daniele Montepietra *
Andoni Ugartemendia Biurrun

PhD students

Annachiara Albanese *
Benedetta Bertoni *
Beatrice Bighi *
Margherita Bini
Giada Bucci *
Lorenzo Castelli
Francesco Cosimo Castellucci
Caterina Chiari *
Sofia Cristiani *
Matteo D'Alessio
Gaia Forghieri *
Payam Habibzadeh Kavkani *
Matteo Lanza
Francesco Lunardelli
Riccardo Magrin Maffei *
Benedetta Masciulli
Alessia Papalini
Leonardo Pierattelli
Giorgia Tori
Andrea Vezzosi *

Gender distribution

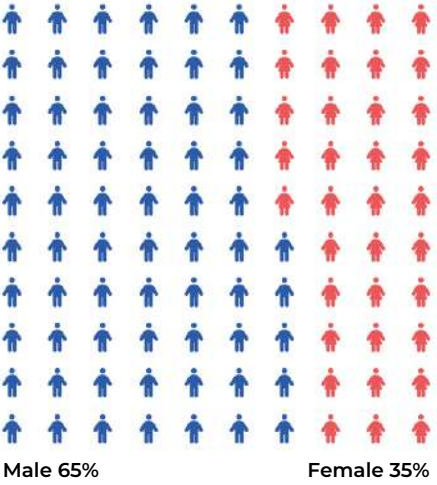

Gender distribution of research personnel.

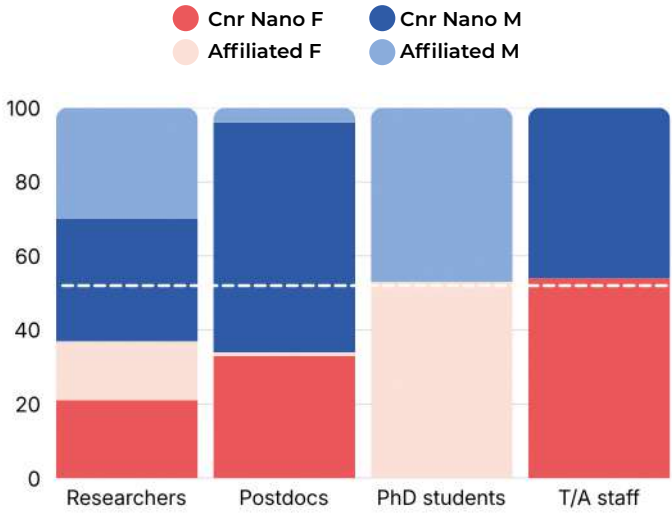

Gender distribution within the Institute personnel
(all categories have been normalized to 100).

Image credits

Cover image
Machine Learning segmentation and labelling of oxide shells in Cu nanoparticles obtained from STEM imaging - allowing quantitative analysis of shell thickness distributions. Courtesy of Giovanni Bertoni (Cnr Nano)

Pag. 7
Scanning electron microscopy image of electrospun polystyrene nanofibers showing beads. Courtesy of Antonella Battisti (Cnr Nano)

Pag. 27
Scanning electron microscopy image of an ordered array of tapered InP nanowires. Courtesy of Valentina Zannier (Cnr Nano)

Pag. 45
Scanning tunnelling microscopy topography (3D view) of gallium atoms intercalated in epitaxial graphene. Courtesy of Stefano Veronesi (Cnr Nano)

Pag. 71
Scanning electron microscopy micrograph of piezoelectric nanopillars based on cellulose nanocrystals for energy harvesting. Courtesy of Luana Persano (Cnr Nano)

Pag. 93
A snapshot from the simulation of an Intrinsically Fluorescent Proteins dense aqueous solution, with some of them flashing. Courtesy of Margherita Bini (SNS) and Valentina Tozzini (Cnr Nano)

Printed in May 2026.
Editorial project: Maddalena Scandola, Cnr Nano.
Graphic design: mediamo.net, Modena.

CNRNANO

ISTITUTO NANOSCIENZE CONSIGLIO NAZIONALE DELLE RICERCHE